Mechanisms of Synaptic Zinc Plasticity in Mouse Dorsal Cochlear Nucleus

by

Nathan W. Vogler

B.S., University of Pittsburgh, 2014

Submitted to the Graduate Faculty of the

School of Medicine in partial fulfillment

of the requirements for the degree of

Doctor of Philosophy

University of Pittsburgh

2019

UNIVERSITY OF PITTSBURGH

SCHOOL OF MEDICINE

This dissertation was presented

by

Nathan W. Vogler

It was defended on

November 26, 2019

and approved by

Dr. Elias Aizenman, Professor, Neurobiology

Dr. Yan Dong, Professor, Neuroscience

Dr. Stephen Meriney, Professor, Neuroscience and Psychiatry

Dr. Anne-Marie Oswald, Associate Professor, Neuroscience

Dr. Laurence Trussell, Professor of Otolaryngology, Oregon Health & Science University

Dissertation Advisor: Dr. Thanos Tzounopoulos, Endowed Professor and Vice Chair of Research, Otolaryngology

Mechanisms of Synaptic Zinc Plasticity in Mouse Dorsal Cochlear Nucleus

Nathan W. Vogler, PhD

University of Pittsburgh, 2019

In many brain areas, such as the neocortex, limbic structures, and the auditory brainstem, glutamatergic nerve terminals also contain zinc in their synaptic vesicles (synaptic zinc). Synaptic zinc is co-released with glutamate to modulate neurotransmission at excitatory synapses, and synaptic zinc modulates sensory processing and behavior. In many zinc-containing brain areas, sensory experience causes long-term changes in synaptic zinc levels and/or signaling, termed here *synaptic zinc plasticity*. However, the mechanisms underlying synaptic zinc plasticity and the effects of this plasticity on long-term glutamatergic plasticity remain unknown. To study these mechanisms, we employed *in vitro* and *in vivo* models in zinc-rich, glutamatergic dorsal cochlear nucleus parallel fiber synapses. Our results demonstrate bidirectional activity-dependent plasticity of synaptic zinc signaling. High-frequency stimulation of parallel fiber synapses induced long-term depression of synaptic zinc signaling (Z-LTD), as evidenced by reduced zinc-mediated inhibition of excitatory postsynaptic currents. Low-frequency stimulation induced long-term potentiation of synaptic zinc signaling (Z-LTP), as evidenced by enhanced zinc-mediated inhibition. Pharmacological inhibition of Group 1 metabotropic glutamate receptors (mGluRs) eliminated both Z-LTD and Z-LTP. Pharmacological activation of Group 1 mGluRs induced bidirectional synaptic zinc plasticity, associated with bidirectional changes in presynaptic zinc levels. Therefore, Group 1 mGluR activation is necessary and sufficient for inducing bidirectional long-term synaptic zinc plasticity. Exposure of mice to loud sound caused Group 1 mGluR-dependent zinc plasticity in parallel fiber synapses, consistent with our *in vitro* results. To study

the downstream mechanisms by which Group 1 mGluRs modulate presynaptic zinc signaling, we further employed our *in vitro* models in dorsal cochlear nucleus slices, using electrophysiology, pharmacology, and fluorescent imaging. Z-LTD requires a rise in postsynaptic Ca^{2+}. Furthermore, depletion of Ca^{2+} stores from the endoplasmic reticulum is sufficient to induce Z-LTD, and reduces presynaptic zinc levels. These results demonstrate a role of postsynaptic Ca^{2+} stores underlying Z-LTD, and suggest a role of retrograde signaling in synaptic zinc plasticity. Together, this work reveals a novel mechanism underlying activity- and experience-dependent plasticity of synaptic zinc signaling, which may be a general plasticity mechanism in zinc-containing synapses throughout the brain.

Table of Contents

List of Figures

Preface

I would first like to thank my mentor, Dr. Thanos Tzounopoulos, for his rigorous and attentive training during my graduate education. This dissertation is a product of his mentorship, and I am extremely grateful for his guidance, support, and friendship during my time in his laboratory. Next, I would like to thank my committee members at the University of Pittsburgh – Dr. Anne-Marie Oswald, Dr. Elias Aizenman, Dr. Yan Dong, and Dr. Stephen Meriney – for their valuable discussions and guidance throughout my research. I would also like to thank Dr. Laurence Trussell for his time and effort serving as the external examiner for my thesis defense.

I would like to thank all of the current and former members of the Tzounopoulos lab for all of their help, friendship, and support during my time in graduate school, especially Rebecca Krall and Amanda Henton. I would also like to thank Dr. Charles Anderson for his advice and training during my first few years in the lab.

Last but not least, I would like to thank my wife, Elise, and all of my family and friends for their support during my time in graduate school.

Funding: This work was supported by NIH grants F31-DC015924 (to Nathan W. Vogler) and R01-DC007905 (to Thanos Tzounopoulos).

1.0 Introduction

Zinc is found in all cells in the body, and is essential for life (Kambe, Tsuji, Hashimoto, & Itsumura, 2015; MacDonald, 2000). Zinc stabilizes proteins, DNA, and ribosomes, serves as a co-factor for many enzymes, and functions as an intra- and inter-cellular signal (MacDonald, 2000; Sensi et al., 2011; Vallee & Falchuk, 1993). In fact, genes that encode zinc-binding proteins account for up to 10% of the human genome (Andreini, Banci, Bertini, & Rosato, 2006; Blasie & Berg, 2002). However, while essential for proper cellular functioning, zinc is also involved in cell death signaling pathways, and excess intracellular zinc is toxic (Aizenman et al., 2000; Choi, Yokoyama, & Koh, 1988; Sensi et al., 2011; Sensi, Yin, Carriedo, Rao, & Weiss, 1999). As such, it is imperative that cellular zinc levels and signaling are tightly regulated. Intracellular zinc levels are maintained, in part, by metallothioneins. Metallothioneins are cysteine-rich zinc-binding proteins that buffer intracellular zinc by binding or releasing zinc when there is an excess or shortage of zinc in the cytoplasm (Krezel & Maret, 2008; Vallee, 1995). The other major regulatory mechanisms are the myriad of dedicated zinc transporter proteins, which transport zinc into or out of the cytoplasm. One family of zinc transporters, the Zrt, Irt-like protein (ZIP) family, composed of 14 members, transports zinc into the cytoplasm from the extracellular space or from zinc-containing organelles (Gaither & Eide, 2001; Kambe et al., 2015). The other family is the zinc transporter (ZnT) family, composed of 10 members, which transport zinc from the cytoplasm out of the cell or into cellular compartments, including endosomes or secretory vesicles (Cousins, Liuzzi, & Lichten, 2006; Kambe et al., 2015). Highlighting zinc's role as an intercellular signal, in the 1990s it was discovered that the zinc transporter ZnT3 loads zinc into synaptic vesicles in the central nervous system (Palmiter, Cole, Quaife, & Findley, 1996; Wenzel, Cole, Born,

Schwartzkroin, & Palmiter, 1997). This *synaptic zinc* is released from presynaptic nerve terminals, functioning as a neurotransmitter that modulates basic neurotransmission as well as synaptic plasticity (Frederickson, Koh, & Bush, 2005; McAllister & Dyck, 2017; Paoletti, Vergnano, Barbour, & Casado, 2009). Despite the critical roles of zinc in many cellular processes, for the purposes of this dissertation we will focus on ZnT3-dependent, synaptic zinc.

1.1 Synaptic zinc in the brain

The first evidence that zinc is released from neurons came from hippocampal slice preparations, where it was discovered that electrical stimulation or chemical depolarization with potassium led to increased zinc in the extracellular medium (Assaf & Chung, 1984; Howell, Welch, & Frederickson, 1984). The subsequent discovery of ZnT3 provided insight into the origin of synaptically released zinc – vesicles in presynaptic nerve terminals (Palmiter et al., 1996; Wenzel et al., 1997). In the brain, while most zinc is tightly bound to proteins, vesicular zinc comprises a pool of "free zinc" – zinc ions that are not protein-bound (Frederickson, 1989; Maret, 2014). Because this zinc is "free" or "chelatable," it can be visualized using histochemical procedures, such as silver-sulphide or zinc-selenium staining (Danscher, 1981, 1982; Danscher & Stoltenberg, 2005). These staining procedures revealed a striking anatomical distribution of zinc in the brain. Zinc-containing fibers are found throughout the telencephalon, predominantly in the hippocampus, neocortex, striatum, and amygdala. However, they are generally absent in the thalamus, midbrain, and brainstem (with the notable exception of the dorsal cochlear nucleus, see section 1.8) (Danscher & Stoltenberg, 2005; McAllister & Dyck, 2017). Within the neocortex, cortical layers I-III, V, and VI contain high levels of zinc; whereas, little is found in layer IV,

where thalamocortical projections terminate (R. Dyck, Beaulieu, & Cynader, 1993; Paoletti et al., 2009). After ZnT3 was identified, a knock-out mouse (ZnT3 KO) was generated which lacked ZnT3, and thus lacked vesicular zinc (Cole, Wenzel, Kafer, Schwartzkroin, & Palmiter, 1999). Anatomical studies using ZnT3 KO mice confirmed that the zinc identified via histochemical staining is indeed vesicular zinc, because zinc staining is absent in these mice (Cole et al., 1999). Moreover, experiments in hippocampal slices from ZnT3 KO mice showed no zinc release in response to synaptic stimulation, thus confirming the vesicular origin of activity-dependent zinc release (Qian & Noebels, 2005, 2006).

Vesicular (synaptic) zinc is found in a subset of nerve terminals that contain and release glutamate, the major excitatory neurotransmitter in the brain (Beaulieu, Dyck, & Cynader, 1992; Slomianka, 1992). In some brain regions, such as the striatum radiatum region of the hippocampus, it is estimated that up to ~50% of glutamatergic terminals also contain zinc (Sindreu, Varoqui, Erickson, & Perez-Clausell, 2003). As such, studies of synaptic zinc have largely focused on its effects on glutamatergic neurotransmission via modulation of glutamate receptors (Figure 1) (Nakashima & Dyck, 2009; Paoletti et al., 2009). It is important to note that zinc is also known to modulate many other types of neurotransmission, including GABAergic, glycinergic, and neurotrophic signaling (McAllister & Dyck, 2017). In addition, zinc activates a specific zinc-sensing metabotropic receptor, mZnR/GPR39, which modulates synaptic activity via modulation of the chloride transporter KCC2 as well as triggering endocannabinoid synthesis (Besser et al., 2009; Chorin et al., 2011; Perez-Rosello et al., 2013; Saadi et al., 2012). However, in this dissertation, we will focus on the effects of synaptic zinc on glutamate receptors.

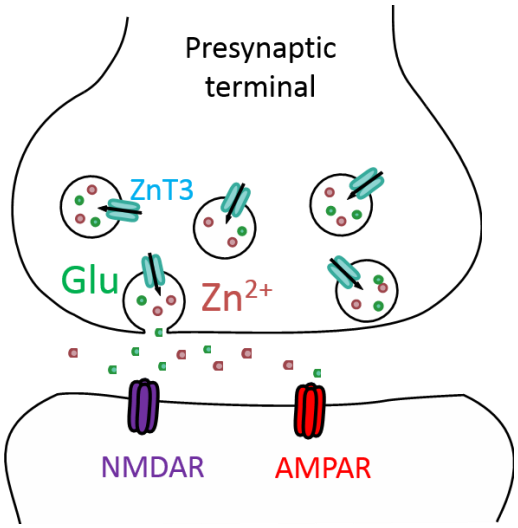

Figure 1: ZnT3-dependent synaptic zinc

Legend for Figure 1:

The zinc transporter ZnT3 loads zinc into presynaptic vesicles in a subset of glutamatergic nerve terminals. Synaptic zinc (Zn^{2+}) is co-released with glutamate (Glu), and modulates neurotransmission, including modulation of postsynaptic NMDA receptors (NMDARs) and AMPA receptors (AMPARs).

1.2 Intracellular zinc and ZnT3

Intracellular zinc is involved in cell death pathways and apoptosis (Frederickson et al., 2005). Zinc causes oxidative stress, triggers the production of reactive oxygen species from mitochondria, enhances potassium efflux via Src kinase and p38 MAPK, and causes caspase activation and cell death (Frederickson et al., 2005; McCord & Aizenman, 2014). As such, excess intracellular zinc is toxic (Aizenman et al., 2000; Choi et al., 1988; Sensi et al., 2011; Sensi et al.,

1999), and the levels of free intracellular zinc are tightly regulated. For proper cellular functioning, the concentration of free zinc in the cytosol is maintained in the picomolar range (Colvin, Holmes, Fontaine, & Maret, 2010). At the organismal level, proper zinc levels are maintained through a balance between zinc uptake (via dietary sources) and excretion. At the cellular level, the ZIP and ZnT transporters move zinc into or out of the cytoplasm, respectively (Kambe et al., 2015). The major mechanism by which cells buffer intracellular zinc is via metallothioneins. Each metallothionein (MT) protein can bind up to seven zinc ions, with different affinities for different MT isoforms ranging from picomolar to nanomolar (Krezel & Maret, 2008). Therefore, MTs buffer zinc over a range of concentrations and regulate the high-affinity zinc binding of other proteins (Krezel & Maret, 2008). The genes that encode MTs are regulated by intracellular zinc levels via the zinc-binding transcription factor MTF1, which is found in the cytoplasm but translocates into the nucleus upon zinc binding (Andrews, 2000). Thus, cells modulate the expression of MTs, and zinc buffering, in response to increased or decreased levels of intracellular zinc.

Regarding the concentration of zinc in presynaptic vesicles, the regulation of synaptic zinc is less understood. Interestingly, the metallothionein isoform MT-III is preferentially expressed synaptic zinc-containing neurons, and is thought to play a role in the loading of zinc into vesicles (Cole, Robbins, Wenzel, Schwartzkroin, & Palmiter, 2000; Knipp, Meloni, Roschitzki, & Vasak, 2005; Masters et al., 1994). The ZnT transporters (including ZnT3) load zinc into vesicles by functioning as a Zn^{2+}/H^{+} antiporter, exchanging zinc ions from the cytoplasm with protons in vesicles (Ohana et al., 2009). These findings suggest that cytosolic zinc levels may impact the concentration of zinc in vesicles.

The targeting of ZnT3 to synaptic vesicles is regulated by the adaptor protein 3 (AP-3) complex (Salazar, Love, Werner, et al., 2004). As such, mutant mice lacking AP-3, known as *mocha* mice, exhibit reduced ZnT3 expression and less vesicular zinc content (Kantheti et al., 1998; Stoltenberg, Nejsum, Larsen, & Danscher, 2004). Furthermore, ZnT3 interacts with the vesicular glutamate transporter 1 (VGlut1) and chloride channel 3, which are also targeted to vesicles by AP-3 (Salazar, Craige, Love, Kalman, & Faundez, 2005; Salazar, Love, Styers, et al., 2004). It has been shown in cultured glutamatergic neurons that the vesicular loading of glutamate and zinc influence each other – increased glutamate loading by VGlut1 increases the loading of zinc by ZnT3 (Salazar et al., 2005). Yet, not all glutamatergic vesicles also contain zinc, as ZnT3-containing vesicles form only a subset of vesicles in zinc-containing presynaptic terminals (Salazar, Love, Werner, et al., 2004). It has been shown that zinc-rich vesicles are preferentially released during higher levels of neuronal activity (Lavoie et al., 2011); however, little is understood regarding the distinct physiological properties of these presynaptic vesicle subpopulations. While the regulation of presynaptic zinc is relatively unknown, in the past few decades investigators have revealed considerable insight into the postsynaptic effects of synaptically released zinc on glutamate receptors.

1.3 Zinc-mediated modulation of NMDA receptors and synaptic plasticity

In the 1980s, it was discovered that application of zinc inhibits excitatory responses mediated by NMDA receptors (NMDARs) in cultured hippocampal neurons and cortical neurons (Peters, Koh, & Choi, 1987; Westbrook & Mayer, 1987). We now know that NMDARs contain a binding site for zinc on the N-terminal domain of the receptor, where zinc acts as an allosteric

inhibitor by reducing the channel opening probability (Paoletti, Ascher, & Neyton, 1997; Traynelis et al., 2010; Vergnano et al., 2014). Furthermore, the affinity of NMDARs for zinc depends on subunit composition. NMDARs are composed of two GluN1 subunits and two GluN2 subunits (Traynelis et al., 2010). GluN2A-containing NMDARs have nanomolar affinity for zinc; whereas, GluN2B-containing NMDARs have micromolar affinity (Hansen, Ogden, Yuan, & Traynelis, 2014; Paoletti et al., 1997; Rachline, Perin-Dureau, Le Goff, Neyton, & Paoletti, 2005; Tovar & Westbrook, 2012).

Exogenous application of micromolar concentrations of zinc inhibits NMDAR excitation in hippocampal mossy fiber and Schaffer collateral synapses, which contain synaptic zinc (Izumi, Auberson, & Zorumski, 2006; Vergnano et al., 2014; Vogt, Mellor, Tong, & Nicoll, 2000). In order to study the potential effects of endogenously released zinc on NMDARs, investigators used zinc chelators to bind and remove zinc from the synapse; however, these studies produced mixed results. For example, at hippocampal mossy fiber synapses, application of the zinc chelator CaEDTA potentiates NMDAR activity, and this effect is absent in ZnT3 KO mice, suggesting that endogenous zinc inhibits NMDARs (Molnar & Nadler, 2001; Vogt et al., 2000). However, others reported no effect of zinc chelation, using the zinc chelators CaEDTA or tricine, on NMDAR activity (in normal physiological Mg^{2+} concentrations), at hippocampal mossy fiber or Schaffer collateral synapses (Vergnano et al., 2014).

NMDARs are known to mediate multiple forms of synaptic plasticity (Malenka & Bear, 2004). Activity-dependent changes in synaptic activity result in increases (long-term potentiation, LTP) or decreases (long-term depression, LTD) in synaptic strength, long thought to be the neural

basis for learning and memory (Citri & Malenka, 2008; Malenka & Bear, 2004; Malenka & Nicoll, 1993). Because zinc inhibits NMDARs, there has been considerable interest in the potential role of zinc in modulating synaptic plasticity (McAllister & Dyck, 2017; Paoletti et al., 2009). However, similar to the results regarding endogenous zinc inhibition of NMDARs, studies on the role of zinc in hippocampal synaptic plasticity have yielded mixed results. At Schaffer collateral-CA1 synapses, which demonstrate LTP mediated by NMDARs, LTP induced by high-frequency stimulation is enhanced in mice that lack the high-affinity GluN2A zinc binding site (Vergnano et al., 2014). Furthermore, LTP induction is prevented when zinc is chelated with CaEDTA (Izumi et al., 2006). At mossy fiber synapses, which exhibit NMDAR-independent LTP, it was initially reported that CaEDTA has no effect on LTP, and LTP is normal in ZnT3 KO mice (Lavoie et al., 2011; Vogt et al., 2000). However, exogenous application of zinc inhibits mossy fiber LTP induction (Xie & Smart, 1994), and another study found that a higher concentration of CaEDTA prevents LTP induction (Li, Hough, Frederickson, & Sarvey, 2001). The effects of zinc on NMDAR-independent mossy fiber LTP are thought to be mediated by zinc-mediated activation of TrkB receptors (Huang, Pan, Xiong, & McNamara, 2008; Li et al., 2001; Pan et al., 2011).

Potentially explaining the conflicting results using zinc chelators, it is now known that the most commonly used extracellular zinc chelators, tricine and CaEDTA, are insufficient to prevent fast, high-affinity zinc binding (Anderson et al., 2015; Pan et al., 2011; Radford & Lippard, 2013). Therefore, these chelators may not adequately block fast zinc release during synaptic transmission and prevent binding to the nanomolar affinity site on GluN2A-containing NMDARs (Anderson et al., 2015; Pan et al., 2011). Fortunately, recent years saw the development of a new zinc chelator, ZX1, that is high affinity (K_d = 1 nM) and fast (rate constant = 0.027) (Anderson et al., 2015; Pan

et al., 2011; Radford & Lippard, 2013). Thus, ZX1 is more efficient than CaEDTA or tricine in blocking synaptic zinc transmission, and is the ideal zinc chelator for studying the effects of endogenous synaptic zinc signaling (Anderson et al., 2015).

Using ZX1, Anderson et al. showed that at zinc-containing glutamatergic synapses, synaptically released inhibits NMDARs closer to the synapse, whereas non-synaptic "tonic" zinc inhibits NMDARs further from the synapse (Anderson et al., 2015). Furthermore, the use of ZX1 clarified the role of synaptic zinc in mossy fiber LTP: Pan et al. showed that chelation of zinc with ZX1 prevents the induction of presynaptic NMDAR-independent mossy fiber LTP (Pan et al., 2011). However, ZX1 also unmasks a postsynaptic form of mossy fiber LTP in mutant mice that lack presynaptic LTP (Pan et al., 2011). Their findings suggest that synaptic zinc in mossy fibers both promotes presynaptic LTP and inhibits postsynaptic LTP, which may explain other observations that mossy fiber LTP appears normal in ZnT3 KO mice (Lavoie et al., 2011; Pan et al., 2011).

1.4 Zinc-mediated modulation of AMPA receptors

In addition to the inhibition of NMDARs, zinc has also been shown to modulate AMPA receptors (AMPARs), the major ionotropic glutamatergic receptor responsible for fast excitatory neurotransmission (Traynelis et al., 2010). However, unlike the known direct zinc binding of NMDARs, the mechanism of zinc-mediated AMPAR modulation is far less understood (McAllister & Dyck, 2017; Paoletti et al., 2009). Studies using exogenous application of zinc have yielded mixed results: low micromolar concentrations of zinc potentiate AMPAR responses, but

high micromolar and millimolar concentrations inhibit AMPAR responses (Blakemore & Trombley, 2004; Bresink, Ebert, Parsons, & Mutschler, 1996; Dreixler & Leonard, 1994; Rassendren, Lory, Pin, & Nargeot, 1990). It has recently been suggested that the potentiation of AMPARs by zinc is due to a zinc-mediated reduction of receptor desensitization, but the mechanism of zinc-mediated inhibition remains unknown (Blakemore & Trombley, 2019). Moreover, the effects of zinc may be subunit specific. AMPARs are composed of four subunits, GluA1-4 (Traynelis et al., 2010), and it has been suggested that zinc potentiates GluA3-containing receptors, but not GluA2-containing receptors (Dreixler & Leonard, 1994). However, the crystal structure of the GluA2 AMPAR subunit suggests the presence of zinc binding sites in the ligand-binding domain of the receptor (Armstrong & Gouaux, 2000). Thus, the mechanism of zinc-mediated AMPAR modulation has remained largely unknown.

Furthermore, because most previous studies used exogenous application of zinc to examine zinc modulation of AMPARs, it remained unknown whether endogenous synaptically released zinc could modulate AMPARs. Fortunately, the development of ZX1 enabled the demonstration that endogenous synaptic zinc inhibits AMPAR excitatory postsynaptic currents (EPSCs) at zinc-containing glutamatergic synapses (Kalappa, Anderson, Goldberg, Lippard, & Tzounopoulos, 2015). This is evidenced by the potentiation of AMPAR EPSCs upon application of ZX1, which is absent in ZnT3 KO mice (Kalappa et al., 2015). Importantly, this study demonstrates that in addition to inhibiting NMDARs and modulating synaptic plasticity, endogenous synaptic zinc is capable of modulating basic excitatory neurotransmission by AMPARs.

1.5 The role of synaptic zinc in sensory processing and behavior

Despite the known effects of zinc on modulating glutamatergic neurotransmission, and the prevalence of zinc in the neocortex and limbic brain areas, the potential impacts of synaptic zinc signaling on *in vivo* sensory processing and behavior were elusive until recently. When the ZnT3 KO mouse was first developed and characterized, these mice exhibited strikingly few abnormalities, performing normally in a barrage of behavioral and cognitive tasks (Cole, Martyanova, & Palmiter, 2001). These initial studies suggested that the loss of synaptic zinc largely does not impact cognition or behavior (Cole et al., 2001). Over time, however, further studies began to reveal subtler abnormalities in these mice. For example, it was found that ZnT3 KO mice exhibit impaired fear memory in response to tone/shock pairings, and impaired long-term memory when recognizing novel versus previously encountered objects (Martel, Hevi, Friebely, Baybutt, & Shumyatsky, 2010; Martel, Hevi, Kane-Goldsmith, & Shumyatsky, 2011). Moreover, ZnT3 KO mice exhibit mild deficits in spatial navigation and memory, and exacerbated age-related cognitive decline compared to wild-type controls (Adlard, Parncutt, Finkelstein, & Bush, 2010; Martel et al., 2011). More recently, it was demonstrated that male ZnT3 KO mice exhibit autism-like phenotypes, evidenced by reduced social interaction and increased repetitive behaviors (Yoo, Kim, Yoon, & Koh, 2016). Therefore, there is converging evidence that synaptic zinc may be more crucial for normal cognition and behavior than previously thought.

Consistent with this notion, several recent studies discovered that synaptic zinc contributes to normal sensory processing *in vivo*. Specifically, ZnT3 KO mice display a reduced ability to discriminate between textures using their whiskers, suggesting that synaptic zinc in the somatosensory cortex contributes to the integration of somatosensory information (Patrick Wu &

Dyck, 2018). Furthermore, studies in the auditory cortex of mice revealed the contribution of synaptic zinc to auditory processing, at both the behavioral and neuronal levels (Anderson, Kumar, Xiong, & Tzounopoulos, 2017; Kumar, Xiong, Tzounopoulos, & Anderson, 2019). These experiments utilized ZX1 to chelate zinc while measuring the sound-evoked activity of auditory cortical neurons in awake mice using two-photon calcium imaging. Strikingly, ZX1 reduces the responsiveness (gain) of auditory cortical principal neurons, and enhances the gain of interneurons (Anderson et al., 2017). Moreover, in similar experiments, ZX1 increases the range of frequencies to which auditory cortical neurons respond, suggesting a role of synaptic zinc in auditory frequency discrimination (Kumar et al., 2019). Consistent with these effects of zinc at the neuronal level, reduced frequency discrimination in a behavioral task was observed after infusion of ZX1 into the auditory cortex, and in ZnT3 KO mice (Kumar et al., 2019). Together, these studies position synaptic zinc as a major modulator of synaptic transmission as well as *in vivo* sensory processing.

1.6 Experience-dependent plasticity of synaptic zinc

Given the role of zinc in modulating neurotransmission, synaptic plasticity, and sensory processing, it is particularly intriguing that the levels of zinc in synaptic vesicles, and the distribution of zinc-containing synapses, undergo plasticity in response to changes in sensory experience. The experience-dependent plasticity of synaptic zinc has been shown in multiple brain areas (McAllister & Dyck, 2017; Nakashima & Dyck, 2009). In monkeys, monocular deprivation increases the levels of vesicular zinc in the primary visual cortex, indicated by increased zinc staining (R. H. Dyck, Chaudhuri, & Cynader, 2003). In rodents, changes in vesicular zinc are well documented in the somatosensory (barrel) cortex. The rodent somatosensory cortex is organized

into ‘barrels,’ where each barrel represents a whisker, and zinc staining of the mouse barrel cortex reveals this somatotopic organization (Czupryn & Skangiel-Kramska, 1997). Plucking or trimming a whisker increases zinc staining in the corresponding barrel (Brown & Dyck, 2002). Interestingly, the increase in vesicular zinc declines as the whisker regrows, suggesting that this plasticity is activity-dependent (Brown & Dyck, 2002). Whisker plucking also increases the proportion of excitatory synapses that contain zinc, suggesting that non-zinc-containing synapses can be converted to zinc-containing synapses (Nakashima & Dyck, 2010). Importantly, changes in vesicular zinc are bidirectional: whereas whisker plucking increases vesicular zinc, stimulation of a whisker decreases zinc staining in the corresponding barrel (Brown & Dyck, 2005).

The fact that vesicular zinc is bidirectionally modulated by experience places this “*synaptic zinc plasticity*” as a potential mechanism by which synapses in the central nervous system adapt to changing sensory environments and experience. Given the role of synaptic zinc in neurotransmission and normal sensory processing, zinc plasticity would have major impacts on neurotransmission, cellular signaling, and experience-dependent plasticity across the brain. Indeed, in the retina, damage to the optic nerve increases vesicular zinc levels, which in turn inhibit optic nerve regeneration and promote cell death (Li et al., 2017). The role of zinc in modulating auditory cortical gain suggests a potential contribution of zinc plasticity to pathological central gain adaptation, such as in tinnitus and hyperacusis after hearing loss (Anderson et al., 2017; Auerbach, Rodrigues, & Salvi, 2014). Moreover, pathological zinc signaling has been implicated in a variety of neurological disorders, highlighting the potential clinical implications of synaptic zinc plasticity.

1.7 Synaptic zinc signaling in neurological disorders

Alzheimer's disease is characterized by the accumulation of beta-amyloid (Aβ) plaques, and zinc contributes to Aβ formation and precipitation (Bush et al., 1994; Deshpande, Kawai, Metherate, Glabe, & Busciglio, 2009). Furthermore, ZnT3-dependent zinc released during synaptic activity contributes to the binding of Aβ in excitatory synapses (Deshpande et al., 2009). Zinc and ZnT3 protein are found in precipitated amyloid plaques, and in mouse models of Alzheimer's disease plaques are more abundant in vesicular zinc-rich cortical regions (Stoltenberg et al., 2007; L. H. Zhang et al., 2008). Alzheimer's patients exhibit a more pronounced decline in ZnT3 expression with age compared to healthy controls (Adlard et al., 2010; Olesen et al., 2016), and treatment with a zinc ionophore ameliorates age-related cognitive decline in mice (Adlard et al., 2015). Therefore, the evidence that synaptic zinc contributes to Alzheimer's disease suggests zinc signaling, and zinc plasticity, as potential targets for therapeutic interventions.

Synaptic zinc is also implicated in Autism Spectrum Disorder. As mentioned previously, ZnT3 KO mice exhibit autism-like social behaviors (Yoo et al., 2016). Moreover, treatment with a zinc ionophore rescues behavioral phenotypes in mouse models of autism (Lee et al., 2015). Prenatal zinc deficiency contributes to the development of autism, and zinc supplementation has been proposed as a potential therapeutic approach (S. Grabrucker et al., 2014; Hagmeyer, Sauer, & Grabrucker, 2018). The prevailing theory is that synaptic zinc release, and subsequent translocation of zinc into postsynaptic neurons, binds and stabilizes Shank postsynaptic scaffolding proteins, which are mutated and implicated in autism (A. M. Grabrucker, 2014).

In addition to the involvement of zinc in Alzheimer's disease and autism, polymorphisms in the ZnT3 gene are associated with increased risk of developing schizophrenia (Perez-Becerril, Morris, Mortimer, McKenna, & de Belleroche, 2016). This is especially interesting given the now known role of synaptic zinc in normal sensory processing (Anderson et al., 2017; Kumar et al., 2019; Patrick Wu & Dyck, 2018). Moreover, variants in the ZnT3 gene increase the risk of febrile seizures, and ZnT3 KO mice are more susceptible to seizures (Cole et al., 2000; Hildebrand et al., 2015). Therefore, there is converging evidence that pathological synaptic zinc signaling contributes to a wide variety of neurological disorders. Together these studies highlight the need to understand the cellular and synaptic mechanisms that modulate synaptic zinc levels and signaling. Elucidating these mechanisms will provide crucial insight into the functional role of synaptic zinc in normal neurotransmission and sensory processing, the molecular pathways that may lead to pathological zinc signaling when disrupted, and potential pharmacological targets for treating pathological zinc signaling in disease states.

1.8 Dissertation goal

Synaptic zinc contributes to neurotransmission, sensory processing, and cognition in both healthy and disease states, and synaptic zinc signaling is bidirectionally modulated. However, the mechanisms underlying synaptic zinc plasticity have remained unknown. In order to understand the functional role of the dynamic modulation of synaptic zinc, and how it contributes to synaptic plasticity in general, we must identify the underlying cellular and molecular mechanisms. The goal of this dissertation is to elucidate these previously unknown mechanisms.

1.9 The dorsal cochlear nucleus as a model for synaptic zinc plasticity

In order to investigate the mechanisms underlying synaptic zinc plasticity, we must first identify a model system amenable to experimental interrogation both *in vitro* and *in vivo*. To this end, we turn to the dorsal cochlear nucleus (DCN) (Figure 2).

1.9.1 The functional role of the dorsal cochlear nucleus

The DCN is an auditory brainstem nucleus that receives afferent input from auditory nerve fibers that relay acoustic information from the cochlea (Oertel & Young, 2004; Osen, 1970). The main output neurons of the DCN, fusiform cells, receive this auditory nerve input on their basal dendrites in the DCN deep layer, and also receive input from granule cells on their apical dendrites in the superficial molecular layer (Oertel & Young, 2004). Fusiform cells project to the inferior colliculus, thus relaying auditory information throughout the central auditory pathway (Oertel & Young, 2004). Granule cell terminals comprise the parallel fibers in the DCN molecular layer, and provide excitatory (glutamatergic) input to fusiform cells as well as cartwheel cells, which are glycinergic inhibitory interneurons in the molecular layer that provide feedforward inhibition of fusiform cells (Davis & Young, 1997; Roberts & Trussell, 2010; Rubio & Juiz, 1998; Waller, Godfrey, & Chen, 1996). Granule cells receive input from multimodal brain areas, including auditory, somatosensory, and vestibular regions (Ryugo, Haenggeli, & Doucet, 2003). Thus, the DCN is well-positioned to integrate acoustic signals (via the auditory nerve) with multimodal information (via the parallel fibers).

Based on the ability of the DCN to integrate auditory cues with somatosensory and vestibular information, the DCN is thought to be involved in sound localization (Oertel & Young, 2004). DCN lesions impair animals' ability to orient toward sound stimuli (May, 2000). Moreover, fusiform cells are tonotopically organized and detect features of sounds such as peaks and notches in sound spectra, which are important for sound localization (Oertel & Young, 2004). Furthermore, somatosensory stimuli, such as ear muscle movement, strongly activate DCN neurons (Oertel & Young, 2004). Recent research has suggested that somatosensory information conveyed via the parallel fibers enables the DCN to act as a filter to cancel self-generated sounds (Singla, Dempsey, Warren, Enikolopov, & Sawtell, 2017). Fusiform cells respond preferentially to external sounds rather than self-generated sounds, whereas cartwheel cells respond to non-auditory signals related to behavior (Singla et al., 2017).

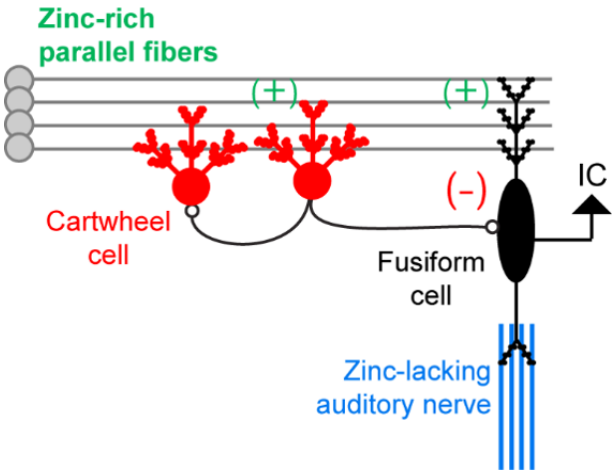

Figure 2: Dorsal cochlear nucleus circuitry

Legend for Figure 2:

Glutamatergic granule cell terminals comprise the synaptic zinc-rich parallel fibers, which excite cartwheel cells and fusiform cells. Glycinergic cartwheel cells provide feedforward inhibition of fusiform cells, which receive sensory input from the zinc-lacking auditory nerve and comprise the main output of the dorsal cochlear nucleus to the inferior colliculus (IC).

1.9.2 Zinc in the dorsal cochlear nucleus

While vesicular zinc is largely absent from most brainstem nuclei, a high concentration of zinc is found in the DCN parallel fibers (Danscher & Stoltenberg, 2005; Frederickson, Howell, Haigh, & Danscher, 1988; Rubio & Juiz, 1998). Interestingly, the zinc-containing parallel fibers exhibit bidirectional activity-dependent synaptic plasticity such as LTP and LTD; however, the zinc-lacking auditory nerve fibers do not exhibit such plasticity (Fujino & Oertel, 2003; Tzounopoulos, Kim, Oertel, & Trussell, 2004). Due to the circuit organization of the DCN (Figure 2), and specifically the segregation of parallel fibers and auditory nerve fibers in the molecular and

deep layers, respectively, parallel fiber activation can be isolated and studied *in vitro* using DCN brain slices (Fujino & Oertel, 2003; Oertel & Wu, 1989; Tzounopoulos et al., 2004).

At the synapses between parallel fibers and cartwheel cells, high-frequency stimulation of parallel fibers results in LTP of synaptic strength; whereas, low-frequency stimulation results in LTD (Fujino & Oertel, 2003). Parallel fibers also exhibit spike timing-dependent plasticity leading to LTP (via NMDAR activation) or LTD (via endocannabinoid signaling) (Tzounopoulos et al., 2004; Tzounopoulos, Rubio, Keen, & Trussell, 2007). Importantly, synaptic zinc signaling is known to modulate glutamatergic neurotransmission and plasticity in these synapses. Synaptic zinc recruits endocannabinoid signaling, by activation of the metabotropic zinc receptor GPR39, which subsequently modulates presynaptic glutamate release and short-term plasticity in response to trains of synaptic activation (Kalappa & Tzounopoulos, 2017; Perez-Rosello et al., 2013). Furthermore, synaptic zinc inhibits NMDARs and AMPARs in cartwheel cells, evidenced by the potentiation of NMDAR and AMPAR EPSCs upon application of the zinc chelator ZX1 (Anderson et al., 2015; Kalappa et al., 2015). The DCN slice preparation, and parallel fiber activation, is therefore proven to be a valuable tool for studying the role of synaptic zinc in glutamatergic neurotransmission.

Crucial for the study of synaptic zinc plasticity, vesicular zinc levels in DCN parallel fibers are modulated by auditory experience. Using an intracellular fluorescent zinc sensor, DA-ZP1, to track zinc levels in parallel fibers, Kalappa et al. showed that *in vivo* exposure to loud sound reduces vesicular zinc levels (Kalappa et al., 2015). This reduction is accompanied by reduced synaptic zinc release, as well as reduced potentiation of AMPAR EPSCs by ZX1 (Kalappa et al.,

2015). Together, these studies position the DCN parallel fibers as an ideal model system to study the mechanisms of synaptic zinc plasticity.

1.10 Dissertation overview

This dissertation examines the mechanisms underlying synaptic zinc plasticity in DCN parallel fibers, using electrophysiology, pharmacology, and fluorescent imaging. We utilize recently developed tools, such as ZX1 and the fluorescent zinc sensor DA-ZP1, to study these mechanisms. While experience-dependent reductions in vesicular zinc have been shown after sound exposure (Kalappa et al., 2015), it has remained unknown whether synaptic zinc plasticity can be induced *in vitro* in response to parallel fiber activation. We demonstrate activity-dependent bidirectional synaptic zinc plasticity in parallel fiber synapses: high-frequency stimulation reduces synaptic zinc signaling, and low-frequency stimulation increases synaptic zinc signaling. We reveal, for the first time to our knowledge, that synaptic zinc plasticity is mediated by Group 1 metabotropic glutamate receptors, both *in vitro* and *in vivo* in response to sound exposure (Chapter 1). Furthermore, we identify a role of postsynaptic calcium in the long-term depression of synaptic zinc signaling (Chapter 2). This novel plasticity mechanism may be a general mechanism underlying activity- and experience-dependent plasticity in zinc-containing synapses throughout the brain. Additionally, we characterize a novel photoactivatable fluorescent zinc sensor (Appendix A), paving the way for future studies.

2.0 Chapter 1: Bidirectional Long-Term Synaptic Zinc Plasticity at Mouse Glutamatergic Synapses

2.1 Overview

Synaptic zinc is co-released with glutamate to modulate neurotransmission in many excitatory synapses. In the auditory cortex, synaptic zinc modulates sound frequency tuning and enhances frequency discrimination acuity. In auditory, visual, and somatosensory circuits, sensory experience causes long-term changes in synaptic zinc levels and/or signaling, termed here *synaptic zinc plasticity*. However, the mechanisms underlying synaptic zinc plasticity and the effects of this plasticity on long-term glutamatergic plasticity remain unknown. To study these mechanisms, we used male and female mice and employed *in vitro* and *in vivo* models in zinc-rich, glutamatergic dorsal cochlear nucleus (DCN) parallel fiber (PF) synapses. High-frequency stimulation of DCN PF synapses induced long-term depression of synaptic zinc signaling (Z-LTD), as evidenced by reduced zinc-mediated inhibition of AMPA receptor (AMPAR) excitatory postsynaptic currents (EPSCs). Low-frequency stimulation induced long-term potentiation of synaptic zinc signaling (Z-LTP), as evidenced by enhanced zinc-mediated inhibition of AMPAR EPSCs. Thus, Z-LTD is a new mechanism of LTP and Z-LTD is a new mechanism of LTP. Pharmacological inhibition of Group 1 metabotropic glutamate receptors (G1 mGluRs) eliminated Z-LTD and Z-LTP. Pharmacological activation of G1 mGluRs induced Z-LTD and Z-LTP, associated with bidirectional changes in presynaptic zinc levels. Finally, exposure of mice to loud sound caused G1 mGluR-dependent Z-LTD in DCN PF synapses, consistent with our *in vitro* results. Together,

we show that G1 mGluR activation is necessary and sufficient for inducing bidirectional long-term synaptic zinc plasticity.

2.2 Introduction

In many brain areas, including the neocortex, limbic structures, and the auditory brainstem, glutamatergic vesicles are loaded with zinc (Danscher & Stoltenberg, 2005; Frederickson et al., 2005). This pool of mobile, synaptic zinc is co-released with glutamate. Synaptically released zinc inhibits synaptic and extrasynaptic NMDA receptor (NMDAR) EPSCs, and modulates AMPA receptor (AMPAR) EPSCs (Anderson et al., 2015; Kalappa et al., 2015; Kalappa & Tzounopoulos, 2017; Vergnano et al., 2014; Vogt et al., 2000). Namely, synaptic zinc inhibits AMPAR EPSCs during baseline synaptic activity via postsynaptic mechanisms, but enhances steady-state AMPAR EPSCs during higher frequencies of synaptic stimulation (Kalappa et al., 2015; Kalappa & Tzounopoulos, 2017). The enhancing effect of synaptic zinc on AMPAR EPSCs is short-lasting and is mediated by short-term, zinc-mediated changes in presynaptic glutamatergic neurotransmission (Kalappa & Tzounopoulos, 2017; Perez-Rosello et al., 2013). Thus, synaptic zinc is a major modulator of baseline neurotransmission and short-term plasticity of glutamatergic synapses.

In awake mice, synaptic zinc enhances the responsiveness (gain) of auditory cortical principal neurons to sound, but reduces the gain of cortical interneurons (Anderson et al., 2017). Furthermore, synaptic zinc sharpens the sound frequency tuning of auditory cortical principal neurons, and enhances frequency discrimination acuity (Kumar et al., 2019). Sensory experience

bidirectionally modulates the levels of vesicular zinc and synaptic zinc signaling in several sensory brain areas (Kalappa et al., 2015; Li et al., 2017; McAllister & Dyck, 2017; Nakashima & Dyck, 2009). In the somatosensory cortex, whisker plucking increases zinc levels, whereas whisker stimulation reduces zinc levels (Brown & Dyck, 2002, 2005). In the primary visual cortex, monocular deprivation increases vesicular zinc levels (R. H. Dyck et al., 2003). In the retina, optic nerve damage increases zinc levels, which in turn inhibit optic nerve regeneration and promote cell death (Li et al., 2017). In the dorsal cochlear nucleus (DCN), an auditory brainstem nucleus, exposure to loud sound reduces vesicular zinc levels and synaptic zinc signaling (Kalappa et al., 2015). Yet, the cellular and molecular mechanisms underlying the long-term experience-dependent plasticity of synaptic zinc signaling, termed here synaptic zinc plasticity, and the relationship of synaptic zinc plasticity to long-term glutamatergic synaptic plasticity remain unknown. Elucidating these mechanisms is crucial for understanding how the brain adapts during normal sensory processing, and why it fails to properly adjust in sensory disorders associated with pathological central adaptation, such as in tinnitus (Auerbach et al., 2014).

To determine the mechanisms of long-term synaptic zinc plasticity and its effects on LTP and LTD, we developed *in vitro* and *in vivo* models. Namely, we used electrophysiology, pharmacology, and fluorescent imaging in the DCN, which contains granule cell endings, parallel fibers (PFs), with high levels of synaptic zinc (Frederickson et al., 1988; Kalappa et al., 2015; Rubio & Juiz, 1998). We investigated these mechanisms *in vitro*, in response to electrical synaptic activation in brain slices, as well as *in vivo*, in response to loud sound exposure. Our results demonstrate that bidirectional activity-dependent synaptic zinc plasticity is a previously unknown,

Group 1 mGluR-dependent mechanism of LTP and LTD at zinc-containing glutamatergic synapses.

2.3 Results

2.3.1 Bidirectional activity-dependent long-term synaptic zinc plasticity requires Group 1 mGluR activation

To investigate the mechanisms underlying synaptic zinc plasticity, we first determined whether we could induce long-term synaptic zinc plasticity in DCN PF synapses in mouse brain slices. In these synapses, synaptic zinc inhibits AMPAR and NMDAR EPSCs via postsynaptic mechanisms. This has been evidenced by application of ZX1, a fast, high-affinity extracellular zinc chelator, which potentiates AMPAR and NMDAR EPSCs (Anderson et al., 2015; Kalappa et al., 2015; Kalappa & Tzounopoulos, 2017). This *ZX1 potentiation* of AMPA and NMDAR EPSCs is dependent on ZnT3, the transporter that loads zinc into synaptic vesicles (Cole et al., 1999; Palmiter et al., 1996). Moreover, reductions in ZX1 potentiation reflect reductions in synaptic zinc levels and release (Kalappa et al., 2015). Therefore, in this study, we used the amount of ZX1 potentiation of AMPAR and NMDAR EPSCs to monitor synaptic zinc signaling, and long-term synaptic zinc plasticity in DCN PF synapses.

Consistent with previous studies, we found that ZX1 potentiated postsynaptic PF AMPAR EPSCs in DCN cartwheel cells (CWCs), a class of inhibitory interneurons (Figure 3 A-B) (Kalappa et al., 2015; Kalappa & Tzounopoulos, 2017). We then tested whether we can induce long-term

synaptic zinc plasticity by using patterns of synaptic activation that induce long-term plasticity of glutamatergic synaptic strength in DCN PF synapses, such as LTP and LTD (Fujino & Oertel, 2003; Tzounopoulos et al., 2004; Tzounopoulos et al., 2007). We started by examining the effect of ZX1 on AMPAR EPSCs following high-frequency stimulation of PFs (HFS, 3 x 100 Hz for 1 sec, 10 sec inter-stimulus interval), which induces LTP (Fujino & Oertel, 2003). After applying HFS and inducing LTP (Figure 3 C), we renormalized AMPAR EPSC amplitude to quantify the amount of ZX1 potentiation (Figure 3 C). After HFS, ZX1 application did not potentiate AMPAR EPSCs (Figure 3 C, blue); whereas, ZX1 potentiated AMPAR EPSCs in control experiments without HFS (Figure 3 C, red). Furthermore, we analyzed the ZX1 potentiation (% increase from baseline) after HFS compared to control (without HFS), and observed a significant reduction in ZX1 potentiation after HFS (Figure 3 D). The loss of ZX1 potentiation indicates a loss of zinc-mediated inhibition of AMPARs, suggesting that HFS caused a long-term reduction in synaptic zinc signaling, termed *Z-LTD* (Figure 3 D). To confirm that the reduction of ZX1 potentiation is not due to a gradual decline in EPSC amplitude after HFS, we performed an additional control experiment where we delivered HFS but did not apply ZX1 (Figure 3 E). EPSC amplitude remained elevated and stable following HFS, over the duration of our recordings (Figure 3 E). This result supports that the reduced ZX1 potentiation after HFS (Figure 3 C, blue) cannot be explained by a gradual decline in EPSC amplitude after HFS, further supporting our conclusion that ZX1 does not potentiate AMPAR EPSCs after HFS, due to a reduction in zinc signaling. In Figure 3F, we show 3 example cells without renormalization after HFS, in which ZX1 was applied at the exact same time. These data show that ZX1 potentiates EPSCs in a control cell where no HFS was applied (Figure 3 F, red) but does not potentiate EPSCs in a cell that received HFS (Figure 3 F, blue; ZX1 was not applied in gray). However, to quantify the average effect of ZX1 after HFS, we

renormalized EPSCs to the baseline before ZX1 application, because not every cell reached a new stable baseline at the same time following HFS (~20-25 min after HFS), and thus ZX1 was not always applied at the exact same time. Taken together, these results suggest that Z-LTD, by reducing zinc-mediated inhibition of AMPAR EPSCs and thus enhancing baseline synaptic strength, is a new mechanism of HFS-induced LTP. For a discussion on the impact of synaptic zinc plasticity in the context of other long-term plasticity mechanisms, see *Discussion* section 2.4.3, *Implications of Z-LTP and Z-LTD for LTD and LTP*.

After establishing that HFS caused Z-LTD, we then studied the underlying mechanisms. NMDARs contribute to the induction of LTP and LTD in the DCN and most central synapses (Fujino & Oertel, 2003; Malenka & Nicoll, 1993; Tzounopoulos et al., 2004; Tzounopoulos et al., 2007). To test the role of NMDARs in the induction of Z-LTD, we blocked NMDARs with APV (NMDAR antagonist, 50 μM; Figure 4 A). Similar to the lack of ZX1 potentiation after HFS alone, ZX1 did not potentiate AMPAR EPSCs after HFS in the presence of APV (Figure 4 A, pink), indicating that NMDARs are not required for the induction of Z-LTD.

Parallel fiber synapses in the DCN also exhibit glutamatergic plasticity that involves metabotropic glutamate receptor (mGluR) signaling (Fujino & Oertel, 2003). Furthermore, Group 1 (G1) mGluRs are expressed in CWCs and in the DCN molecular layer, where PF terminals reside (Bilak & Morest, 1998; Wright, Blackstone, Huganir, & Ryugo, 1996). We therefore tested whether G1 mGluR activation is necessary for Z-LTD. To test this hypothesis, we repeated the experiment shown in Figure 4A, but we now blocked G1 mGluRs with LY367385 (100 μM, mGluR1-selective antagonist) and MPEP (4 μM, mGluR5-selective antagonist) (Figure 4 B).

Under these conditions, ZX1 potentiation was observed after HFS, indicating that LY367385/MPEP blocked HFS-induced Z-LTD (Figure 4 B-C, green). Furthermore, ZX1 potentiation after HFS with APV and LY367385/MPEP was not different compared to experiments where APV and LY367385/MPEP were applied but HFS was not delivered (Figure 4 B-C). Together, these results demonstrate that blockade of G1 mGluRs eliminated HFS-induced Z-LTD; therefore, G1 mGluR activation is necessary for Z-LTD induction.

Glutamatergic plasticity is bidirectional: synapses undergo LTP or LTD in response to high- or low-frequency stimulation, respectively (Fujino & Oertel, 2003; Malenka & Nicoll, 1993; Mulkey & Malenka, 1992). To determine whether long-term synaptic zinc plasticity is bidirectional, we tested whether low-frequency stimulation (LFS) increases zinc signaling (Figure 5 A). Because the induction of Z-LTD is NMDAR-independent and requires mGluR activation (Figure 4), we used an LFS stimulation protocol previously shown to favor mGluR-dependent synaptic plasticity (Oliet, Malenka, & Nicoll, 1997). Namely, we used LFS (5 Hz, 3 min), blockade of NMDARs with APV, and high extracellular concentrations of divalent ions (4 mM Ca^{2+} and Mg^{2+}) (Oliet et al., 1997). Compared to interleaved control experiments, LFS increased the amount of subsequent ZX1 potentiation (Figure 5 A, C). Increased ZX1 potentiation indicates increased zinc-mediated inhibition of AMPARs, suggesting that LFS caused a long-term increase in synaptic zinc signaling, termed *Z-LTP* (Figure 5 C). By enhancing zinc-mediated inhibition of AMPAR EPSCs, Z-LTP is a new mechanism of LFS-induced LTD. Note that LFS did not induce LTD, despite increasing synaptic zinc signaling (Figure 5 A). This is consistent with previous studies using this LFS protocol when GABAergic signaling is blocked (Oliet et al., 1997), as done here (see *Materials and Methods* section 2.5.3). Moreover, this result suggests that LFS also induced

an LTP that counterbalances the LTD effect of Z-LTP (see *Discussion* section 2.4.3, *Implications of Z-LTP and Z-LTD for LTD and LTP*.

Note that control ZX1 potentiation in these conditions (Figure 5 A, C, red) was slightly less, albeit not significantly different (p=0.11, unpaired t test), than previous control experiments performed in ACSF with 2.4/1.3 mM of extracellular Ca^{2+}/Mg^{2+} (Figure 3 B). This is likely due to reduced neuronal excitability in higher divalent concentrations (Kalappa et al., 2015; Oliet et al., 1997). Together, these results show that LFS induced Z-LTP, thus demonstrating that activity-dependent plasticity of zinc signaling is bidirectional: HFS induces long-term depression of zinc signaling (Z-LTD), whereas LFS induces long-term potentiation of zinc signaling (Z-LTP).

We next tested whether G1 mGluR activation is necessary for the induction of Z-LTP. After delivering LFS in the presence of LY367385/MPEP, ZX1 potentiation was reduced compared to LFS alone (Figure 5 B-C, green), and was similar to ZX1 potentiation in control experiments where LY367385/MPEP were applied but LFS was not delivered (Figure 5 B-C, red). This result indicates that LY367385/MPEP blocked LFS-induced Z-LTP. To confirm that the changes in ZX1 potentiation after LFS (or LFS with LY367385/MPEP) are not due to gradual changes in EPSC amplitude after LFS, we performed additional control experiments where we delivered either LFS alone or LFS with LY367385/MPEP, but did not apply ZX1 (Figure 5 D). In these experiments, EPSC amplitude remained stable following LFS, further supporting our conclusion that the observed changes in ZX1 potentiation after LFS are due to changes in zinc signaling. These results indicate that G1 mGluR activation is necessary for the induction of Z-

LTP. Together, these results reveal that activation of G1 mGluR signaling is necessary for both LFS-induced Z-LTP and HFS-induced Z-LTD.

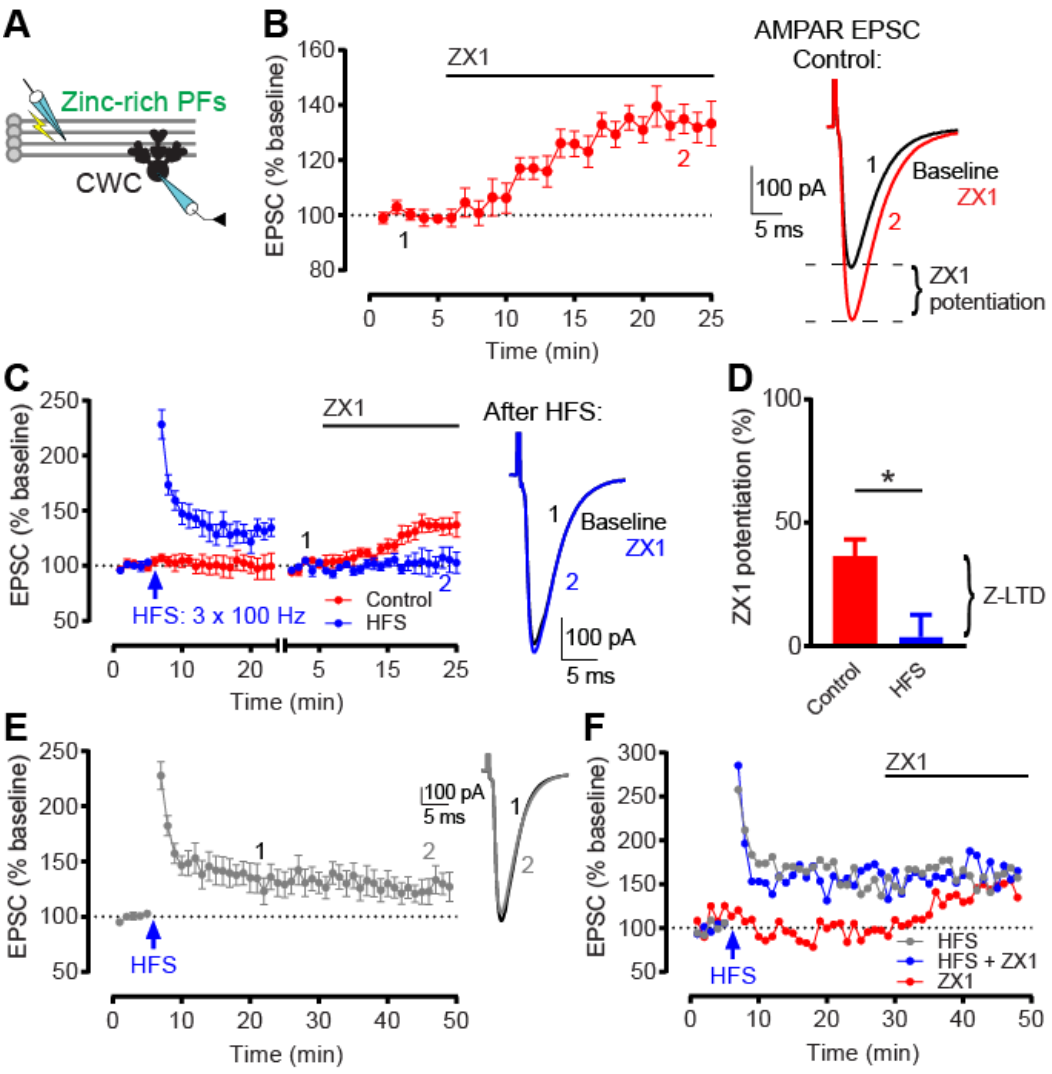

Figure 3: High-frequency stimulation (HFS) induces Z-LTD in DCN parallel fiber synapses

Legend for Figure 3:

(A) Schematic of experimental setup illustrating stimulation of zinc-rich glutamatergic DCN parallel fibers (PFs) and whole-cell recording of a postsynaptic cartwheel cell (CWC). **(B)** *Left*: Time course of AMPAR EPSC amplitude before and after ZX1 application, normalized to baseline before ZX1 application (100 μM). ZX1 significantly potentiated AMPAR EPSCs (n=10, *p=002, Wilcoxon matched-pairs signed rank test). *Right*: Example AMPAR EPSCs before and after ZX1 application, showing ZX1 potentiation. **(C)** *Left*: Time course of AMPAR EPSC amplitude before

and after HFS, and before and after subsequent ZX1 application (blue), and similar time course in control experiments (without HFS, red). After obtaining a stable baseline, HFS was delivered (3 x 100 Hz for 1 sec, 10 sec ISI). HFS induced LTP (n=7, *p=0.02, paired t test). To examine ZX1 potentiation after HFS, after obtaining a stable baseline after HFS, AMPAR EPSC amplitude was renormalized to the new baseline before ZX1 application. The renormalization is indicated by a gap and restart of timing in the x-axis. In control experiments (red), ZX1 potentiated EPSCs (n=6, *p=0.03, Wilcoxon matched-pairs signed rank test). After HFS (blue), ZX1 did not potentiate EPSCs (n=7, n.s. p=0.86, paired t test). *Right*: Example AMPAR EPSCs showing no ZX1 potentiation after HFS. **(D)** Average ZX1 potentiation (% increase from baseline) during the last 5 min of ZX1 application (mins. 21-25). 'Control' (n=6) vs. 'HFS' (n=7): *p=0.016, unpaired t test. The reduction in ZX1 potentiation is termed Z-LTD. **(E)** Time course of AMPAR EPSC amplitude before and after HFS, without subsequent ZX1 application. HFS induced LTP (n=8, *p=0.027, paired t test). After HFS, EPSCs remained stable for the duration of the recording (mins. 19-23 vs. mins. 45-49: n=5, n.s. p=0.12, paired t test). Example traces show AMPAR EPSCs from mins. 19-23 and mins. 45-49. **(F)** Example time courses from 3 individual cells, without renormalization, where ZX1 was applied at the exact same time. Blue: HFS was delivered and ZX1 was subsequently applied. Red: HFS was not delivered and ZX1 was applied. Gray: HFS was delivered but ZX1 was not applied. For all figures, values represent mean ± SEM. Star (*) indicates $p<0.05$. For detailed values and statistical tests for all Chapter 1 figures, see section 2.5.9 *Detailed values and statistical tests for Chapter 1 Figures*.

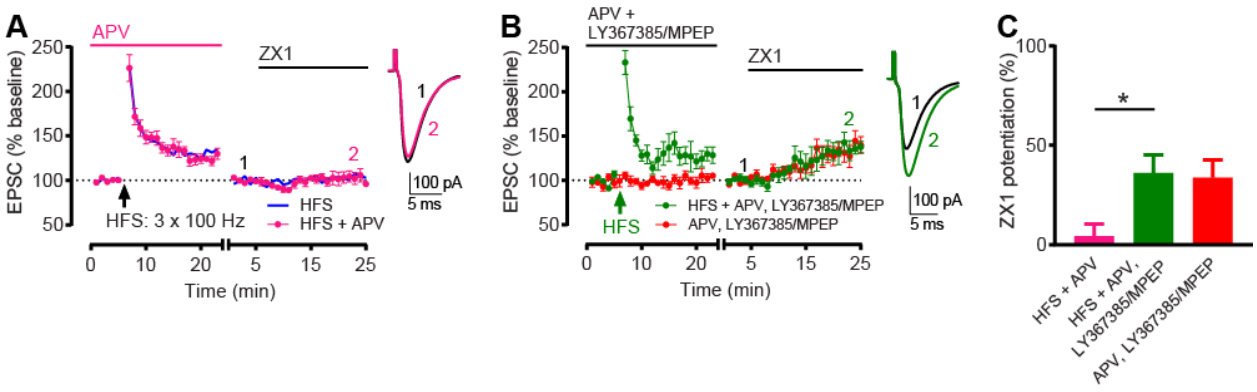

Figure 4: Group 1 mGluR activation is required for HFS-induced Z-LTD

Legend for Figure 4:

(A) Time course of AMPAR EPSC amplitude before and after HFS in the presence of APV (50 μM), and before and after subsequent ZX1 application (pink). HFS induced LTP (n=9, *p=0.001, paired t test). After HFS + APV, ZX1 did not potentiate EPSCs (n=9, n.s. p=0.82, Wilcoxon matched-pairs signed rank test). Blue line shows HFS time course replotted from **3 C**. The presence of APV during HFS did not affect the induction of Z-LTD. ZX1 potentiation (%) 'HFS' vs. 'HFS + APV': n.s. p=0.96, unpaired t test. **(B)** Similar time course as in **A** but with HFS in the presence of LY367385 (100 μM), MPEP (4 μM), and APV (50 μM) (green), compared to cells with LY367385, MPEP, and APV but without HFS (red). HFS induced LTP (n=6, *p=0.029, paired t test). After HFS + APV, LY367385/MPEP, ZX1 potentiated EPSCs (n=5, *p=0.02, paired t test. For **(A-B)**, to examine ZX1 potentiation after HFS, similar approach and renormalization as in **3 C** was performed. Example traces show AMPAR EPSCs before and after ZX1. **(C)** Average ZX1 potentiation (% increase from baseline) during the last 5 min of ZX1 application (mins. 21-25). 'HFS + APV, LY367385/MPEP' (n=5) increased ZX1 potentiation compared to 'HFS + APV' (n=9) (*p=0.0181), and was not different from 'APV, LY367385/MPEP' (n=5) (n.s. p>0.99). One-way ANOVA/Bonferroni. Values represent mean ± SEM. Star (*) indicates p<0.05.

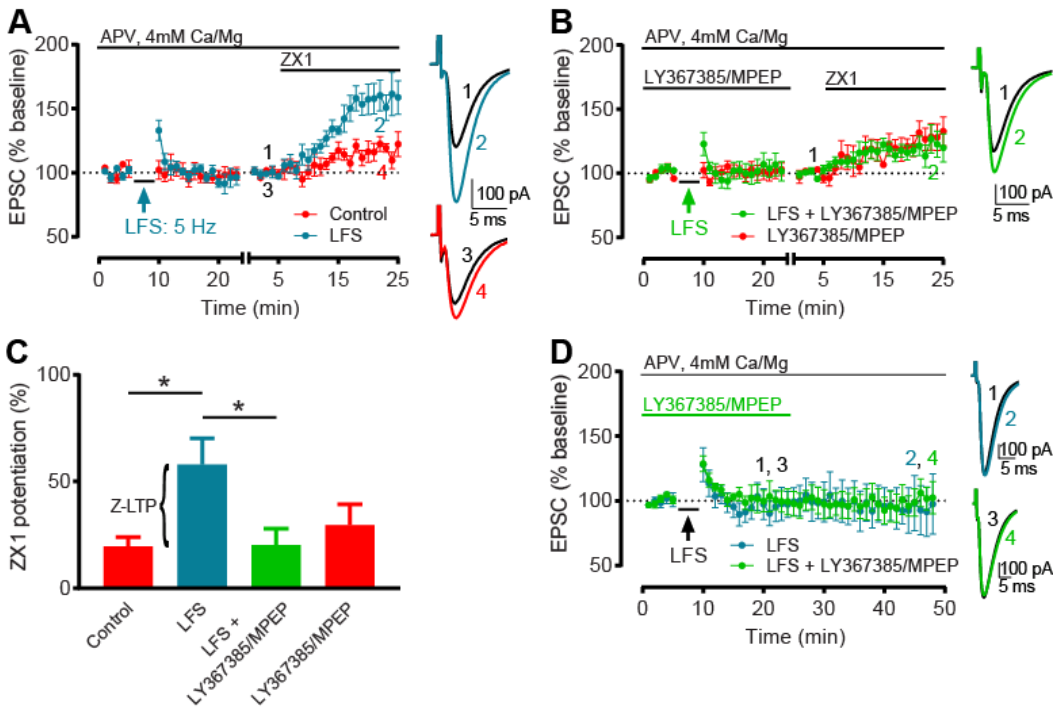

Figure 5: Low frequency stimulation (LFS) induces Z-LTP, which requires Group 1 mGluR activation

Legend for Figure 5:

(A) Time course of AMPAR EPSC amplitude before and after LFS (5 Hz, 3 min), and before and after subsequent ZX1 application (cyan); and similar time course in interleaved control experiments (without LFS, red). LFS did not induce LTD (n=8, n.s. p=0.22, paired t test). ZX1 potentiated EPSCs after LFS (n=6, *p=0.0025, paired t test) and in controls (n=5, *p=0.019, paired t test). **(B)** Similar time course as in **A** but with LFS in the presence of LY367385 (100 μM) and MPEP (4 μM) (green), compared to cells with LY367385 and MPEP but without LFS (red). LFS + LY367385/MPEP did not induce LTD (n=6, n.s. p=0.69, paired t test). ZX1 potentiated EPSCs after LFS (n=6, *p=0.02, paired t test) and without LFS (n=6, *p=0.015, paired t test). For **(A-B)**, to examine the ZX1 potentiation after LFS, similar approach and renormalization as in **3 C** was performed. Example traces show AMPAR EPSCs before and after ZX1. **(C)** Average ZX1

potentiation (% increase from baseline) during the last 5 min of ZX1 application (mins. 21-25). 'Control': n=5; 'LFS': n=6; 'LFS + LY367385/MPEP': n=6; 'LY367385/MPEP': n=6. LFS increased ZX1 potentiation compared to control (*p=0.03); this increase was blocked by LY367385 and MPEP (*p=0.027); and LFS + LY367385/MPEP was not different from LY367385/MPEP alone (n.s. p>0.99). One-way ANOVA/Bonferroni. The increase in ZX1 potentiation is termed Z-LTP. **(D)** Time course of AMPAR EPSC amplitude before and after LFS, with and without LY367385/MPEP. After LFS, EPSCs remained stable for the duration of the recording. 'LFS': n=4; mins. 19-23 vs. mins. 44-48: n.s. p=0.32, paired t test. 'LFS + LY367385/MPEP': n=4, mins. 19-23 vs. mins 44-48: n.s. p=0.87, Wilcoxon patched-pairs signed rank test. Example traces show AMPAR EPSCs from mins. 19-23 and mins. 44-48. Values represent mean ± SEM. Star (*) indicates p<0.05.

2.3.2 Group 1 mGluR activation is sufficient to induce bidirectional long-term synaptic zinc plasticity

Is activation of G1 mGluRs sufficient to induce Z-LTP and Z-LTD? Because G1 mGluRs are required for both increases and decreases in synaptic zinc signaling by different stimulation paradigms, we hypothesized that the direction of plasticity depends on the differential activation of G1 mGluRs during HFS and LFS. To test this, we applied high or low concentrations of DHPG (G1 mGluR agonist, 50 μM or 5 μM). Consistent with previous studies, application of 50 μM DHPG caused a significant depression of synaptic strength (Figure 6 A, cyan) (Huber, Roder, & Bear, 2001; Snyder et al., 2001; Wisniewski & Car, 2002). After applying 50 μM DHPG, obtaining a new stable baseline, and then applying ZX1, we observed that the ZX1 potentiation of EPSCs was significantly increased compared to control experiments (Figure 6 A-B). This result indicates

that 50 μM DHPG increases synaptic zinc signaling: G1 mGluR activation is sufficient to induce Z-LTP. Because Z-LTP and Z-LTD induced by LFS and HFS depend on G1 mGluR activation (Figures 4 and 5), we next tested whether application of a lower concentration of DHPG causes Z-LTD. After applying 5 μM DHPG and obtaining a new stable baseline, ZX1 did not potentiate EPSCs, consistent with Z-LTD induction (Figure 6 A-B, purple). To confirm that the changes in ZX1 potentiation after 50 μM or 5 μM DHPG are not due to changes in EPSC amplitude after DHPG (in the absence of ZX1), we performed additional control experiments where we applied 50 μM or 5 μM DHPG, but did not apply ZX1 (Figure 6 C). We found that after application of 50 μM DHPG, EPSCs remained depressed and stable for the duration of the recording (Figure 6 C, cyan), and after application of 5 μM DHPG, EPSCs remained stable for the duration of the recording (Figure 6 C, purple). These results further support our conclusions that the changes in ZX1 potentiation after 50 μM DHPG and 5 μM DHPG are due to increased and decreased zinc signaling, respectively. Together, these results demonstrate that G1 mGluR activation is sufficient to cause bidirectional zinc plasticity. Furthermore, the direction of zinc plasticity depends on the concentration of DHPG: 50 μM DHPG causes Z-LTP, whereas 5 μM DHPG causes Z-LTD (Figure 6 B). These results are consistent with the notion that bidirectional zinc plasticity depends on differential activation of G1 mGluRs by either LFS/HFS or high/low concentrations of DHPG.

Electrical synaptic stimulation with LFS/HFS or pharmacological activation of G1 mGluRs with high/low concentrations of DHPG induce bidirectional synaptic zinc plasticity; however, it is unknown whether these two different methods induce mechanistically similar synaptic zinc plasticity. To explore this, we compared the amount of Z-LTP elicited by applying sequential LFS and 50 μM DHPG to the amount of Z-LTP elicited by LFS or 50 μM DHPG alone. If electrical

and pharmacological manipulations induce Z-LTP by different mechanisms, then LFS and 50 μM DHPG application should yield an additive effect on Z-LTP, and subsequent ZX1 potentiation should be greater than that following LFS alone or application of 50 μM DHPG alone. To test this, we performed interleaved experiments to determine the effect of 50 μM DHPG alone, under the conditions used for LFS-induced Z-LTP as in Figure 5, with experiments involving stimulation with LFS and subsequent DHPG application (Figure 6 D-E). Under these conditions, ZX1 potentiation following application of 50 μM DHPG was similar to ZX1 potentiation following LFS (Figure 6 D, F). Importantly, ZX1 potentiation after sequential LFS and 50 μM DHPG was not significantly greater than ZX1 potentiation after LFS or DHPG alone (Figure 6 E-F). Together, these results show that LFS occluded the effect of 50 μM DHPG; thus, LFS and DHPG induce Z-LTP likely via a common mechanistic pathway.

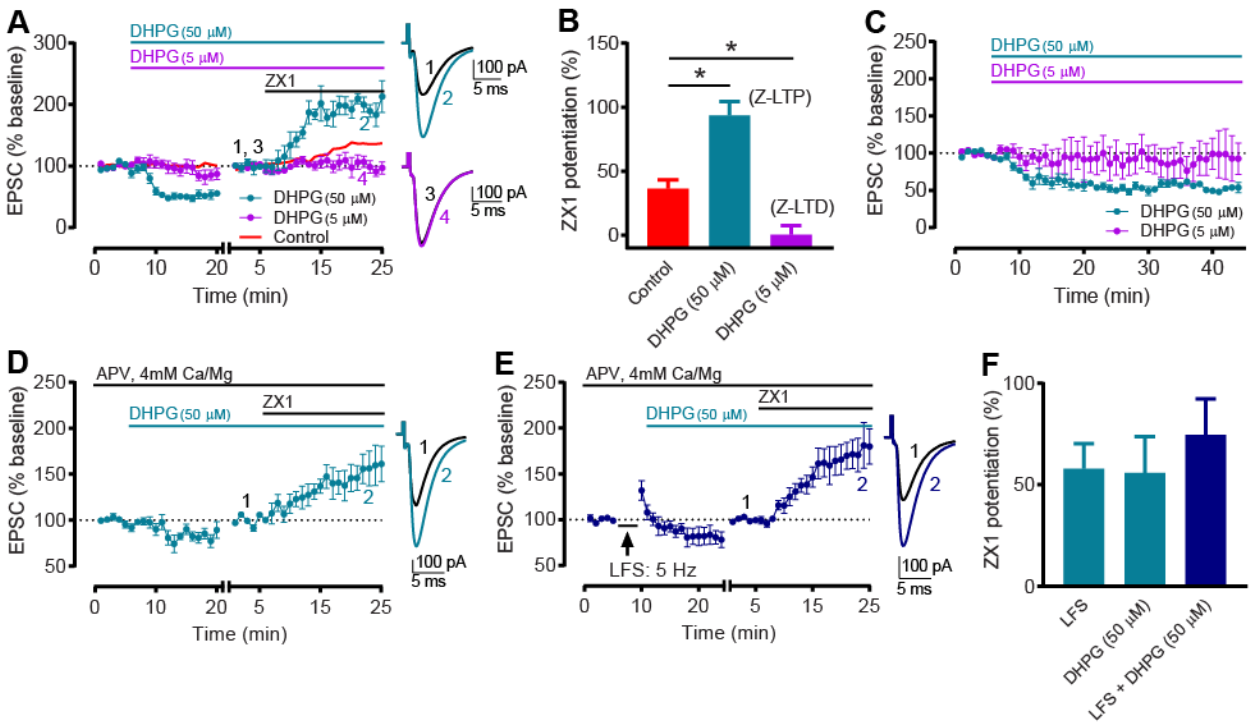

Figure 6: Group 1 mGluR activation is sufficient to induce Z-LTP and Z-LTD

Legend for Figure 6:

(A) Time course of AMPAR EPSC amplitude before and after application of 50 μM DHPG (cyan) or 5 μM DHPG (purple), and before and after subsequent ZX1 application. Red line shows Control time course replotted from **3 C**. 50 μM DHPG caused synaptic depression (n=6, *p=0.003, paired t test), and ZX1 potentiated EPSCs (n=5, *p=0.02, paired t test). 5 μM DHPG did not cause synaptic depression (n=6, n.s. p=0.14, paired t test), and ZX1 did not potentiate EPSCs (n=5, n.s. p=0.81, paired t test). To examine the ZX1 potentiation after DHPG application, after obtaining a stable baseline after DHPG, AMPAR EPSC amplitude was renormalized to the new baseline before ZX1 application. The renormalization is indicated by a gap and restart of timing in the x-axis. Example traces show AMPAR EPSCs before and after ZX1. **(B)** Average ZX1 potentiation (% increase from baseline) during the last 5 min of ZX1 application (mins. 21-25), compared to

Control from **3 C-D**. 'DHPG (50 μM)': n=5; 'DHPG (5 μM)': n=5. DHPG (50 μM) increased ZX1 potentiation compared to control (*p=0.0006), whereas DHPG (5 μM) reduced ZX1 potentiation compared to control (*p=0.029). One-way ANOVA/Bonferroni. Increased and decreased ZX1 potentiation correspond to Z-LTP and Z-LTD, respectively. **(C)** Time course of AMPAR EPSC amplitude before and after application of 50 μM DHPG (cyan) or 5 μM DHPG (purple). After 50 μM DHPG, EPSCs remained depressed and stable for the duration of the recording (mins. 16-20 vs. mins. 40-44: n=5, n.s. p=0.21, paired t test). After 5 μM DHPG, EPSCs remained stable for the duration of the recording (mins. 16-20 vs. mins 40-44: n=4, n.s. p=0.35, paired t test. **(D)** Similar time course as in **A** (cyan), but in same extracellular conditions as in **5 A-B**. 50 μM DHPG caused synaptic depression (n=5, *p=0.04, paired t test). ZX1 potentiated EPSCs (n=5, *p=0.026, paired t test). **(E)** Time course of AMPAR EPSC amplitude before and after sequential LFS (5 Hz, 3 min) and application of 50 μM DHPG, and before and after subsequent ZX1 application, in same conditions as in **D**. ZX1 potentiated EPSCs (n=5, *p=0.004, paired t test). For **(D-E)**, to examine the ZX1 potentiation, similar approach and renormalization as in **A** was performed. Example traces show AMPAR EPSCs before and after ZX1. **(F)** Average ZX1 potentiation (% increase from baseline) during the last 5 min of ZX1 application (mins. 21-25) for the experiments in **D-E**, with LFS data from **5 C**. 'DHPG (50 μM)': n=5; 'LFS + DHPG (50 μM)': n=5. Sequential LFS and DHPG (50 μM) did not increase ZX1 potentiation compared to LFS (n.s. p=0.92) or DHPG (50 μM) alone (n.s. p=0.855). One-way ANOVA/Bonferroni. Values represent mean ± SEM. Star (*) indicates $p<0.05$.

2.3.3 Group 1 mGluR activation modulates presynaptic zinc levels

We used activity-dependent changes in the amount of ZX1 potentiation of AMPAR EPSCs for assessing changes in synaptic zinc signaling (Z-LTP and Z-LTD). However, ZX1 potentiation is determined by the postsynaptic zinc-mediated inhibition of AMPAR EPSCs, as well as the amount of presynaptic zinc release (Kalappa et al., 2015). Because previous studies demonstrated sensory experience-dependent, long-term modulation of presynaptic zinc levels (Kalappa et al., 2015; Nakashima & Dyck, 2009), we hypothesized that Z-LTP and Z-LTD are expressed, at least in part, by the modulation of presynaptic zinc levels. To quantify potential changes in presynaptic zinc levels, we used DA-ZP1, a fluorescent intracellular zinc sensor capable of tracking presynaptic zinc levels in PF terminals (Kalappa et al., 2015; Zastrow et al., 2016). DA-ZP1 produces a band of fluorescence within the DCN molecular layer in wild type mice. This fluorescent signal is absent in mice lacking the vesicular ZnT3 transporter, thus demonstrating that the signal is due to ZnT3-dependent, synaptic zinc (Kalappa et al., 2015; Zastrow et al., 2016). To induce Z-LTP and Z-LTD, we applied DHPG, which is mechanistically similar to electrically-induced Z-LTP and Z-LTD (Figure 6 F) and capable of inducing robust synaptic zinc plasticity in many terminals in the slice. To test for changes in presynaptic zinc levels, we imaged DA-ZP1 fluorescence in the same region of the same DCN slice before and after DHPG application (50 μM or 5 μM) (Figure 7 A; see *Materials and Methods* section 2.5.4). Application of 50 μM DHPG increased DA-ZP1 fluorescence, indicating increased presynaptic zinc levels in PF terminals, which is consistent with Z-LTP (Figure 7 A, C). In contrast, application of 5 μM DHPG reduced DA-ZP1 fluorescence, indicating reduced zinc levels, which is consistent with Z-LTD (Figure 7 B-C).

Together, these results demonstrate that differential activation of G1 mGluRs, by application of different concentrations of DHPG, causes bidirectional modulation of presynaptic zinc levels. Furthermore, these results are consistent with our electrophysiological experiments: 50 μM DHPG results in Z-LTP by increasing presynaptic zinc levels, whereas 5 μM DHPG results in Z-LTD by reducing presynaptic zinc levels. Although these results do not rule out potential postsynaptic mechanisms of Z-LTP and Z-LTD, they demonstrate that Z-LTP and Z-LTD are associated with modulation of presynaptic zinc levels.

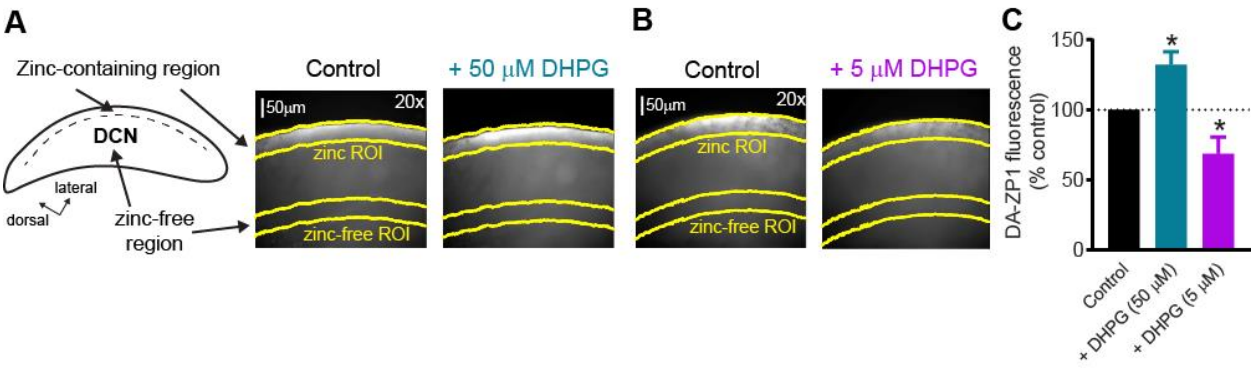

Figure 7: Group 1 mGluR activation bidirectionally modulates presynaptic zinc levels

Legend for Figure 7:

(A) *Left*: Schematic of the DCN, showing the presynaptic zinc-containing region near the ependymal surface, where parallel fiber terminals reside, and the zinc-free region. *Right*: 20x image of DA-ZP1 fluorescence, demonstrating the zinc-containing ROI (zinc ROI) and the zinc-free ROI, before and after application of 50 μM DHPG. **(B)** Same approach as in **A**, before and after application of 5 μM DHPG. **(C)** Average DA-ZP1 fluorescence after application of 50 μM or 5 μM DHPG, normalized to baseline fluorescence before DHPG application. 50 μM DHPG increased DA-ZP1 fluorescence (n=9, *p=0.0004, paired t test). 5 μM DHPG reduced DA-ZP1 fluorescence (n=8, *p=0.0078, Wilcoxon matched-pairs signed rank test). Values represent mean ± SEM. Star (*) indicates $p<0.05$.

2.3.4 G1 mGluR-dependent Z-LTD reduces zinc inhibition of NMDARs

Z-LTP and Z-LTD involve modulation of presynaptic zinc signaling (Figure 7). Based on this finding, the induction of long-term synaptic zinc plasticity should also affect postsynaptic NMDAR EPSCs, which are inhibited by zinc via direct high-affinity NMDAR allosteric modulation (Paoletti et al., 1997; Vergnano et al., 2014). To test this prediction, we quantified the ZX1 potentiation of NMDAR EPSCs after inducing Z-LTD with HFS. To monitor NMDAR EPSCs, we used a short train of presynaptic stimulation (5 pulses at 20 Hz) to activate extrasynaptic NMDARs, for NMDAR EPSCs recorded in somata of CWCs are mostly mediated by extrasynaptic NMDARs activated by glutamate spillover during this short train (Anderson et al., 2015). To avoid keeping CWCs at +40 mV for too long while recording NMDAR EPSCs, and to maintain the same induction protocol used in our previous experiments, we initially recorded AMPAR EPSCs at -70 mV and then applied HFS (Figure 8 A). Subsequently, we blocked AMPARs with DNQX (20 μM, AMPA/kainate receptor antagonist) and recorded at +40 mV to obtain a stable baseline of NMDAR EPSCs before applying ZX1 (Figure 8 A). Consistent with our results on AMPAR EPSCs, HFS significantly reduced ZX1 potentiation of NMDAR EPSCs (Figure 8 A-B, blue) compared to control experiments where HFS was not applied (Figure 8 A-B, red). These results demonstrate that Z-LTD reduces zinc-mediated inhibition of NMDARs. To determine whether this plasticity shares the same mechanism as Z-LTD evidenced by changes in the ZX1 potentiation of AMPAR EPSCs, we tested whether G1 mGluR activation is required. Indeed, after HFS in the presence of LY367385/MPEP, we observed ZX1 potentiation of NMDAR EPSCs (Figure 8 A-B, green), demonstrating that G1 mGluR activation is necessary for Z-LTD assessed by NMDAR EPSCs. Together, our results suggest that G1 mGluR-dependent synaptic zinc plasticity modulates zinc-mediated inhibition of AMPARs and NMDARs similarly,

suggesting that it is independent of the mode of action of synaptic zinc on its postsynaptic targets. This supports our findings that zinc plasticity is expressed, at least in part, by changes in presynaptic zinc levels.

However, the contribution of postsynaptic mechanisms in synaptic zinc plasticity cannot be excluded. To address this possibility, we tested whether activity-dependent changes in postsynaptic NMDAR subunit composition could modulate zinc sensitivity. NMDARs are composed of two GluN1 subunits and two GluN2 subunits (Traynelis et al., 2010). GluN2A-containing NMDARs (GluN1/GluN2A diheteromers and GluN2/GluN2A/GluN2B triheteromers) have nanomolar affinity for zinc, whereas GluN1/GluN2B diheteromers have micromolar affinity (Hansen et al., 2014; Paoletti et al., 1997; Rachline et al., 2005; Tovar & Westbrook, 2012). Therefore, the reduced zinc-mediated inhibition of NMDAR EPSCs after HFS, evidenced by reduced ZX1 potentiation (Figure 8 A-B), could be explained by an increase in the proportion of GluN2B subunits. We therefore tested whether HFS increases the sensitivity of NMDAR EPSCs to ifenprodil, a GluN2B-selective antagonist (Figure 8 C-D) (Hansen et al., 2014; Tovar & Westbrook, 2012). Compared to control experiments (without HFS), HFS did not affect the ifenprodil sensitivity (IC_{50}) of NMDAR EPSCs (Figure 8 C-D). This indicates that HFS-induced plasticity does not alter the proportions of GluN2B vs. GluN2A NMDAR subunits, suggesting that Z-LTD is not due to reduced zinc sensitivity caused by a decrease in the relative contribution of GluN2A vs. GluN2B in the NMDAR EPSC. Therefore, these results further support that zinc plasticity is expressed by changes in presynaptic zinc levels, rather than postsynaptic receptor modifications.

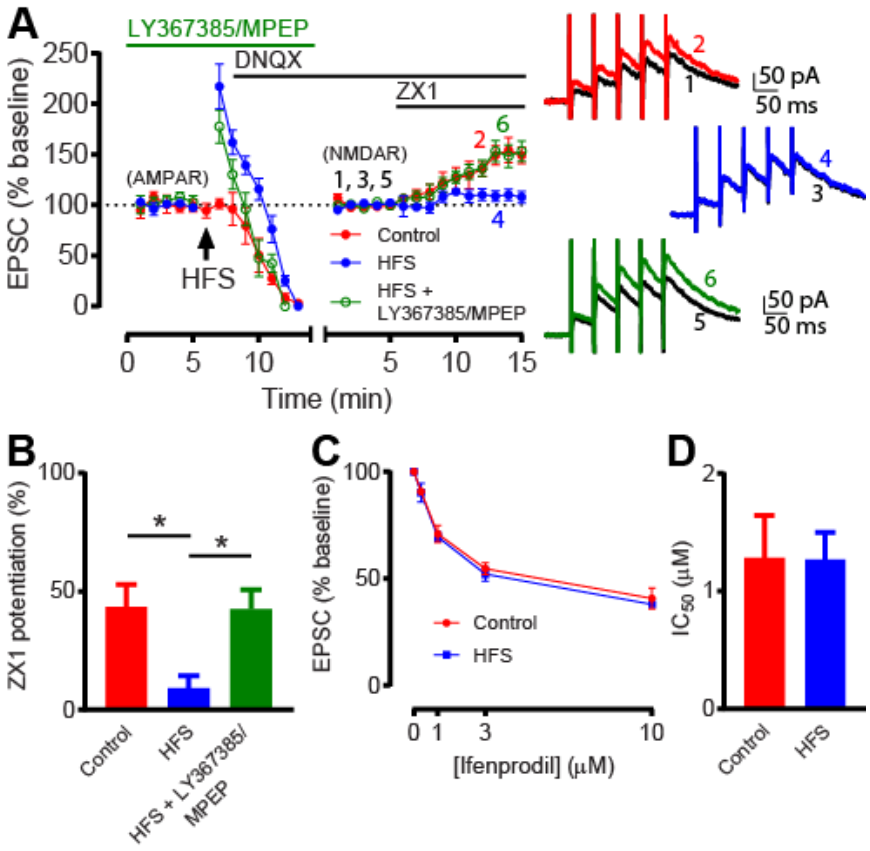

Figure 8: Group 1 mGluR-dependent Z-LTD reduces zinc inhibition of NMDARs

Legend for Figure 8:

(A) *Left*: Time course of AMPAR EPSC amplitude before and after HFS, and NMDAR EPSC amplitude before and after subsequent ZX1 application (blue); similar time course in control experiments (without HFS, red); and similar time course with HFS in the presence of LY367385 (100 μM) and MPEP (4 μM) (green). After obtaining a stable baseline of AMPAR EPSCs, HFS was delivered, then DNQX (20 μM) was applied. NMDAR EPSCs were then recorded at +40 mV, normalized to the baseline NMDAR EPSC amplitude before ZX1 application. The switch from AMPAR to NMDAR EPSC time course, and the renormalization of EPSC amplitude are indicated by a gap and restart of timing in the x-axis. In controls, ZX1 potentiated NMDAR EPSCs (n=5,

*p=0.027, paired t test). After HFS, ZX1 did not potentiate NMDAR EPSCs (n=6, n.s. p=0.16, paired t test). After HFS + LY367385/MPEP, ZX1 potentiated NMDAR EPSCs (n=5, *p=0.038, paired t test). *Right*: Example NMDAR EPSCs before and after ZX1 application. **(B)** Average ZX1 potentiation (% increase from baseline) during the last 5 min of ZX1 application (mins. 11-15). 'Control': n=5; 'HFS': n=6; 'HFS + LY367385, MPEP': n=5. HFS reduced ZX1 potentiation compared to control (*p=0.012); this reduction was blocked by LY367385 and MPEP (*p=0.015). One-way ANOVA/Bonferroni. **(C)** Dose-response of NMDAR EPSCs (% baseline) for increasing concentrations of ifenprodil, in controls (red) and after HFS (blue). 'Control': n=3-5 per concentration; 'HFS': n=3-4 per concentration. **(D)** IC_{50} of ifenprodil, from dose-responses in **C**. n.s. p=0.97, comparison of fits, extra sum-of-squares F test. Values represent mean ± SEM. Star (*) indicates $p<0.05$.

2.3.5 Sound-induced zinc plasticity requires Group 1 mGluRs *in vivo*

Our experiments described here, using *in vitro* brain slice electrophysiology in the DCN point toward a mechanism of bidirectional long-term synaptic zinc plasticity dependent on G1 mGluR activation. We therefore hypothesized that G1 mGluR activation may also be necessary for the reduction in synaptic zinc signaling observed in the DCN after exposure to loud sound (Kalappa et al., 2015). To test this hypothesis, we quantified the ZX1 potentiation of PF EPSCs in DCN slices from mice exposed to loud sound (116 dB, 4 hours). Consistent with sound-induced Z-LTD and previous studies (Kalappa et al., 2015), we did not observe ZX1 potentiation in slices from noise-exposed (N.E.) mice (Figure 9 A-B, gray). To test whether G1 mGluRs are necessary for the reduced zinc signaling in slices from N.E. mice, we administered a systemic, blood brain barrier-permeable G1 mGluR antagonist (AIDA, i.p., 2 mg/kg; twice: 30 min before and 1.5 hours

after beginning the noise exposure). Indeed, we observed ZX1 potentiation in slices from N.E. mice treated with AIDA (Figure 9 A-B, orange), suggesting that *in vivo* inhibition of G1 mGluR activity blocked the sound-induced Z-LTD.

Although AIDA treatment blocked Z-LTD in DCN PF synapses (Figure 9 A-B), it did not affect assays that are sensitive to presynaptic glutamate release probability, such as paired-pulse ratio (PPR) and coefficient of variation (CV) analysis (Figure 9 C). This indicates that sound-induced G1 mGluR-dependent Z-LTD specifically modulates synaptic zinc signaling, without affecting presynaptic glutamate signaling in PFs. Furthermore, AIDA treatment did not affect sound-induced hearing loss in N.E. mice, quantified with Auditory Brainstem Responses (ABRs) (Figure 9 D). ABRs reflect the synchronous activity, arising from the auditory nerve (Wave I), of auditory brainstem nuclei to the inferior colliculus (Waves II-V) in response to sound stimuli. Elevated ABR thresholds indicate increased hearing thresholds. However, similar ABR thresholds may be accompanied by differences in the suprathreshold response of Wave I, which could reflect differential degeneration of the auditory nerve (Kujawa & Liberman, 2009). AIDA treatment did not affect noise-induced changes in either ABR thresholds or Wave I amplitude (Figure 9 E), thus indicating that the effect of AIDA on blocking Z-LTD is not due to differential noise-induced hearing loss after AIDA treatment. Together, these results demonstrate that sound-induced Z-LTD requires G1 mGluR activation, consistent with our *in vitro* results.

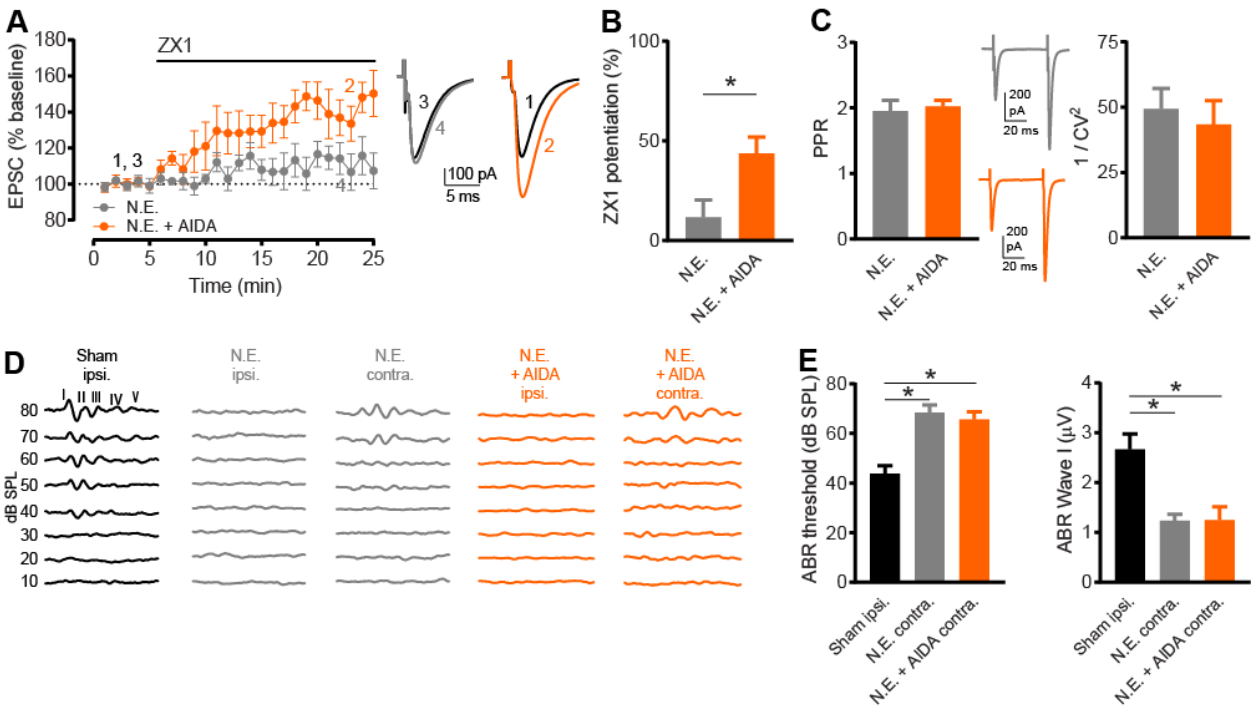

Figure 9: Sound-induced Z-LTD requires Group 1 mGluR activation

Legend for Figure 9:

(A) Time course of AMPAR EPSC amplitude before and after ZX1 application in slices from N.E. mice (gray) and N.E. AIDA-treated mice (orange). In N.E. mice, ZX1 did not potentiate EPSCs (n=5, n.s. p=0.23, paired t test). In N.E. AIDA-treated mice, ZX1 potentiated EPSCs (n=6, *p=0.005, paired t test). Example traces show AMPAR EPSCs before and after ZX1. **(B)** Average ZX1 potentiation (% increase from baseline) during the last 5 min of ZX1 application (mins. 21-25). 'N.E.' (n=5) vs. 'N.E. + AIDA' (n=6): *p=0.024, unpaired t test. **(C)** *Left*: Average paired-pulse ratio (PPR, pulse 2 / pulse 1) of baseline AMPAR EPSCs in slices from N.E. mice and N.E. AIDA-treated mice. 'N.E.' (n=6) vs. 'N.E. + AIDA' (n=8): n.s. p=0.70, unpaired t test. Example traces show AMPAR EPSCs in response to two pulses. *Right*: coefficient of variation (CV) analysis ($1/CV^2$) of baseline AMPAR EPSCs (pulse 1) in slices from N.E. mice and N.E. AIDA-treated mice. 'N.E.' (n=6) vs. 'N.E. + AIDA' (n=8): n.s. p=0.49, Mann Whitney test. **(D)** Example

Auditory Brainstem Responses (ABRs, 10-80 dB SPL sound stimuli) from sham-exposed mice (recorded from sham-exposed, ipsilateral ear, black), N.E. mice (gray), and N.E. AIDA-treated mice (orange). Because no ABRs were detected in the ipsilateral ears of N.E. mice, ABRs were measured from ears contralateral to noise exposure. **(E)** *Left*: Average ABR thresholds (dB SPL). 'Sham ipsi.': n=8; 'N.E. contra.': n=6; 'N.E. + AIDA contra.': n=7. N.E. increased ABR thresholds compared to sham-exposed (*p=0.0002), but AIDA and N.E. did not affect increases in ABR thresholds compared to N.E. alone, Kruskal-Wallis test/Dunn. *Right*: Average ABR Wave I amplitude (μV). 'Sham ipsi.': n=8; 'N.E. contra.': n=6; 'N.E. + AIDA contra.': n=7. N.E. decreased ABR Wave I amplitude compared to sham-exposed (*p=0.0024), but AIDA and N.E. did not affect decreases in ABR Wave I amplitude compared to N.E. alone, Kruskal-Wallis test/Dunn. Values represent mean ± SEM. Star (*) indicates $p<0.05$.

2.4 Discussion

Our results show that long-term synaptic zinc plasticity is an experience-, G1 mGluR-dependent mechanism that bidirectionally modulates synaptic zinc signaling in the DCN. Whereas the exact synaptic, natural, and ethologically relevant stimuli that elicit Z-LTP and Z-LTD remain unknown, here we developed *in vitro* and *in vivo* models for studying Z-LTP and Z-LTD. This is a crucial step towards further elucidation of the detailed natural stimuli eliciting long-term synaptic zinc plasticity, as well as the precise cellular and molecular mechanisms underlying the induction and expression of Z-LTP and Z-LTD.

2.4.1 Mechanisms of Group 1 mGluR-dependent Z-LTP and Z-LTD

Our results show that differential activation of G1 mGluRs, by either LFS/HFS or high/low concentrations of DHPG, determines the induction and direction of long-term synaptic zinc plasticity. Prolonged LFS causes Z-LTP, similarly to G1 mGluR activation with 50 μM DHPG; whereas, brief HFS causes Z-LTD, similarly to activation with 5 μM DHPG. Although the precise dynamics of mGluR activation during LFS and HFS are unknown, these results are consistent with the notion that prolonged LFS may lead to greater G1 mGluR activation than brief HFS.

Group 1 mGluRs, mGluR1 and mGluR5, are linked to the IP_3-Diacylglycerol (DAG) signaling pathway, leading to intracellular rises in Ca^{2+} from intracellular stores (Abdul-Ghani, Valiante, Carlen, & Pennefather, 1996; Conn & Pin, 1997; Kim, Lee, Lee, & Roche, 2008). In the hippocampus, LFS induces G1 mGluR-mediated LTD via postsynaptic AMPAR endocytosis involving Ca^{2+} release from endoplasmic reticulum (ER) stores and dendritic protein synthesis (Holbro, Grunditz, & Oertner, 2009; Huber, Kayser, & Bear, 2000; Luscher & Huber, 2010; Pick & Ziff, 2018). Moreover, in the hippocampus, HFS or theta-burst stimulation induces G1 mGluR-mediated LTP, also involving ER Ca^{2+} release, resulting in postsynaptic AMPAR/NMDAR trafficking or enhanced presynaptic glutamate release (Anwyl, 2009; Topolnik, Azzi, Morin, Kougioumoutzakis, & Lacaille, 2006; Wu, Harney, Rowan, & Anwyl, 2008). It remains unknown whether G1 mGluR-dependent Z-LTP and Z-LTD are downstream effects of the same signaling pathways that induce LTD and LTP, or occur through separate mechanisms. Nonetheless, we propose, albeit not tested here, that differential G1 mGluR activation by LFS/HFS leads to subsequent release of different amounts or types of intracellular Ca^{2+} signals. Different Ca^{2+}

signals may in turn activate diverse signaling pathways that ultimately lead to increased and decreased synaptic zinc signaling. An analogue that comes to mind is the mechanism via which differential activation of NMDARs, by various levels of synaptic activity, leads to variable Ca^{2+} levels and signaling, ultimately determining the induction of both LTP and LTD (Malenka & Bear, 2004).

Our results suggest that increases or decreases in synaptic zinc signaling, evidenced by increased or decreased ZX1 potentiation of EPSCs, are mediated by bidirectional modulation of vesicular zinc levels and subsequent synaptic zinc release. High or low concentrations of DHPG, which induce Z-LTP and Z-LTD, increase or decrease presynaptic zinc levels in PF terminals (Figure 7). Furthermore, synaptic zinc plasticity modulates zinc-mediated inhibition of NMDARs as well as AMPARs, and this effect on NMDARs cannot be explained by postsynaptic changes in the relative contributions of GluN2A vs. GluN2B subunits in the NMDAR EPSCs (Figure 8). Although we cannot fully exclude potential contributions of postsynaptic mechanisms in synaptic zinc plasticity, our results support that synaptic zinc plasticity is mainly mediated by activity-dependent modulation of presynaptic zinc levels and signaling, and are consistent with previous studies demonstrating experience-dependent modulation of vesicular zinc levels in the somatosensory cortex (Brown & Dyck, 2002, 2005), visual cortex (R. H. Dyck et al., 2003), optic nerve (Li et al., 2017), and the DCN (Kalappa et al., 2015).

Cartwheel cells express G1 mGluRs, particularly mGluR1, suggesting that the locus of induction of zinc plasticity is postsynaptic (Wright et al., 1996). Because Z-LTP and Z-LTD involve modulation of presynaptic zinc levels, one suggestion is the presence of a retrograde signal

from CWCs involved in the expression of Z-LTP and Z-LTD in PFs. Alternatively, the presence of mGluR1 on axon terminals in the DCN molecular layer may support a presynaptic locus of induction (Bilak & Morest, 1998). Because ZnT3 determines vesicular zinc levels (Cole et al., 1999; Palmiter et al., 1996), modulation of ZnT3 expression or function may underlie the expression of Z-LTP and Z-LTD. While our results reveal a role for G1 mGluRs in Z-LTP and Z-LTD, future experiments will be necessary to determine the detailed induction and expression mechanisms.

2.4.2 Implications of Z-LTP and Z-LTD for short-term plasticity

Previous studies in DCN PF synapses revealed that synaptic zinc triggers endocannabinoid synthesis, which inhibits presynaptic glutamate release and modulates short-term plasticity (Kalappa & Tzounopoulos, 2017; Perez-Rosello et al., 2013). During high-frequency (50 Hz) trains, synaptic zinc inhibits AMPAR EPSCs during the first few stimuli, but enhances steady-state EPSCs in subsequent stimuli by recruiting endocannabinoid signaling and enhancing synaptic facilitation (Kalappa & Tzounopoulos, 2017). Therefore, long-term increases in zinc signaling (Z-LTP) would enhance endocannabinoid activation during subsequent stimulus trains, increase synaptic facilitation, and further enhance steady-state EPSCs. Conversely, long-term decreases in zinc signaling, via Z-LTD, would reduce endocannabinoid activation, decrease synaptic facilitation, and suppress steady-state EPSCs.

Following stimulus trains, zinc-mediated endocannabinoid activation causes short-term depression and inhibits short-term facilitation (Perez-Rosello et al., 2013). Therefore, Z-LTP and Z-LTD are expected to shift the balance between short-term facilitation and short-term depression

in DCN synapses. Z-LTP will enhance subsequent zinc-mediated short-term depression, whereas Z-LTD will enhance short-term facilitation. Taken together, our results highlight a powerful mechanism by which long-term bidirectional zinc plasticity may modulate short-term glutamatergic synaptic plasticity.

2.4.3 Implications of Z-LTP and Z-LTD for LTD and LTP

In central synapses, including DCN PF synapses, the direction and size of LTP or LTD are determined by the combination of multiple simultaneous LTP and LTD mechanisms (Bender, Bender, Brasier, & Feldman, 2006; O'Connor, Wittenberg, & Wang, 2005; W. Shen, Flajolet, Greengard, & Surmeier, 2008; Tzounopoulos et al., 2007; Zhao & Tzounopoulos, 2011). In DCN PF synapses, LTP and LTD are influenced by the coactivation of pre- and postsynaptic signaling mechanisms including NMDARs, mGluRs, muscarinic acetylcholine receptors, and endocannabinoid signaling (Fujino & Oertel, 2003; Tzounopoulos et al., 2007; Zhao & Tzounopoulos, 2011). Therefore, bidirectional zinc plasticity likely acts together with these other known mechanisms to shape the size and direction of synaptic plasticity.

Several of our results are consistent with this notion. As shown in Figure 4, blockade of NMDARs did not block either HFS-induced LTP or Z-LTD. This indicates that NMDAR-independent LTP was induced, suggesting that Z-LTD contributes to NMDAR-independent LTP (Figure 4 A). G1 mGluR antagonists blocked HFS-induced Z-LTD (Figure 4 B). Therefore, the induced LTP under these conditions is NMDAR-, G1 mGluR-, and Z-LTD-independent. G1 mGluR activation with 5 µM DHPG induced Z-LTD, which reduces zinc-mediated inhibition of AMPAR EPSCs, but did not induce LTP (Figure 6 A, C). This suggests that 5 µM DHPG also

induced an LTD that counterbalances the LTP effect of Z-LTD. As shown in Figure 5 A, LFS induced Z-LTP, which enhances zinc-mediated inhibition of AMPAR EPSCs. However, LFS did not induce LTD (Figure 5 A), suggesting that LFS also induced an LTP that counterbalances the LTD effect of Z-LTP. This is consistent with previous studies showing that LTP and LTD mechanisms occur simultaneously in DCN PF synapses (Tzounopoulos et al., 2007). G1 mGluR activation with 50 µM DHPG induced LTD, as well as Z-LTP evidenced by increased synaptic zinc signaling (Figure 6 A-B) and increased zinc levels (Figure 7 A, C), suggesting that Z-LTP is associated with G1 mGluR-dependent LTD. Taken together, all these results are consistent with previous studies and further support the notion that LTP and LTD are the result of coactivation of different signaling pathways of long-term plasticity in the DCN (Fujino & Oertel, 2003; Tzounopoulos et al., 2007; Zhao & Tzounopoulos, 2011). Nevertheless, our results add Z-LTP and Z-LTD as new mechanisms of LTD and LTP at zinc-containing glutamatergic synapses.

In DCN PFs, mGluR activation contributes to both HFS-induced LTP and LFS-induced LTD (Fujino & Oertel, 2003). In response to HFS, Fujino & Oertel, 2003 showed mGluR- and NMDAR- independent LTP of an unknown mechanism (Fujino & Oertel, 2003), which is consistent with our findings on HFS-induced LTP in CWCs (Figure 4 B). However, Fujino & Oertel showed LFS-induced NMDAR-dependent LTD, whereas we did not observe LFS-induced LTD (Figure 5). This discrepancy could be explained by the use of different LFS induction protocols (5 Hz for 3 min here, vs. 1 Hz for 5 min paired with postsynaptic depolarization) and extracellular solutions (4/4 mM Ca^{2+}/Mg^{2+} here, vs. 2.4/1.3 mM Ca^{2+}/Mg^{2+}).

In addition to DCN PF synapses, we propose, although not tested here, that Z-LTP and Z-LTD may contribute to LTD and LTP in other synaptic zinc-containing brain areas which express G1 mGluR-dependent LTD and LTP, such as the hippocampus, amygdala, and striatum (Anwyl, 2009; Chen, Hu, Jiang, Potegal, & Li, 2017; Gubellini et al., 2003; Huber et al., 2000; Luscher & Huber, 2010; McAllister & Dyck, 2017; Oliet et al., 1997; Topolnik et al., 2006; Wu et al., 2008). In the hippocampus, LFS induces G1 mGluR-mediated LTD, whereas HFS induces LTP (Anwyl, 2009; Huber et al., 2000; Oliet et al., 1997; Topolnik et al., 2006; Wu et al., 2008). Therefore, LFS-induced Z-LTP would likely further enhance the effects of G1 mGluR-LTD, by increasing zinc inhibition of AMPARs; whereas HFS-induced Z-LTD would further enhance the effects of LTP, by reducing zinc inhibition of AMPARs. Thus, synaptic zinc plasticity likely serves as a positive feedback mechanism to enhance the effects of G1 mGluR-dependent LTP or LTD on glutamatergic synaptic transmission.

2.4.4 Implications of Z-LTP and Z-LTD for metaplasticity

Our results reveal that the induction of Z-LTP and Z-LTD is NMDAR-independent. However, zinc inhibits NMDARs and thus modulates the induction of NMDAR-dependent LTP and LTD in the hippocampus (Izumi et al., 2006; Takeda, Fuke, Ando, & Oku, 2009; Vergnano et al., 2014). As such, long-term synaptic zinc plasticity may contribute to ‘metaplasticity’, the modulation of subsequent LTP and LTD (Abraham & Tate, 1997). Z-LTD, by reducing the inhibitory effect of zinc on NMDARs, may promote subsequent NMDAR-dependent LTP and decrease subsequent NMDAR-dependent LTD. Conversely, Z-LTP, by enhancing the inhibitory effect of zinc on NMDARs, may promote subsequent NMDAR-LTD over NMDAR-LTP.

Therefore, zinc plasticity likely serves as a positive feedback mechanism for NMDAR-dependent metaplasticity.

Synaptic zinc contributes to mossy fiber presynaptic LTP in response to HFS, via activation of TrkB receptors (Huang et al., 2008; Pan et al., 2011). Therefore, if HFS induces Z-LTD in mossy fiber synapses, it would act as a negative feedback mechanism by reducing subsequent LTP induction. Taken together, we propose that the role of Z-LTD and Z-LTP in LTP and LTD depends on the specific mechanisms underlying LTP and LTD, but overall, Z-LTD and Z-LTP likely act as positive feedback mechanisms to enhance G1 mGluR-dependent LTP and LTD, and NMDAR-dependent metaplasticity.

2.4.5 Clinical and translational implications of zinc plasticity

In the context of zinc plasticity as a positive feedback signal for NMDAR-dependent metaplasticity, it is interesting that exposure to loud sound – known to induce tinnitus – causes Z-LTD in the DCN. Although not tested here, it is possible that Z-LTD could potentially lead to runaway excitation due to enhanced LTP and decreased LTD, and thus to pathological DCN hyperactivity associated with tinnitus (Tzounopoulos, 2008). Noise-induced pathological hyperexcitability through LTP/LTD-like mechanisms in the DCN PF synapses has been hypothesized and recently implicated in tinnitus treatment (Marks et al., 2018; Tzounopoulos, 2008), therefore suggesting that noise-induced reductions in synaptic zinc might contribute to tinnitus.

2.5 Materials and Methods

2.5.1 Animals and Ethical Approval

Male or female ICR mice (Envigo) were used in this study, aged between postnatal day 17 (P17) to P29. Mice had access to food and water *ad libitum*. All steps were taken to minimize animals' pain and suffering. All animal procedures were approved by the Institutional Animal Care and Use Committee of the University of Pittsburgh, Pittsburgh, PA.

2.5.2 Brain slice preparation

Mice were deeply anesthetized with isoflurane (3% in O_2), then immediately decapitated and their brains were removed. Brain slices were prepared in artificial cerebrospinal fluid (ACSF, 34°C) containing the following (in mM): 130 NaCl, 3 KCl, 1.2 $CaCl_2 \cdot 2H_2O$, 1.3 $MgCl_2 \cdot 6H_2O$, 20 $NaHCO_3$, 3 HEPES, and 10 D-Glucose, saturated with 95% O_2/5% CO_2 (vol/vol), pH = 7.25-7.35, ~300 mOsm. Using a Vibratome (VT1200S; Leica), coronal brain slices (210 μm thickness) containing the left dorsal cochlear nucleus (DCN) were cut, then placed in a chamber containing warm (34°C) ACSF, and incubated for 60 min at 34°C, then room temperature (no longer than 3 hours) before beginning electrophysiology experiments. Incubating ACSF was the same as cutting ACSF, except it was stirred with Chelex 100 resin (Bio-Rad) for 1 hour to remove contaminating zinc, then filtered using Nalgene rapid flow filters lined with polyethersulfone (0.2 μm pore size). After filtering, high purity $CaCl_2 \cdot 2H_2O$ and $MgCl_2 \cdot 6H_2O$ (99.995%; Sigma Aldrich) were added. All plastic and glassware used for these experiments were washed with 5% nitric acid.

2.5.3 Electrophysiology

Whole-cell recordings. DCN slices were transferred to the recording chamber and perfused with ACSF (1-2 mL/min), maintained at ~34°C using an inline heating system (Warner Instruments). Recording ACSF was the same as incubating ACSF (see above), except it contained 2.4 mM $CaCl_2 \cdot 2H_2O$. Whole-cell recordings from cartwheel cells were performed using glass micropipettes (3-6 MΩ; Sutter Instruments). Cartwheel cells were identified by the presence of complex spikes in cell-attached configuration before break-in or in response to current injections in current-clamp mode after break-in (Manis, Spirou, Wright, Paydar, & Ryugo, 1994; Tzounopoulos et al., 2004; S. Zhang & Oertel, 1993). Recording pipettes were filled with a potassium-based internal solution (except for Figure 8, see below) containing the following (in mM): 113 K-gluconate, 4.5 $MgCl_2.6H_2O$, 14 Tris-phosphocreatine, 9 HEPES, 0.1 EGTA, 4 Na_2ATP, 0.3 Tris-GTP, and 10 sucrose (pH = 7.25, 295 mOsm, junction potential -12 mV). For experiments shown in Figure 8 measuring NMDAR EPSCs, recordings were performed using a cesium-based internal solution containing the following (in mM): 128 $Cs(CH_3O_3S)$, 10 HEPES, 4 $MgCl_2 \cdot 6H_2O$, 4 Na_2ATP, 0.3 Tris-GTP, 10 Tris-phosphocreatine, 1 EGTA, 1 QX-314, and 3 Na-ascorbate (pH = 7.25, 300 mOsm, junction potential -9 mV). Voltages were not corrected for junction potentials. Recordings were performed using ephus (Suter et al., 2010) and a MultiClamp 700B amplifier (Axon Instruments). Data were sampled at 10 kHz and low-pass-filtered at 4 kHz. Series resistance (R_s, < 25 MΩ) was not compensated and was monitored during the recording period by delivering -5 mV voltage steps for 50 ms. R_s was calculated by dividing the -5 mV voltage step by the peak current generated immediately after the voltage step. Input resistance (R_m) was monitored and calculated by dividing the -5 mV voltage step by the difference between the baseline and steady-state hyperpolarized current, then subtracting R_s. Data were excluded if R_s or

R_m changed by more than 20% from the baseline period. EPSCs were evoked using an Isoflex stimulator (A.M.P.I., 0.1 ms pulses) through a glass ACSF-containing theta electrode to stimulate the zinc-rich parallel fibers. The average AMPAR EPSC amplitude during the initial baseline period was 376.5 ± 8.9 pA, which was approximately 50% of maximum EPSC amplitude. Cells were considered stable during the baseline period if the EPSC amplitude for every minute during the baseline period varied by <10% from the overall mean EPSC amplitude during the baseline period (Fujino & Oertel, 2003). After breaking into whole-cell configuration, the average time until the beginning of the baseline period was 9.1 ± 0.5 min. All EPSCs were recorded in the presence of SR95531 (20 μM, $GABA_AR$ antagonist) and strychnine (1 μM, GlyR antagonist). AMPAR EPSCs were recorded in voltage-clamp mode at -70 mV. For paired-pulse experiments, the inter-stimulus interval was 50 ms. NMDAR EPSCs were evoked by a 5-pulse stimulus train (20 Hz) (Anderson et al., 2015), recorded in voltage clamp mode at +40 mV, and in the presence of DNQX (20 μM, AMPA/kainate receptor antagonist). Zinc signaling was examined by applying ZX1 (100 μM), a fast, high-affinity extracellular zinc chelator (Anderson et al., 2015; Kalappa et al., 2015; Kalappa & Tzounopoulos, 2017; Pan et al., 2011). All drugs were always bath applied.

Induction of plasticity. High-frequency stimulation (HFS) consisted of 3 trains of 100 Hz pulses for 1 sec, with 10 sec between trains. Neurons were voltage-clamped at -70 mV during HFS. For experiments measuring NMDAR EPSCs after HFS (Figure 8), DNQX (20 μM) was added after HFS, then cells were voltage-clamped at +40 mV for the remainder of the experiment to record NMDAR EPSCs. For ifenprodil experiments (Figure 8 C-D), ZX1 was applied prior to ifenprodil to chelate extracellular zinc, because zinc affects NMDAR ifenprodil sensitivity (Hansen et al., 2014). The time course of these experiments (Figure 8 C-D) was similar to the

experiments shown in Figure 8 A, except ZX1 was applied with DNQX, after the HFS. After obtaining a stable baseline of NMDAR EPSCs, ifenprodil (300 nM, 1 μM, 3 μM, or 10 μM) was applied, and EPSCs (% baseline) were measured 10 min after ifenprodil application. Low-frequency stimulation (LFS) consisted of 5 Hz pulses for 3 min. During LFS, cells were held at -80 mV in current-clamp mode (Oliet et al., 1997). To promote mGluR-mediated plasticity, all LFS experiments were performed in the presence of APV (50 μM, NMDAR antagonist), and with external ACSF containing 4 mM $CaCl_2 \cdot 2H_2O$ and 4 mM $MgCl_2 \cdot 6H_2O$ (Oliet et al., 1997). The interleaved experiments shown in Figure 6 D, examining the effect of 50 μM DHPG application, were also performed in these conditions. For normalized EPSCs (% baseline), EPSC amplitudes were normalized to the average EPSC amplitude during the 5 min baseline period before HFS/LFS, DHPG, ifenprodil, or ZX1 application. To quantify ZX1 potentiation after HFS/LFS or DHPG application, EPSC amplitudes were renormalized to the average EPSC amplitude of the new baseline period 5 min before ZX1 application. ZX1 potentiation (shown in bar graphs) was quantified as the percent increase in the average EPSC amplitude during the last 5 min of ZX1 application (min 11-15 in Figure 8 A, min 21-25 in all other figures) compared to the 5 min baseline period before ZX1 application.

2.5.4 Vesicular zinc imaging with DA-ZP1

After preparation and incubation of DCN slices (described above), slices were transferred to the imaging chamber and perfused with recirculating ACSF (2-3 mL/min) maintained at ~34°C. Imaging of presynaptic vesicular zinc levels in DCN parallel fibers was performed using DA-ZP1, a high-affinity, membrane permeable fluorescent zinc sensor (Zastrow et al., 2016). DA-ZP1 (0.5-1.0 μM) was added to the ACSF, and allowed to incubate for at least 20 min before imaging.

Images were acquired using an upright microscope (Olympus BX5) with epifluorescence optics through a 20x water immersion objective (Olympus). Green fluorescent signals were isolated using a Pinkel filter set (Semrock LF488/543/625-3X-A-000) in response to excitation by an ephus-driven blue LED (M470L2; Thorlabs), and images were acquired using a CCD camera (Retiga 2000R, QImaging). Images consisted of 20 frames captured at 0.067 Hz which were then averaged together and analyzed in MATLAB (Mathworks). The DCN molecular layer, which contains the vesicular zinc-rich parallel fibers, extends ~75 μm deep from the ependymal surface, while deeper layers lack vesicular zinc (zinc-free region) (Frederickson et al., 1988; Rubio & Juiz, 1998; Ryugo & Willard, 1985). Thus, DA-ZP1 produces a band of fluorescence within the molecular layer near the ependymal surface, consistent with the distribution of zinc-rich parallel fiber terminals (Frederickson et al., 1988; Kalappa et al., 2015; Zastrow et al., 2016). The DA-ZP1 fluorescence band is absent in ZnT3 KO mice lacking vesicular zinc, indicating that it specifically labels vesicular zinc (Kalappa et al., 2015; Zastrow et al., 2016). To control for slice-to-slice variability in the molecular layer volume, which in turn might lead to variability in DA-ZP1 brightness, we compared DA-ZP1 fluorescence in the same region of the same slice before and after DHPG application (Figure 7). DA-ZP1 fluorescence 15-20 min after DHPG application was normalized to baseline fluorescence before DHPG application, shown in Figure 7 C. To quantify DA-ZP1 fluorescence, we quantified two ROIs within each slice: one within the zinc-containing molecular layer (zinc ROI) and the other within the zinc-free region (zinc-free ROI) (Kalappa et al., 2015; Zastrow et al., 2016). Because the DCN molecular layer is curved along the ependymal surface, to define the zinc ROI, we used a MATLAB routine to automatically detect the abrupt increase in fluorescence intensity between the background and the ependymal surface of the slice. Then the zinc ROI was automatically selected to include 50 μm depth from the ependymal surface,

consistent with the extent of the zinc-containing parallel fiber terminals (Frederickson et al., 1988). The length of the ROI was 450 µm. The zinc-free ROI was identical to the zinc ROI, except located 200-250 µm from the border of the slice, within the zinc-free region (deep or fusiform cell layers) (Frederickson et al., 1988; Ryugo & Willard, 1985). Thus, all ROIs contained the same cross-sectional area. The automatically generated ROI borders are shown with yellow lines in Figure 7. Fluorescence intensity was averaged within each ROI, and the zinc-sensitive fluorescence was calculated by subtracting the zinc-free ROI fluorescence from the zinc ROI fluorescence.

2.5.5 Noise exposure

Noise exposure was performed based on previously published methods (Kalappa et al., 2015). Sham- or noise-exposed mice were anesthetized using 3% isoflurane during induction and 1-1.5% during maintenance. Noise-exposed mice were exposed for 4 hours to narrow bandpass noise at 116 dB sound pressure level (SPL), centered at 16 kHz with a 1.6 kHz bandwidth. Noise was presented unilaterally (left ear) through a pipette tip inserted into the left ear canal, with the other end attached to a calibrated speaker (CF-1; Tucker Davis Technologies). Insertion of the pipette tip into the ear canal did not produce a seal. Sham-exposed mice underwent an identical procedure except without any noise exposure. For mice given intraperitoneal injections of AIDA (2 mg/kg), one injection was given 30 min prior to exposure, and a second injection was given 2 hours later. After noise- or sham-exposure, ABRs were collected and mice recovered from anesthesia, then DCN slices were prepared (within 30 min after exposure).

2.5.6 ABRs

Auditory Brainstem Responses (ABRs) were measured based on previously published methods (Kalappa et al., 2015). ABRs were recorded immediately after noise- or sham-exposure. During ABR measurements, mice were anesthetized using 3% isoflurane during induction and 1-1.5% during maintenance. Mice were placed in a sound attenuating chamber and temperature was maintained at ~37°C using a heating pad. A subdermal electrode was placed at the vertex, the ground electrode placed ventral to the right pinna, and the reference electrode placed ventral to the left pinna (sham- or noise-exposed ear). In noise-exposed mice, because no ABRs were detected when recording from the exposed (ipsilateral) ear, we recorded ABRs from the non-exposed (contralateral) ear (Figure 9 D). For ABR measurements from contralateral ears of noise-exposed mice, the reference electrode was placed ventral to the right pinna (contralateral ear) and the ground electrode placed ventral to the left pinna. ABRs were detected in response to 1 ms click sound stimuli, presented through a pipette tip inserted into the ear canal, with the other end attached to the speaker (CF-1; Tucker Davis Technologies). ABRs were recorded in response to clicks presented in 10 dB steps, ranging from 0-80 dB SPL. 1 ms clicks were presented at a rate of 18.56/sec using System 3 software package from Tucker Davis Technologies, and ABRs were averaged 512 times and filtered using a 300-3,000 Hz bandpass filter. ABR threshold was defined as the lowest stimulus intensity which generated a reliable Wave 1 in the response waveform. Wave 1 amplitude was measured as the peak-to-trough amplitude of the first wave in the ABR waveform (latency ~2 ms), in response to 80 dB SPL clicks.

2.5.7 Drugs

All chemicals used for ACSF and internal solutions were purchased from Sigma-Aldrich. The following drugs were purchased from HelloBio: SR95531 hydrobromide, DL-AP5, DNQX disodium salt, ifenprodil, MPEP hydrochloride, LY367385, and (S)-3,5-Dihydroxyphenylglycine (DHPG). Strychnine hydrochloride was purchased from Abcam. (RS)-1-Aminoindan-1,5-dicarboxylic acid (AIDA) was purchased from Tocris. ZX1 was purchased from STREM Chemicals. DA-ZP1 was generously provided by Drs. Stephen Lippard and Jacob Goldberg.

2.5.8 Statistical Analysis

All data analysis was performed using Matlab (Mathworks), Excel (Microsoft), or Prism 7 (GraphPad). For statistical tests within groups, to determine whether HFS, LFS, DHPG, or ZX1 significantly changed EPSC amplitude we used paired t tests (for normally distributed data) or Wilcoxon matched-pairs signed rank tests (for non-normally distributed data). Data were considered normally distributed if they passed the Shapiro-Wilk normality test. For paired tests, we compared the average EPSC amplitude (in pA) of the 5 min baseline period to the average EPSC amplitude (in pA) during a 5 min period after HFS, LFS, DHPG, or ZX1. The exact time points that were used for each test are stated in *Detailed values and statistical tests for Chapter 1 Figures*, section 2.5.9. To determine whether 50 µM or 5 µM DHPG changed DA-ZP1 fluorescence, we used paired t tests or Wilcoxon matched-pairs signed rank tests to compare the zinc-sensitive fluorescence (in arbitrary units) before DHPG application to the zinc-sensitive fluorescence (in arbitrary units) 15-20 min after DHPG application. For comparisons between groups, we used unpaired t tests (for normally distributed data) or Mann Whitney tests (for non-

normally distributed data). All statistical tests were two-tailed. For comparisons between three or more groups, we used ordinary one-way ANOVA with Bonferroni's multiple comparisons test (for normally distributed data), or Kruskal-Wallis test with Dunn's multiple comparisons test (for non-normally distributed data). IC_{50} was calculated using the Hill equation by fitting the dose-response curve with a nonlinear least squares fit. The IC_{50} of each fit was compared using the extra sum-of-squares F test. Significance levels are defined as $p < 0.05$. Group data are presented as mean ± SEM unless otherwise noted.

2.5.9 Detailed values and statistical tests for Chapter 1 Figures

Figure 3: **(3B)** Baseline (avg. of mins. 1-5) vs. ZX1 (avg. of mins. 21-25) (pA): n=10, *p=0.002, Wilcoxon matched-pairs signed rank test. **(3C)** 'HFS': baseline (avg. of mins. 1-5) vs. after HFS (avg. of mins. 19-23) (pA): n=7, t=3.074 df=6, *p=0.0218, paired t test; baseline vs. ZX1 (avg. of mins. 21-25) (pA): n=7, t=0.1837 df=6, n.s. p=0.8603, paired t test. 'Control': baseline vs. ZX1 (avg. of mins. 21-25) (pA): n=6, *p=0.0313, Wilcoxon matched-pairs signed rank test. **(3D)** ZX1 potentiation (%): 'Control': 36.45 ± 6.852%, n=6. 'HFS': 3.777 ± 8.838%, n=7. 'Control' vs. 'HFS': t=2.844 df=11, *p=0.016, unpaired t test. **(3E)** n=5-8: 3 cells did not remain stable for the entire time course and were included up to min 35. Baseline vs. mins. 30-49 (pA): n=8, t=2.796 df=7, *p=0.0267, paired t test. Mins. 19-23 vs. mins. 45-49 (pA): n=5, t=1.971 df=4, n.s. p=0.12, paired t test.

Figure 4: **(4A)** 'HFS+APV': baseline vs. after HFS+APV (mins. 19-23): n=9, t=4.949 df=8, *p=0.0011, paired t test. Baseline vs. ZX1 (mins. 21-25): n=9, n.s. p=0.8203, Wilcoxon matched-pairs signed rank test. ZX1 potentiation (%): 'HFS+APV' vs. 'HFS': t=0.04826 df=14,

n.s. p=0.9622. **(4B)** 'HFS + APV, LY367385/MPEP': baseline vs. after HFS + APV, LY367385/MPEP (mins. 19-23): n=6, t=3.022 df=5, *p=0.0293, paired t test. Baseline vs. ZX1 (mins. 21-25): n=5, t=3.669 df=4, *p=0.0214, paired t test. One cell was included for analysis of EPSCs following HFS, but did not remain stable throughout subsequent ZX1 application and was excluded from analysis following ZX1 application. 'APV, LY367385/MPEP': baseline vs. ZX1 (mins. 21-25): n=5, t=3.22 df=4, *p=0.0323, paired t test. **(4C)** ZX1 potentiation (%): 'HFS + APV': 4.28 ± 6.08%, n=9. 'HFS + APV, LY367385/MPEP': 36.07 ± 9.05%, n=5. 'APV, LY367385/MPEP': 33.76 ± 8.96%, n=5. One-way ANOVA: F= 6.048, *p=0.0111. 'HFS + APV' vs. 'HFS + APV, LY367385/MPEP': *p=0.0181; 'HFS + APV, LY367385/MPEP' vs. 'APV, LY367385/MPEP': n.s. p>0.9999; Bonferroni's multiple comparisons test.

Figure 5: **(5A)** 'LFS': Baseline vs. after LFS (mins. 19-23): n=8, t=1.344 df=7, n.s. p=0.2209, paired t test. Baseline vs. ZX1 (mins. 21-25): n=6, t=5.621 df=5, *p=0.0025, paired t test. Two cells were included for analysis of EPSCs following LFS, but did not remain stable throughout subsequent ZX1 application and were excluded from analysis following ZX1 application. 'Control': baseline vs. ZX1 (mins. 21-25): n=5, t=3.785 df=4, *p=0.0194, paired t test. **(5B)** 'LFS + LY367385/MPEP': baseline vs. after LFS (mins. 19-23): n=6, t=0.4227 df=5, n.s. p=0.6901, paired t test. Baseline vs. ZX1 (mins. 21-25): n=6, t=3.29 df=5, *p=0.0217, paired t test. 'LY367385/MPEP': Baseline vs. ZX1 (mins. 21-25): n=6, t=3.668 df=5, *p=0.0145, paired t test. **(5C)** ZX1 potentiation (%): 'Control': 19.65 ± 4.3%, n=5. 'LFS': 57.86 ± 12.4%, n=6. 'LFS + LY367385/MPEP': 20.19 ± 7.68%, n=6. 'LY367385/MPEP': 29.54 ± 9.73%, n=6. One-way ANOVA: F=3.737, *p=0.0289. 'Control' vs. 'LFS': *p=0.0334; 'LFS' vs. 'LFS + LY367385/MPEP': *p=0.0271; 'LFS + LY367385/MPEP' vs. 'LY367385/MPEP': n.s. p>0.999;

Bonferroni's multiple comparisons test. **(5D)** 'LFS': Mins. 19-23 vs. mins. 44-48: n=4, t=1.186 df=3, n.s. p=0.3211, paired t test. 'LFS + LY367385/MPEP': Mins. 19-23 vs. mins. 44-48: n=4, p=0.875, Wilcoxon matched-pairs signed rank test.

Figure 6: **(6A)** 'DHPG (50 μM)': Baseline vs. mins 16-20: n=6, t=5.438 df=5, *p=0.0029, paired t test. Baseline vs. ZX1 (mins. 21-25): n=5, t=3.717 df=4, *p=0.0205, paired t test. One cell was included for analysis of EPSCs following 50 μM DHPG, but did not remain stable throughout subsequent ZX1 application and was excluded from analysis following ZX1 application. 'DHPG (5 μM)': Baseline vs. mins. 16-20: n=6, t=1.736 df=5, n.s. p=0.1431, paired t test. Baseline vs. ZX1 (mins. 21-25): n=5, t=0.2619 df=4, n.s. p=0.8063, paired t test. One cell was included for analysis of EPSCs following 5 μM DHPG, but did not remain stable throughout subsequent ZX1 application and was excluded from analysis following ZX1 application. **(6B)** ZX1 potentiation (%): 'DHPG (50 μM)': 93.51 ± 10.92%, n=5. 'DHPG (5 μM)': 0.44 ± 7.08%, n=5. One-way ANOVA: F=23.19, *p<0.0001. 'Control' vs. 'DHPG (50 μM)': *p=0.0006; 'Control' vs. 'DHPG (5 μM)': *p=0.0285; Bonferroni's multiple comparisons test. **(6C)** 'DHPG (50 μM)': Mins. 16-20 vs. mins 40-44: n=5, t=1.499 df=4, n.s. p=0.2083, paired t test. 'DHPG (5 μM)': Mins. 16-20 vs. mins. 40-44: n=4, t=1.093 df=3, n.s. p=0.3544, paired t test. **(6D)** Baseline vs. mins. 16-20: n=5, t=2.923 df=4, *p=0.0431, paired t test. Baseline vs. ZX1 (mins. 21-25): n=5, t=3.462 df=4, *p=0.0258, paired t test. **(6E)** Baseline vs. mins. 20-24: n=5, t=2.086 df=4, n.s. p=0.1053, paired t test. Baseline vs. ZX1 (mins. 21-25): n=5, t=5.932 df=4, *p=0.004, paired t test. **(6F)** ZX1 potentiation (%): 'DHPG (50 μM)': 55.83 ± 17.9%, n=5. 'LFS + DHPG (50 μM)': 74.65 ± 17.6%, n=5. One-way ANOVA: F=0.4126, n.s. p=0.6703. 'LFS + DHPG (50 μM)' vs. 'LFS': n.s.

p=0.9181; ‘LFS + DHPG (50 μM)’ vs. ‘DHPG (50 μM)’: n.s. p=0.8553; Bonferroni's multiple comparisons test.

Figure 7: **(7C)** DA-ZP1 fluorescence (% control): ‘+ DHPG (50 μM)’: 132.3 ± 9.096%, n=9; before vs. after 50 μM DHPG (a.u.): t=5.924 df=8, *p=0.0004, paired t test. ‘+ DHPG (5 μM)’: 68.73 ± 11.99%, n=8; before vs. after 5 μM DHPG (a.u.): *p=0.0078, Wilcoxon matched-pairs signed rank test.

Figure 8: **(8A)** ‘Control’: baseline vs. ZX1 (mins. 11-15): n=5, t=3.398 df=4, *p=0.0273, paired t test. ‘HFS’: baseline vs. ZX1 (mins. 11-15): n=6, t=1.658 df=5, n.s. p=0.1583, paired t test. ‘HFS + LY367385/MPEP’: baseline vs. ZX1 (mins. 11-15): n=5, t=3.061 df=4, *p=0.0376, paired t test. **(8B)** ZX1 potentiation (%): ‘Control’: 43.5 ± 9.4%, n=5. ‘HFS’: 9.2 ± 5.2%, n=6. ‘HFS + LY267385/ MPEP’: 42.6 ± 8.2%, n=5. One-way ANOVA: F=7.115, *p=0.0082. ‘Control’ vs. ‘HFS’: *p=0.0123; ‘HFS’ vs. ‘HFS + LY367385, MPEP’: *p=0.0148; Bonferroni’s multiple comparisons test. **(8C)** EPSC (% baseline): ‘Control’: 300nM: n=3, 90.68 ± 1.051%; 1μM: n=5, 70.89 ± 3.943%; 3μM: n=5, 54.61 ± 2.791%; 10μM: n=3, 40.72 ± 4.845%. ‘HFS’: 300nM: n=3, 90.24 ± 4.327%; 1μM: n=4, 69.52 ± 2.208%; 3μM: n=4, 52.1 ± 3.214%; 10μM: n=3, 37.89 ± 1.533%. Nonlinear fits: ‘Control’: Hill Slope=1.095, R^2=0.9472. ‘HFS’: Hill Slope=1.128, R^2=0.9765. **(8D)** IC_{50} (μM): ‘Control’: 1.284 ± 0.3566. ‘HFS’: 1.267 ± 0.2321. Extra sum-of-squares F test: n.s. p=0.9687.

Figure 9: **(9A)** ‘N.E.’: baseline vs. ZX1 (mins. 21-25): n=5, t=1.419 df=4, n.s. p=0.2289, paired t test. ‘N.E. + AIDA’: n=6, t=4.775 df=5, *p=0.005, paired t test. **(9B)** ZX1 potentiation

(%): ‘N.E.’: 11.7 ± 8.56%, n=5. ‘N.E. + AIDA’: 43.8 ± 8.05%, n=6. ‘N.E.’ vs. ‘N.E. + AIDA’: t=2.724 df=9, *p=0.024, unpaired t test. **(9C)** PPR: ‘N.E.’: 1.954 ± 0.16, n=6. ‘N.E. + AIDA: 2.023 ± 0.09, n=8. ‘N.E.’ vs. ‘N.E. + AIDA’: t=0.3901 df=12, n.s. p=0.7033, unpaired t test. $1/CV^2$: ‘N.E.’: 49.35 ± 7.77, n=6. ‘N.E. + AIDA’: 43.42 ± 9.06, n=8. ‘N.E.’ vs. ‘N.E. + AIDA’: n.s. p=0.4908, Mann Whitney test. **(9E)** ABR threshold (dB SPL): ‘Sham ipsi.’: 43.75 ± 3.24, n=8. ‘N.E. contra.’: 68.33 ± 3.07, n=6. ‘N.E. + AIDA contra.’: 65.71 ± 2.97, n=7. Kruskal-Wallis test: *p=0.0002. ‘Sham ipsi.’ vs. ‘N.E. contra.’: *p=0.0042; ‘Sham ipsi.’ vs. ‘N.E. + AIDA contra.’: *p=0.0076; ‘N.E. contra.’ vs. ‘N.E. + AIDA contra.’: n.s. p>0.9999; Dunn's multiple comparisons test. ABR Wave I (μV): ‘Sham ipsi.’: 2.67 ± 0.31, n=8. ‘N.E. contra.’: 1.23 ± 0.13, n=6. ‘N.E. + AIDA contra.’: 1.25 ± 0.27, n=7. Kruskal-Wallis test: *p=0.0024. ‘Sham ipsi.’ vs. ‘N.E. contra.’: *p= 0.0387; ‘Sham ipsi.’ vs. ‘N.E. + AIDA contra.’: *p=0.0107; ‘N.E. contra.’ vs. ‘N.E. + AIDA contra.’: n.s. p>0.9999; Dunn's multiple comparisons test.

3.0 Chapter 2: The Role of Postsynaptic Calcium in Synaptic Zinc Plasticity

3.1 Overview

Synaptic zinc is co-released with glutamate in many excitatory synapses, and modulates neurotransmission and sensory perception. At zinc-containing synapses, the levels of presynaptic zinc, and consequent synaptic zinc signaling, undergo bidirectional plasticity in response to sensory experience and synaptic activity. We previously showed that synaptic zinc plasticity is mediated by Group 1 metabotropic glutamate receptors (mGluRs); however, the downstream mechanisms by which Group 1 mGluRs modulate presynaptic zinc signaling remain unknown. To study these mechanisms, we employed electrophysiology and fluorescent imaging in zinc-rich, glutamatergic dorsal cochlear nucleus (DCN) parallel fiber (PF) synapses. Long-term depression of synaptic zinc signaling (Z-LTD) requires a rise in postsynaptic Ca^{2+}. Furthermore, depletion of Ca^{2+} stores from the endoplasmic reticulum (ER) is sufficient to induce Z-LTD, and reduces presynaptic zinc levels. Together, these results demonstrate a role of postsynaptic Ca^{2+} via ER stores underlying Z-LTD, and suggest a role of retrograde signaling in synaptic zinc plasticity.

3.2 Introduction

In zinc-containing synapses, zinc released from presynaptic terminals inhibits NMDA receptor and AMPA receptor excitatory postsynaptic currents (EPSCs) (Anderson et al., 2015; Kalappa et al., 2015; Kalappa & Tzounopoulos, 2017; Vergnano et al., 2014; Vogt et al., 2000).

In the auditory cortex, synaptic zinc modulates neuronal response gain and frequency tuning (Anderson et al., 2017; Kumar et al., 2019). In many brain areas, including the neocortex, retina, and dorsal cochlear nucleus, sensory experience bidirectionally modulates the levels of vesicular zinc and synaptic zinc signaling (Kalappa et al., 2015; Li et al., 2017; McAllister & Dyck, 2017; Nakashima & Dyck, 2009). Thus, the plasticity of synaptic zinc levels and signaling, termed *synaptic zinc plasticity*, is a major plasticity mechanism that modulates neurotransmission and sensory processing. Until recently, the cellular and molecular mechanisms underlying synaptic zinc plasticity remained unknown. However, recent studies identified a novel role of Group 1 metabotropic glutamate receptors (G1 mGluRs) underlying bidirectional synaptic zinc plasticity (*Chapter 1*, section 2.3). G1 mGluR activation is necessary and sufficient for inducing bidirectional long-term synaptic zinc plasticity. Yet, the downstream mechanisms that link G1 mGluR activation to changes in presynaptic zinc signaling remain unknown. Elucidating these mechanisms is crucial for understanding the cellular and molecular signaling pathways that underlie the plasticity of zinc-containing synapses, and how the brain adapts in response to sensory experience. Furthermore, pathological neuronal zinc signaling is associated with many neuronal disorders, including schizophrenia, Alzheimer's disease, and autism (Adlard et al., 2010; A. M. Grabrucker, 2014; Lee et al., 2015; Olesen et al., 2016; Perez-Becerril et al., 2016; Yoo et al., 2016). Therefore, identifying the signaling pathways that modulate synaptic zinc may provide potential therapeutic targets for treating pathological zinc signaling in disease states.

To study the mechanisms of synaptic zinc plasticity, we employed established models in the dorsal cochlear nucleus (DCN) (*Chapter 1*), using electrophysiology, pharmacology, and fluorescent imaging. Our results demonstrate a role of postsynaptic Ca^{2+} via endoplasmic

reticulum (ER) stores underlying the long-term depression of synaptic zinc signaling, and suggest a role of retrograde signaling in synaptic zinc plasticity.

3.3 Results

3.3.1 Postsynaptic Ca^{2+} signaling is required for synaptic zinc plasticity

In DCN slices, parallel fiber (PF) synapses undergo bidirectional synaptic zinc plasticity in response to synaptic activity. Changes in synaptic zinc signaling are evidenced by changes in the potentiation of EPSCs by the high-affinity extracellular zinc chelator ZX1. Specifically, high-frequency stimulation (HFS) of PFs induces long-term depression of synaptic zinc signaling (Z-LTD), evidenced by the lack of ZX1 potentiation following HFS. Conversely, low-frequency stimulation (LFS) induces long-term potentiation of synaptic zinc signaling (Z-LTP), evidenced by increased ZX1 potentiation following LFS (*Chapter 1*, section 2.3). At the synapses between PFs and cartwheel cells (CWCs), activity-dependent synaptic zinc plasticity requires G1 mGluR activation (*Chapter 1*, section 2.3). However, it remains unknown whether the locus of induction of zinc plasticity is presynaptic or postsynaptic, since both presynaptic and postsynaptic G1 mGluRs are present in these synapses (Bilak & Morest, 1998; Wright et al., 1996). G1 mGluRs are linked to the IP3-Diacylglycerol (DAG) signaling pathway, leading to intracellular rises in Ca^{2+} (Abdul-Ghani et al., 1996; Conn & Pin, 1997; Kim et al., 2008). Therefore, we tested the hypothesis that postsynaptic G1 mGluR-mediated Ca^{2+} signaling underlies zinc plasticity, by inducing Z-LTD while blocking Ca^{2+} signaling in the postsynaptic CWC (Figure 10 A). We delivered HFS, and measured subsequent ZX1 potentiation of AMPAR EPSCs, with intracellular

recording solution containing BAPTA (calcium chelator, 10 mM) to prevent intracellular rises in Ca^{2+} in the postsynaptic CWC (Figure 10 A). After HFS with BAPTA-containing intracellular solution, ZX1 significantly potentiated AMPAR EPSCs (Figure 10 A). Furthermore, the ZX1 potentiation after HFS in the presence of BAPTA was not significantly different from ZX1 potentiation in cells recorded with BAPTA but where HFS was not delivered (Figure 10 B-C). Together, these results demonstrate that postsynaptic BAPTA blocked HFS-induced Z-LTD. Therefore, a postsynaptic rise in Ca^{2+} is necessary for Z-LTD, and these results suggest that the locus of induction of synaptic zinc plasticity is postsynaptic.

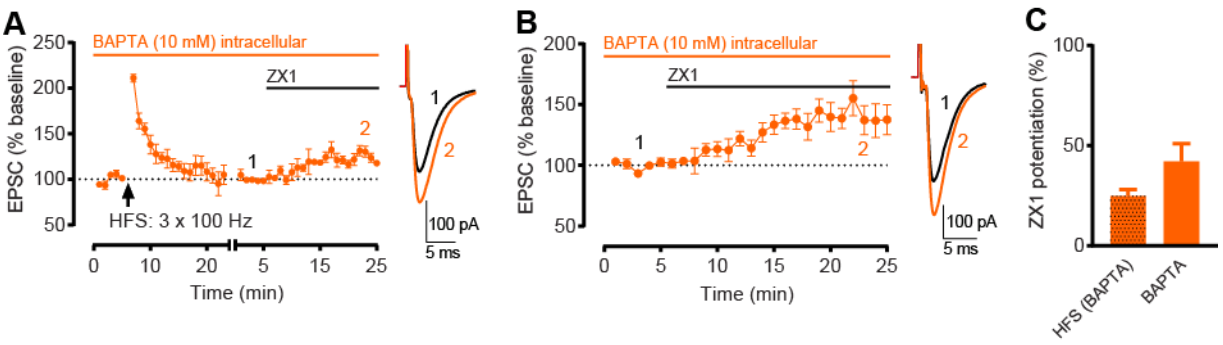

Figure 10: Postsynaptic Ca^{2+} signaling is necessary for Z-LTD

Legend for Figure 10:

(A) Time course of AMPAR EPSC amplitude before and after HFS, and before and after subsequent ZX1 application, with intracellular recording solution containing 10 mM BAPTA. After obtaining a stable baseline, HFS was delivered (3 x 100 Hz for 1 sec, 10 sec ISI). HFS did not induce LTP (n=6, n.s. p=0.39, paired t test). To examine ZX1 potentiation after HFS, after obtaining a stable baseline after HFS, AMPAR EPSC amplitude was renormalized to the new baseline before ZX1 application (100 μM). The renormalization is indicated by a gap and restart of timing in the x-axis. ZX1 significantly potentiated AMPAR EPSCs (n=6, *p=0.002, paired t test). Example traces show AMPAR EPSCs before and after ZX1 application. **(B)** Time course of AMPAR EPSC amplitude before and after ZX1 application, normalized to baseline before ZX1 application, with intracellular recording solution containing 10 mM BAPTA. ZX1 potentiated EPSCs (n=5, *p=0.012, paired t test). Example traces show AMPAR EPSCs before and after ZX1 application. **(C)** Average ZX1 potentiation (% increase from baseline) during the last 5 min of ZX1 application (mins. 21-25). 'HFS (BAPTA)' (n=6) vs. 'BAPTA' (n=5): n.s. p=0.082, unpaired t test. For all figures, values represent mean ± SEM. Star (*) indicates p<0.05. For detailed values

and statistical tests for all Chapter 2 figures, see section 3.5.7 *Detailed values and statistical tests for Chapter 2 Figures*.

3.3.2 Increased postsynaptic Ca^{2+} via ER stores is sufficient to induce Z-LTD

Postsynaptic Ca^{2+} signaling is required for HFS-induced Z-LTD, but what is the source of intracellular Ca^{2+}? G1 mGluRs lead to intracellular rises in Ca^{2+} from stores in the endoplasmic reticulum (ER) (Abdul-Ghani et al., 1996; Conn & Pin, 1997; Kim et al., 2008). To determine if ER Ca^{2+} stores are required for the induction of Z-LTD, we depleted ER Ca^{2+} stores using cyclopiazonic acid (CPA), a specific inhibitor of sarco- or endoplasmic reticulum Ca^{2+}-ATPase (Plenge-Tellechea, Soler, & Fernandez-Belda, 1997; Seidler, Jona, Vegh, & Martonosi, 1989). We tested whether HFS induces Z-LTD in the presence of CPA (Figure 11 A). For these experiments, we pre-treated slices with CPA (20 μM) in the ACSF and maintained CPA throughout the recording (Figure 11 A). After HFS in the presence of CPA, ZX1 did not potentiate AMPAR EPSCs, consistent with the induction of Z-LTD (Figure 11 A). However, depletion of ER Ca^{2+} stores by CPA increases intracellular Ca^{2+} (Demaurex, Lew, & Krause, 1992), and an intracellular rise in Ca^{2+} is required for Z-LTD (Figure 10). Therefore, it is possible that the observed Z-LTD (Figure 11 A) was induced by the CPA treatment alone, by increasing intracellular Ca^{2+}, and potentially occluded the effect of HFS. To test whether CPA treatment induces Z-LTD, we performed interleaved experiments measuring ZX1 potentiation of AMPAR EPSCs in the presence of CPA, and in control experiments without CPA (Figure 11 B). For these experiments, we again pre-treated slices with CPA in the ACSF and maintained CPA throughout the recording. In control experiments, ZX1 potentiated AMPAR EPSCs (Figure 11 B), consistent with previous studies (*Chapter 1*, section 2.3; (Kalappa et al., 2015)). However, in the presence of CPA, ZX1 did not

potentiate EPSCs (Figure 11 B-C). The loss of ZX1 potentiation indicates a reduction of synaptic zinc signaling, suggesting that CPA treatment induced Z-LTD and thus mimics the effect of HFS. Together, these results suggest that depletion of ER Ca^{2+} stores is sufficient to induce Z-LTD, likely by increasing intracellular Ca^{2+}.

The induction of Z-LTD, by reducing synaptic zinc signaling, reduces zinc-mediated inhibition of AMPAR EPSCs. Therefore, if depletion of ER Ca^{2+} stores induces Z-LTD, then application of CPA should increase AMPAR EPSC amplitude. To test this prediction, we measured the effect of CPA application on AMPAR EPSCs (Figure 11 D). Consistent with the induction of Z-LTD by CPA, the application of CPA significantly potentiated AMPAR EPSCs (Figure 11 D). To test whether this *CPA potentiation* is mediated by a reduction of synaptic zinc signaling, we examined the effect of CPA in the presence of extracellular ZX1 to prevent changes in synaptic zinc signaling (Figure 11 D). In the presence of ZX1, CPA did not potentiate AMPAR EPSCs (Figure 11 D-E). This result indicates that zinc signaling is required for CPA potentiation, and suggests that CPA potentiates AMPAR EPSCs by reducing zinc-mediated inhibition. Together, these results further support that depletion of ER Ca^{2+} stores is sufficient to induce Z-LTD.

The induction of Z-LTD by HFS is postsynaptically-mediated (Figure 10) and CPA application induces Z-LTD (Figure 11 B-D). However, because CPA is cell membrane-permeable, it remains possible that CPA induces Z-LTD by a different (potentially presynaptic) mechanism. We therefore sought to confirm whether the Z-LTD induced by CPA application is also mediated by increases in postsynaptic Ca^{2+}. To test this, we measured the effect of CPA application on

AMPAR EPSCs, with intracellular recording solution containing BAPTA (Figure 11 D). With BAPTA-containing intracellular solution, CPA did not potentiate EPSCs (Figure 11 D). This result demonstrates that a rise in postsynaptic Ca^{2+} is necessary for CPA potentiation (Figure 11 D). Finally, if increased postsynaptic Ca^{2+} underlies Z-LTD, then the presence of postsynaptic BAPTA should also prevent the reduction of ZX1 potentiation induced by CPA. To test this prediction, we recorded AMPAR EPSCs with BAPTA-containing intracellular solution and applied CPA, then subsequently measured ZX1 potentiation (Figure 11 F). Indeed, after CPA application with intracellular BAPTA, ZX1 significantly potentiated AMPAR EPSCs (Figure 11 F), indicating that BAPTA prevented CPA-induced Z-LTD. This result demonstrates that a rise in postsynaptic Ca^{2+} is necessary for CPA-induced Z-LTD. Together, all these results demonstrate that depletion of ER Ca^{2+} stores is sufficient to induce Z-LTD, by increasing postsynaptic Ca^{2+}.

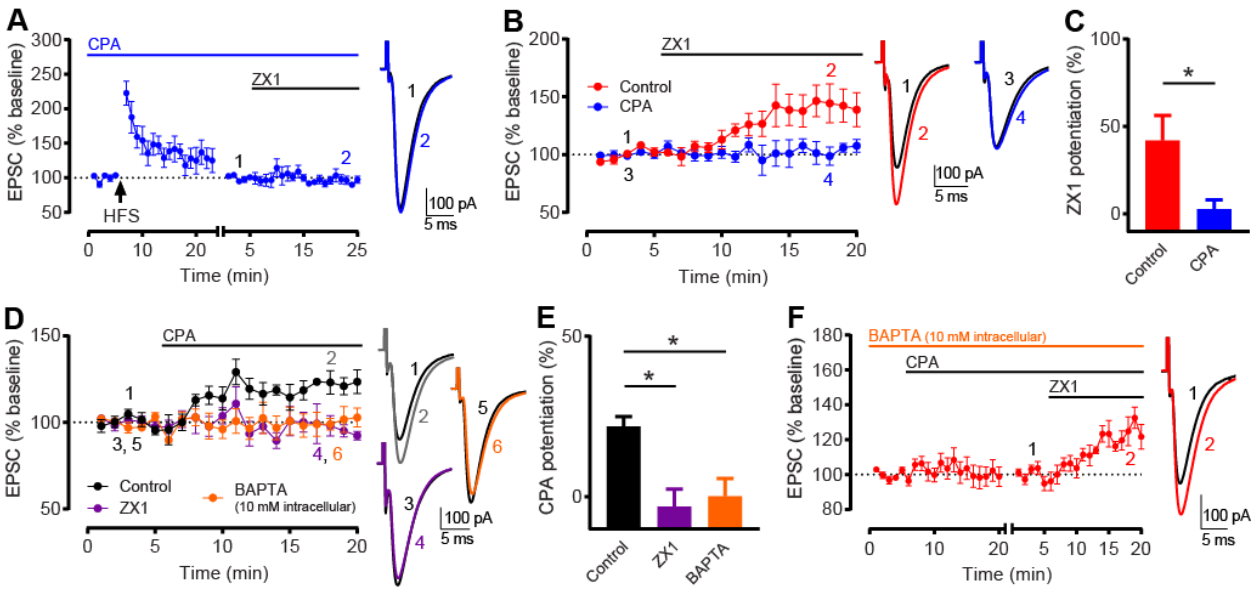

Figure 11: Increased postsynaptic Ca^{2+} via ER stores is sufficient to induce Z-LTD

Legend for Figure 11:

(A) Time course of AMPAR EPSC amplitude before and after HFS, and before and after subsequent ZX1 application, in the presence of CPA (20 µM). HFS did not induce LTP (n=4, n.s. p=0.17, paired t test). To examine ZX1 potentiation after HFS, similar approach and renormalization as in **10 A** was performed. ZX1 did not potentiate EPSCs (n=4, n.s. p=0.44, paired t test). Example traces show AMPAR EPSCs before and after ZX1 application. **(B)** Time course of AMPAR EPSC amplitude before and after ZX1 application, normalized to baseline before ZX1 application, in the presence of CPA (blue) and in controls (without CPA, red). In controls, ZX1 potentiated EPSCs (n=5, *p=0.036, paired t test). In CPA, ZX1 did not potentiate EPSCs (n=5, n.s. p=0.52, paired t test). Example traces show AMPAR EPSCs before and after ZX1 application. **(C)** Average ZX1 potentiation (% increase from baseline) during the last 5 min of ZX1 application (mins. 16-20). 'Control' (n=5) vs. 'CPA' (n=5): *p=0.034, unpaired t test. **(D)** Time course of AMPAR EPSC amplitude before and after CPA application (20 µM), normalized to baseline

before CPA application, in controls (black), in the presence of ZX1 (purple), and with BAPTA-containing intracellular recording solution (orange). In controls, CPA potentiated EPSCs (n=5, *p=0.004, paired t test). In the presence of ZX1, CPA did not potentiate EPSCs (n=4, n.s. p=0.40, paired t test). With intracellular BAPTA, CPA did not potentiate EPSCs (n=6, n.s. p=0.81, paired t test). Example traces show AMPAR EPSCs before and after CPA application. **(E)** Average CPA potentiation (% increase from baseline) during the last 5 min of CPA application (mins. 16-20). Compared to controls (n=5), CPA potentiation was reduced in the presence of ZX1 (n=4, *p=0.011), and with intracellular BAPTA (n=6, *p=0.013). One-way ANOVA/Bonferroni. **(F)** Time course of AMPAR EPSC amplitude before and after CPA application, and before and after subsequent ZX1 application, with BAPTA-containing intracellular recording solution. After obtaining a stable baseline, CPA was applied. To examine ZX1 potentiation after CPA, after obtaining a stable baseline after CPA, AMPAR EPSC amplitude was renormalized to the new baseline before ZX1 application. The renormalization is indicated by a gap and restart of timing in the x-axis. After CPA application with intracellular BAPTA, ZX1 potentiated EPSCs (n=5, *p=0.0016, paired t test). Example traces show AMPAR EPSCs before and after ZX1 application. Values represent mean ± SEM. Star (*) indicates $p<0.05$.

3.3.3 Depletion of ER Ca^{2+} stores reduces presynaptic zinc levels

The induction of Z-LTD by Group 1 mGluR activation is associated with reduced presynaptic zinc levels (*Chapter 1*, section 2.3.3). Because depletion of ER Ca^{2+} stores is sufficient to induce Z-LTD evidenced by reduced ZX1 potentiation (Figure 11), we hypothesized that CPA application induces Z-LTD by reducing presynaptic zinc levels. To test this hypothesis, we measured presynaptic zinc levels in DCN parallel fibers using DA-ZP1, a fluorescent intracellular zinc sensor (*Chapter 1*, section 2.3.3; (Kalappa et al., 2015; Zastrow et al., 2016)). We measured DA-ZP1 fluorescence in control slices and slices incubated with CPA (Figure 12 A-B). Compared to control slices, incubation of slices with CPA significantly reduced DA-ZP1 fluorescence (Figure 12 B). This result demonstrates that CPA reduces presynaptic zinc levels in PFs, thus suggesting that depletion of ER Ca^{2+} stores induces Z-LTD by reducing presynaptic zinc levels. Moreover, these results are consistent with our electrophysiological experiments (Figure 11) and further support that the changes in synaptic zinc signaling observed by changes in ZX1 potentiation are due to changes in presynaptic zinc levels.

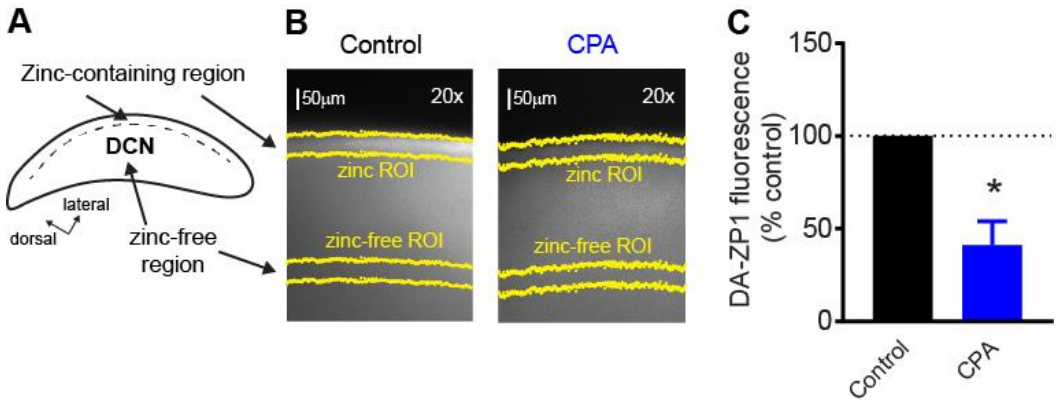

Figure 12: Depletion of ER Ca^{2+} stores reduces presynaptic zinc levels

Legend for Figure 12:

(A) Schematic of the DCN, showing the presynaptic zinc-containing region near the ependymal surface, where parallel fiber terminals reside, and the zinc-free region. **(B)** 20x images of DA-ZP1 fluorescence (0.75 μM), demonstrating the zinc-containing ROI (zinc ROI) and the zinc-free ROI, in a control slice (*left*) and a slice incubated in CPA (20 μM) (*right*) **(C)** Average DA-ZP1 fluorescence in CPA-treated slices, normalized to simultaneously imaged control slices. CPA treatment significantly reduced DA-ZP1 fluorescence (n=5, *p=0.01, one sample t test vs. 100%). Values represent mean ± SEM. Star (*) indicates $p<0.05$.

3.4 Discussion

Our results demonstrate that HFS-induced Z-LTD requires postsynaptic Ca^{2+} signaling, and that depletion of postsynaptic ER Ca^{2+} stores is sufficient to induce Z-LTD. Together, these results suggest that Z-LTD is mediated by activity-dependent rises in postsynaptic Ca^{2+} from intracellular ER stores. This mechanism is consistent with previous results demonstrating a critical role of G1 mGluR activation in synaptic zinc plasticity (*Chapter 1*), and Ca^{2+} mobilization from ER stores downstream of G1 mGluR activation (Abdul-Ghani et al., 1996; Conn & Pin, 1997; Kim et al., 2008). Furthermore, the Z-LTD induced by depletion of ER Ca^{2+} stores is associated with reduced presynaptic zinc levels (Figure 12), which is consistent with previous results demonstrating that Z-LTD induced by G1 mGluR activation is expressed by a reduction of presynaptic zinc levels (*Chapter 1*). Because Z-LTD is postsynaptically induced (Figure 10 A; Figure 11 D), these results suggest the presence of a retrograde signaling mechanism, activated by a rise in postsynaptic Ca^{2+}, that subsequently modulates presynaptic zinc levels. Taken together, we propose a model of activity-dependent synaptic zinc plasticity (Figure 13), in which activation of postsynaptic G1 mGluRs mobilizes postsynaptic Ca^{2+} from ER stores, which activates a retrograde messenger that modulates presynaptic zinc levels and zinc release.

The proposed model (Figure 13) is based on our results demonstrating the role of G1 mGluRs and postsynaptic ER Ca^{2+} stores in Z-LTD. It remains unknown if a similar mechanism, involving postsynaptic ER Ca^{2+} stores and retrograde signaling, also underlies activity-dependent increases in presynaptic zinc levels (Z-LTP). However, previous experiments demonstrated that G1 mGluR activation is necessary and sufficient for both Z-LTD and Z-LTP by differential amounts of G1 mGluR activation (*Chapter 1*). Therefore, it is likely, although not tested here, that

mobilization of postsynaptic Ca^{2+} from ER stores, downstream of G1 mGluR activation, may also underlie Z-LTP. Differential amounts of G1 mGluR activation may mobilize different amounts of Ca^{2+} from intracellular stores, ultimately leading to either Z-LTD or Z-LTP. Consistent with this notion, the depletion of ER Ca^{2+} stores is also known to cause the further influx of Ca^{2+} and other divalent cations (Demaurex et al., 1992), thus suggesting that intracellular Ca^{2+} mobilization may lead to multiple diverse signaling cascades.

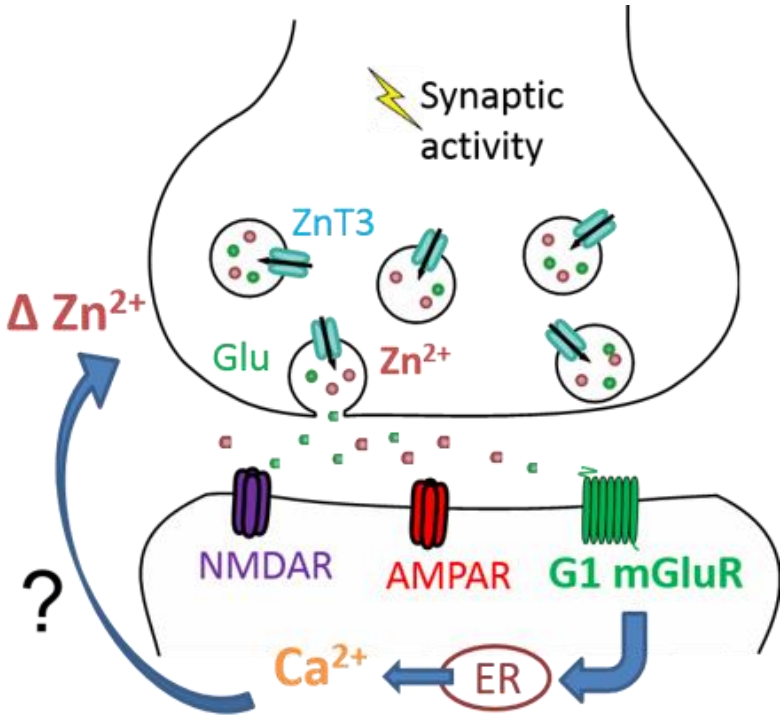

Figure 13: Proposed model of activity-dependent synaptic zinc plasticity

Legend for Figure 13:

In zinc-containing excitatory presynaptic terminals, the vesicular zinc transporter ZnT3 loads zinc into synaptic vesicles. In response to synaptic activity, glutamate and zinc are released. Activation of postsynaptic Group 1 mGluRs mobilizes Ca^{2+} from stores in postsynaptic endoplasmic reticulum. The rise in postsynaptic intracellular Ca^{2+} activates an unknown retrograde messenger, which acts on presynaptic terminals to modulate vesicular zinc levels and synaptic zinc release.

3.4.1 Mechanisms of synaptic zinc plasticity via retrograde signaling

Our results suggest the presence of a retrograde signaling mechanism, induced postsynaptically, that modulates presynaptic zinc levels and zinc release in DCN PFs. In many central synapses, activity-dependent plasticity involves a variety of retrograde messengers, including lipids (such as endocannabinoids), gases (such as nitric oxide), peptides, or growth factors (Araque, Castillo, Manzoni, & Tonini, 2017; Hardingham, Dachtler, & Fox, 2013; Regehr, Carey, & Best, 2009; Turrigiano, 2007). Retrograde messengers are released from postsynaptic neurons in an activity-dependent manner, and modulate synaptic strength via effects on presynaptic neurotransmitter release (Regehr et al., 2009; Suvarna, Maity, & Shivamurthy, 2016). What retrograde messenger(s) could mediate plasticity of presynaptic zinc signaling? One suggestion is nitric oxide (NO). In neurons, NO is synthesized by the enzyme neuronal nitric oxide synthase (nNOS), which is activated by Ca^{2+}/calmodulin (Garthwaite, 2008). Moreover, nNOS is highly expressed in the DCN molecular layer (Baizer et al., 2014), where our studies demonstrate activity-dependent zinc plasticity in PFs. Once synthesized, NO released from dendrites acts on many targets as a volume transmitter, including presynaptic boutons (Garthwaite, 2019; Steinert, Chernova, & Forsythe, 2010). nNOS is commonly known to be coupled to NMDA receptors via interactions with the postsynaptic density protein PSD-95, where it is activated by Ca^{2+} influx through NMDA receptors (Brenman et al., 1996; Sattler et al., 1999). However, nNOS is also localized subcellularly in the endoplasmic reticulum, and Group 1 mGluR activation has been shown to activate nNOS via Ca^{2+} release from ER stores (Batista, de Paula, Cavalcante, & Mendez-Otero, 2001; Hecker, Mulsch, & Busse, 1994; K. Z. Shen & Johnson, 2013). Additionally, NO is known to facilitate the release of zinc from metallothioneins, increase intracellular zinc levels in presynaptic boutons, and modulate presynaptic zinc release (Cuajungco & Lees, 1998;

Frederickson, Cuajungco, LaBuda, & Suh, 2002; Lin, Mohandas, Fontaine, & Colvin, 2007; Pearce et al., 2000). Together, these studies place G1 mGluR-mediated NO synthesis, and retrograde signaling by NO, as a strong candidate underlying synaptic zinc plasticity. It is also possible that while both Z-LTP and Z-LTD require G1 mGluR activation, the differential activation of G1 mGluRs could lead to diverging signaling pathways and recruit different retrograde messengers for Z-LTP and Z-LTD. Future studies will be necessary to determine whether NO, or other retrograde messenger(s), mediate bidirectional synaptic zinc plasticity.

3.4.2 Mechanism of AMPAR inhibition by synaptic zinc

Previous studies, as well as our results, demonstrate that endogenous synaptically released zinc inhibits AMPAR EPSCs, evidenced by the potentiation of AMPAR EPSCs by ZX1 (Kalappa et al., 2015). These results are consistent with the direct binding and modulation of AMPARs by synaptic zinc (Kalappa et al., 2015), which is consistent with structural data showing zinc binding sites in the ligand-binding domain of GluA2 AMPAR subunits (Armstrong & Gouaux, 2000). However, the precise mechanism by which ZX1 potentiates AMPAR EPSCs is unknown. Our results shown in Figure 10 B demonstrate that ZX1 potentiates AMPAR EPSCs in the presence of postsynaptic BAPTA (Figure 10 B), which indicates that ZX1 potentiation of AMPAR EPSCs does not require postsynaptic Ca^{2+} signaling. This result suggests that ZX1 potentiation of AMPAR EPSCs is likely not due to postsynaptic modifications that require intracellular Ca^{2+}, such as AMPAR trafficking (Herring & Nicoll, 2016). Therefore, these data further support that ZX1 potentiation of AMPAR EPSCs likely reveals the direct inhibition of AMPARs by synaptically released zinc.

3.4.3 Clinical implications of the role of Group 1 mGluRs and ER Ca^{2+} stores in zinc plasticity

Pathological neuronal zinc signaling is associated with numerous neurological disorders, such as schizophrenia, Alzheimer's disease, and autism. Variants in the ZnT3 gene are associated with schizophrenia (Perez-Becerril et al., 2016); Alzheimer's patients display reduced levels of ZnT3 expression (Olesen et al., 2016); ZnT3KO mice exhibit cognitive deficits similar to Alzheimer's and autism-like phenotypes (Adlard et al., 2010; Yoo et al., 2016); and a zinc ionophore rescues behavioral phenotypes in mouse models of autism (Lee et al., 2015). Therefore, there is converging evidence that pathological zinc signaling may play a significant role in the cognitive deficits observed in these neurological disorders. As such, understanding the cellular mechanisms that govern the long-term plasticity of zinc levels is a crucial first step in determining the molecular pathways that, when disrupted, may lead to pathological zinc signals. Our results identify Group 1 mGluRs and ER Ca^{2+} stores as novel targets for potential pharmacological interventions that could modulate and treat pathological zinc signaling in disease states.

3.5 Materials and Methods

3.5.1 Animals and Ethical Approval

Male or female ICR mice (Envigo) were used in this study, aged between postnatal day 17 (P17) to P29. Mice had access to food and water *ad libitum*. All steps were taken to minimize

animals' pain and suffering. All animal procedures were approved by the Institutional Animal Care and Use Committee of the University of Pittsburgh, Pittsburgh, PA.

3.5.2 Brain slice preparation

DCN brain slices were prepared as described previously (*Chapter 1*, section 2.5.2). Briefly, coronal brain slices containing the left DCN (210 μm thickness) were cut in artificial cerebrospinal fluid (ACSF, 34°C) containing the following (in mM): 130 NaCl, 3 KCl, 1.2 $CaCl_2 \cdot 2H_2O$, 1.3 $MgCl_2 \cdot 6H_2O$, 20 $NaHCO_3$, 3 HEPES, and 10 D-Glucose, saturated with 95% O_2/5% CO_2 (vol/vol), pH = 7.25-7.35, ~300 mOsm. Incubating ACSF was the same as cutting ACSF, except it was stirred with Chelex 100 resin (Bio-Rad) for 1 hour to remove contaminating zinc, then filtered using Nalgene rapid flow filters lined with polyethersulfone (0.2 μm pore size). After filtering, high purity $CaCl_2 \cdot 2H_2O$ and $MgCl_2.6H_2O$ (99.995%; Sigma Aldrich) were added. All plastic and glassware used for these experiments were washed with 5% nitric acid.

3.5.3 Electrophysiology

Whole-cell recordings. Cartwheel cells were recorded and identified as described previously (*Chapter 1,* section 2.5.3). Recording ACSF was the same as incubating ACSF (see above), except it contained 2.4 mM $CaCl_2 \cdot 2H_2O$. Recording pipettes were filled with a potassium-based internal solution containing the following (in mM): 113 K-gluconate, 4.5 $MgCl_2 \cdot 6H_2O$, 14 Tris-phosphocreatine, 9 HEPES, 0.1 EGTA, 4 Na_2ATP, 0.3 Tris-GTP, and 10 sucrose (pH = 7.25, 295 mOsm). For experiments where intracellular solution contained BAPTA (10 mM) (Figures 10 and 11 D, F), internal solution was the same as potassium-based internal solution except it

contained 73 mM K-gluconate and 10 mM BAPTA-4K$^+$. Voltages were not corrected for junction potentials. Recordings were performed using ephus (Suter et al., 2010) and a MultiClamp 700B amplifier (Axon Instruments). Data were sampled at 10 kHz and low-pass-filtered at 4 kHz. Series resistance (R_s, < 25 MΩ) and input resistance (R_m) were monitored as described previously (*Chapter 1*, section 2.5.3). Data were excluded if R_s or R_m changed by more than 20% from the baseline period. EPSCs were evoked using an Isoflex stimulator (A.M.P.I., 0.1 ms pulses) through a glass ACSF-containing theta electrode to stimulate the zinc-rich parallel fibers. Cells were considered stable during the baseline period of the EPSC amplitude for every minute during the baseline period varied by <10% from the overall mean EPSC amplitude during the baseline period (Fujino & Oertel, 2003). For experiments where intracellular solution contained BAPTA (see above), baseline EPSCs were not recorded until at least 20 min after breaking into whole-cell configuration. All EPSCs were recorded in the presence of SR95531 (20 μM, $GABA_AR$ antagonist) and strychnine (1 μM, GlyR antagonist). AMPAR EPSCs were recorded in voltage-clamp mode at -70 mV. All drugs were always bath applied.

Induction of plasticity. High-frequency stimulation (HFS) consisted of 3 trains of 100 Hz pulses for 1 sec, with 10 sec between trains. Cells were voltage-clamped at -70 mV during HFS. For normalized EPSCs (% baseline), EPSC amplitudes were normalized to the average EPSC amplitude during the 5 min baseline period before HFS, CPA, or ZX1 application. To quantify ZX1 potentiation after HFS or CPA application, EPSC amplitudes were renormalized to the average EPSC amplitude of the new baseline period 5 min before ZX1 application. ZX1 potentiation was quantified as the percent increase in the average EPSC amplitude during the last 5 min of ZX1 application compared to the 5 min baseline period before ZX1 application. CPA

potentiation was quantified as the percent increase in the average EPSC amplitude during the last 5 min of CPA application compared to the 5 min baseline period before CPA application.

3.5.4 Vesicular zinc imaging with DA-ZP1

Imaging of presynaptic vesicular zinc levels in DCN parallel fibers was performed using DA-ZP1 (0.5-1.0 μM) as described previously (*Chapter 1,* section 2.5.4). To quantify DA-ZP1 fluorescence, we quantified two ROIs within each slice: one within the zinc-containing molecular layer (zinc ROI) and the other within the zinc-free region (zinc-free ROI) (Kalappa et al., 2015; Zastrow et al., 2016). The automatically generated ROI borders are shown with yellow lines in Figure 12 B. Fluorescence intensity was averaged within each ROI, and the zinc-sensitive fluorescence was calculated by subtracting the zinc-free ROI fluorescence from the zinc ROI fluorescence. For experiments measuring DA-ZP1 fluorescence after incubation with CPA, CPA (20 μM) was added to the slice incubating chamber at least 20 min before being transferred to the imaging chamber. For these experiments, we simultaneously imaged pairs of control and CPA-treated slices in the same imaging chamber. Zinc-sensitive fluorescence in the CPA-treated slice was normalized to the simultaneously imaged control, non-treated slice (Figure 12 C).

3.5.5 Drugs

All chemicals used for ACSF and internal solutions were purchased from Sigma-Aldrich. SR95531 hydrobromide and cyclopiazonic acid (CPA) were purchased from HelloBio. Strychnine hydrochloride was purchased from Abcam. ZX1 was purchased from STREM Chemicals. DA-ZP1 was generously provided by Drs. Stephen Lippard and Jacob Goldberg.

3.5.6 Statistical Analysis

All data analysis was performed using Matlab (Mathworks), Excel (Microsoft), or Prism 7 (GraphPad). For statistical tests within groups, to determine whether HFS, CPA, or ZX1 significantly changed EPSC amplitude we used paired t tests (for normally distributed data). Data were considered normally distributed if they passed the Shapiro-Wilk normality test. For paired tests, we compared the average EPSC amplitude (in pA) of the 5 min baseline period to the average EPSC amplitude (in pA) during a 5 min period after HFS, CPA, or ZX1. The exact time points that were used for each test are stated in *Detailed values and statistical tests for Chapter 2 Figures*, section 3.5.7. For comparisons between groups, we used unpaired t tests (for normally distributed data). For statistical tests on normalized DA-ZP1 fluorescence, we used one-sample t tests compared to 100%. All statistical tests were two-tailed. For comparisons between three or more groups, we used ordinary one-way ANOVA with Bonferroni's multiple comparisons test (for normally distributed data). Significance levels are defined as $p < 0.05$. Group data are presented as mean ± SEM.

3.5.7 Detailed values and statistical tests for Chapter 2 Figures

Figure 10: **(10A)** Baseline (avg. of mins. 1-5) vs. HFS (avg. of mins. 19-23) (pA): n=6, t=0.9362 df=5, n.s. p=0.3922, paired t test. Baseline vs. ZX1 (mins. 21-25): n=6, t=5.668 df=5, *p=0.0024, paired t test. **(10B)** Baseline vs. ZX1 (mins. 21-25): n=5, t=4.344 df=4, *p=0.0122, paired t test. **(10C)** ZX1 potentiation (%): 'HFS (BAPTA)': 24.93 ± 3.185, n=6. 'BAPTA': 42.15 ± 8.936, n=5. 'HFS (BAPTA)' vs. 'BAPTA': t=1.956 df=9; n.s. p=0.0821, unpaired t test.

Figure 11: **(11A)** Baseline vs. HFS (mins. 19-23): n=4, t=1.796 df=3, n.s. p=0.1703, paired t test. Baseline vs. ZX1 (min 21-25): n=4, t=0.8927 df=3, n.s. p=0.4378, paired t test. **(11B)** 'Control': baseline vs. ZX1 (mins. 16-20): n=5, t=3.116 df=4, *p=0.0357, paired t test. 'CPA': baseline vs. ZX1 (mins. 16-20): n=5, t=0.7067 df=4, n.s. p=0.5187, paired t test. **(11C)** ZX1 potentiation (%): 'Control': 41.93 ± 14.35, n=5. CPA: 2.712 ± 5.347, n=5. 'Control' vs. 'CPA': t=2.561 df=8, *p=0.0336, unpaired t test. **(11D)** 'Control': baseline vs. CPA (mins. 16-20): n=5, t=5.888 df=4, *p=0.0042, paired t test. 'ZX1': baseline vs. CPA (mins. 16-20): n=4, t=0.9784 df=3, n.s. p=0.4000, paired t test. 'BAPTA': baseline vs. CPA (mins. 16-20): n=6, t=0.2515 df=5, n.s. p=0.8114, paired t test. **(11E)** CPA potentiation (%): 'Control': 21.92 ± 3.006, n=5. ZX1: -3.017 ± 5.401, n=4. BAPTA: 0.1296 ± 5.53, n=6. One-way ANOVA: F= 7.434, *p=0.0079; 'Control' vs. 'ZX1': *p=0.0109; 'Control' vs. 'BAPTA': *p=0.0133; Bonferroni's multiple comparisons test. **(11F)** Baseline vs. ZX1 (mins. 16-20): n=5, t=7.558 df=4, *p=0.0016, paired t test.

Figure 12: **(12C)** DA-ZP1 fluorescence (% control): 'CPA': 41.14 ± 12.87%; n=5, t=4.573 df=4, *p=0.0102, one sample t test vs. 100%.

4.0 General Discussion

This dissertation demonstrates bidirectional activity-dependent plasticity of synaptic zinc signaling in DCN parallel fibers. In the DCN, synaptic zinc plasticity is induced via synaptic activation *in vitro*, or sound exposure *in vivo*. Furthermore, Group 1 mGluR activation is necessary and sufficient for bidirectional synaptic zinc plasticity, and our results suggest a role of postsynaptic calcium and retrograde signaling. To our knowledge, this is the first time that a mechanism underlying synaptic zinc plasticity has been revealed. Moreover, synaptic zinc plasticity constitutes a novel mechanism of LTP and LTD in zinc-containing synapses.

Although increases or decreases in vesicular zinc have been previously observed in response to sensory deprivation or stimulation, it was unknown whether this zinc plasticity is an active or passive process. For example, if zinc uptake remains constant, sensory deprivation could lead to the passive accumulation of zinc in presynaptic terminals simply due to reduced neuronal activity. Similarly, sensory stimulation could lead to the passive reduction of zinc levels due to increased synaptic activity and zinc release (McAllister & Dyck, 2017). Our results settle this debate by demonstrating that synaptic zinc plasticity is an active process that dynamically regulates vesicular zinc levels and signaling, via Group 1 mGluR activation. Therefore, synaptic zinc plasticity is likely a critical component of experience-dependent adaptation, rather than merely an epiphenomenon.

4.1 Potential mechanisms underlying the expression of presynaptic zinc plasticity

Our results demonstrate that synaptic zinc plasticity is expressed, at least in part, by the modulation of presynaptic zinc levels (Figures 7 and 12). Because ZnT3 determines vesicular zinc levels (Cole et al., 1999; Palmiter et al., 1996), modulation of ZnT3 expression or function may underlie the expression of Z-LTP and Z-LTD. In the retina, optic nerve injury increases ZnT3 immunostaining, supporting that increases in ZnT3 expression mediate increases in synaptic zinc levels (Li et al., 2017). However, in the barrel cortex, whisker plucking increases the vesicular zinc content and the density of zinc-containing synapses, but does not alter either ZnT3 protein or mRNA levels (Brown & Dyck, 2002; Liguz-Lecznar, Nowicka, Czupryn, & Skangiel-Kramska, 2005; Nakashima, Butt, & Dyck, 2011; Nakashima & Dyck, 2010). Furthermore, in barrel cortical layers IV and V, the density of excitatory synapses remains unchanged despite the increased density of zinc-containing synapses, indicating that some previously excitatory non-zinc-containing synapses were converted to zinc-containing synapses (Nakashima & Dyck, 2010). Together, these studies suggest that changes in vesicular zinc content can occur without affecting glutamatergic synapses. While it remains unknown precisely how loud sound exposure reduces zinc levels in DCN PF synapses, this phenomenon of glutamate-independent zinc modulation may also explain our electrophysiological results after sound exposure, because sound exposure caused Z-LTD without affecting presynaptic glutamate dynamics (Figure 9).

In the context of ZnT3 modulation, it is interesting that the vesicular glutamate transporter 1 (VGlut1), which is co-targeted to synaptic vesicles with ZnT3, increases ZnT3 zinc transport in cultured cells (Salazar et al., 2005). Because VGlut1 is highly expressed in the DCN molecular layer (Zhou, Nannapaneni, & Shore, 2007), one hypothesis is that modulation of VGlut1 may

modulate ZnT3 function in PF terminals. However, the independent modulation of presynaptic glutamate and zinc dynamics after sound exposure (Figure 9) suggests a VGlut1-independent mechanism of ZnT3 modulation.

Because vesicular zinc is localized to a subpopulation of glutamatergic vesicles (Salazar, Love, Werner, et al., 2004), it is possible that activity-dependent changes in the distribution of released vesicles may contribute to the modulation of synaptically released zinc. However, our results using DA-ZP1 suggest that zinc plasticity is expressed by increases or decreases in vesicular zinc content (Figure 7). What mechanisms could mediate changes in the loading of zinc into vesicles? Because ZnT3 is targeted to synaptic vesicles by AP-3 (Salazar, Love, Werner, et al., 2004), modulation of AP-3 expression or function could consequently modulate ZnT3 and vesicular zinc content. It is also possible that changes in cytosolic zinc levels in presynaptic terminals, such as zinc release from metallothioneins, could modulate the loading of zinc into vesicles. As discussed in Chapter 2 *Discussion* (section 3.4), our results suggest a model of activity-dependent zinc plasticity that involves a retrograde messenger that modulates presynaptic zinc levels (Figure 13), and we suggest NO signaling as a candidate mechanism. Although it is not known whether DCN cartwheel cells specifically express nNOS, nNOS is highly expressed in the DCN molecular layer (Baizer et al., 2014), where cartwheel cells reside. NO facilities the release of zinc from metallothioneins, including MT-III which is preferentially expressed in synaptic zinc-containing neurons (Cole et al., 2000; Cuajungco & Lees, 1998; Knipp et al., 2005; Lin et al., 2007). Furthermore, NO-induced changes in intracellular zinc levels modulate the expression of many zinc transporters, including ZnT1, ZnT2 and ZnT4, which transport zinc out of the cytoplasm or into secretory vesicles (Aguilar-Alonso et al., 2008; Kambe et al., 2015). Therefore, NO-

induced changes in presynaptic intracellular zinc levels could modulate the loading of zinc into presynaptic vesicles by ZnT3.

4.2 The role of synaptic zinc in central synapses

Our results show that long-term synaptic zinc plasticity is an experience-, G1 mGluR-dependent mechanism that bidirectionally modulates synaptic zinc signaling in the DCN. Is this a general mechanism that applies to all synaptic zinc-containing brain areas? Synaptic zinc is present throughout the neocortex and other brain structures, such as the amygdala and the hippocampus (McAllister & Dyck, 2017). Moreover, synaptic zinc is modulated by sensory activity throughout the sensory cortex (McAllister & Dyck, 2017), shapes the gain of central sensory responses (Anderson et al., 2017), and when upregulated by optic nerve injury, it inhibits retinal ganglion cell survival and axon regeneration (Li et al., 2017). It is therefore likely, although not tested here, that the reported long-term synaptic zinc plasticity mechanism is a general mechanism that dynamically modulates sensory processing for adaptation to different sensory environments and injury.

The phenomenon, and underlying mechanism, of synaptic zinc plasticity may provide insight into the etiological question of *why* glutamatergic synapses contain and release zinc. Without zinc plasticity, the amount of zinc-mediated inhibition of postsynaptic responses would be constant and zinc would have little relevant impact on glutamatergic neurotransmission. The ability of synapses to modulate zinc signaling affords zinc-containing synapses an additional level of synaptic plasticity. The modulation of zinc signaling enables plasticity of synaptic strength

independent of changes in glutamate release or trafficking of postsynaptic glutamate receptors. An analogy that comes to mind is the functionality of having both an accelerator and a brake in an automobile: while it is possible to increase or decrease the speed of the vehicle simply by pressing or releasing the gas pedal, having a brake enables a far superior level of control. In this analogy, glutamate is the accelerator, and zinc is the brake. Whereas glutamate provides the main excitatory drive, zinc is an inhibitor that can be regulated to fine-tune neuronal responses. Furthermore, because zinc plasticity is mediated by Group 1 mGluRs, this suggests a feedback mechanism by which glutamate signaling (via mGluRs) can dynamically regulate zinc, which modulates the effects of glutamate.

Such a role for synaptic zinc may also help explain the precise anatomical distribution of zinc in the brain. Why do some synapses contain zinc while others do not? Synaptic zinc is present throughout the neocortex and limbic structures such as the hippocampus and amygdala, but it is largely absent from the midbrain and brainstem (except for the dorsal cochlear nucleus) (McAllister & Dyck, 2017). Zinc-containing fibers largely appear to project within the cortex and limbic areas, while long-range projections to or from these regions are zinc-lacking (Brown & Dyck, 2004; Ichinohe & Rockland, 2005; Slomianka, 1992). Notably, the zinc-containing projections within the telencephalon are typically more plastic than the long-range input/output pathways (Frederickson, Suh, Silva, Frederickson, & Thompson, 2000). Together, these observations further suggest that synaptic zinc, and the dynamic modulation of zinc signaling, is particularly important for synaptic plasticity throughout the brain.

4.3 The role of zinc plasticity in the context of other plasticity mechanisms

Given the prevalence of synaptic zinc throughout the brain, activity-dependent zinc plasticity is a phenomenon that future investigators should consider when studying synaptic function and plasticity. For example, for decades the hippocampus has been utilized for dissecting mechanisms of synaptic plasticity (Citri & Malenka, 2008; Malenka & Nicoll, 1993). While many investigators have examined the role of synaptic zinc in the induction of LTP and LTD (Nakashima & Dyck, 2009), the converse should be considered as well – that activity-dependent LTP/LTD induction could modulate the zinc signal itself. Indeed, mGluR activation has been implicated in multiple forms of hippocampal LTP/LTD (Anwyl, 2009; Citri & Malenka, 2008); therefore, Group 1 mGluR-mediated zinc plasticity may contribute to these plasticity mechanisms. As discussed in Chapter 1 *Discussion* (section 2.4), bidirectional synaptic zinc plasticity likely serves as a positive feedback mechanism to further enhance the effects of mGluR-dependent LTD and LTP, by increasing or decreased zinc-mediated inhibition of AMPARs. For example, hippocampal mGluR-dependent LTD involves postsynaptic AMPAR endocytosis (Holbro et al., 2009; Huber et al., 2000; Luscher & Huber, 2010; Pick & Ziff, 2018). Therefore, mGluR-dependent Z-LTP would further promote LTD of synaptic strength, by increasing zinc-mediated inhibition of the remaining AMPARs. Future studies will be needed to dissect whether zinc plasticity is mediated by the same signaling pathways known to mediate mGluR-dependent LTD or LTP, or whether zinc plasticity occurs through other pathways as a separate supplementary mechanism. Nonetheless, zinc plasticity further adds to the complexities of synaptic function and plasticity in zinc-containing synapses. Changes in synaptic zinc signaling may underlie mechanisms of synaptic plasticity that have been previously overlooked.

As discussed in Chapter 1 *Discussion* (section 2.4), zinc plasticity likely acts together with other known plasticity mechanisms to shape the size of LTP or LTD. Why would a synapse need many different plasticity mechanisms? The ability of synapses to undergo multiple mechanisms of plasticity affords flexibility to maintain proper synaptic function and adapt to a variety of changes in synaptic activity or sensory experience. Each neurotransmitter system or plasticity mechanism may increase or decrease synaptic excitability in different ways. Therefore, a separate plasticity mechanism, such as zinc plasticity, may serve to counterbalance these changes and prevent runaway synaptic potentiation or depression. Future studies will be needed to determine precisely how zinc plasticity interacts with other plasticity mechanisms in the brain, and the overall role of zinc in particular synapses.

4.4 The role of synaptic zinc in the DCN

It is intriguing that the DCN parallel fibers contain high concentrations of vesicular zinc, while most other brainstem structures are zinc-lacking (Danscher & Stoltenberg, 2005). What is the role of synaptic zinc in the DCN? The zinc-containing parallel fibers (PFs) exhibit a high degree of synaptic plasticity, while the zinc-lacking auditory nerve fibers do not (Fujino & Oertel, 2003; Oertel & Young, 2004). These findings further suggest that zinc contributes to synaptic plasticity. Furthermore, plasticity of PFs has been implicated in DCN adaptation to auditory experience, such as noise exposure, which can lead to hyperexcitability and tinnitus (Marks et al., 2018; Tzounopoulos, 2008). Our findings on the contributions of synaptic zinc plasticity to LTP/LTD in PFs suggest a potential role of zinc plasticity in this experience-dependent adaptation, in both normal and pathological states.

Loud sound exposure damages auditory nerve fibers, which reduces afferent input to the DCN (Pilati et al., 2012). Yet, sound exposure reduces zinc levels and synaptic zinc signaling in the PFs in the molecular layer of the DCN (Kalappa et al., 2015). How could sound-induced changes in auditory input cause zinc plasticity in PFs? Recent studies showed that superficial stellate cells in the DCN molecular layer are electrically coupled to fusiform cells, which receive auditory nerve input (Apostolides & Trussell, 2013, 2014). These stellate cells, via synapses onto cartwheel cells, are therefore capable of sensing changes in auditory input and subsequently modulating the efficacy of PF activity (Apostolides & Trussell, 2013, 2014). Moreover, noise exposure is known to cause an enhancement of excitatory somatosensory inputs to the DCN, thus enhancing PF activity (Dehmel, Pradhan, Koehler, Bledsoe, & Shore, 2012; Shore, Zhou, & Koehler, 2007). It has been hypothesized that this PF enhancement acts as a compensatory plasticity mechanism to counteract the reduced auditory input resulting from noise-induced auditory nerve damage (Dehmel et al., 2012; Shore et al., 2007). Could synaptic zinc plasticity play a role in this compensatory mechanism? Sound-induced reductions in zinc signaling would contribute to enhanced PF excitation, by reducing zinc-mediated inhibition of AMPARs and NMDARs. Because fusiform cells in the DCN receive input from both the auditory nerve and PFs, enhanced PF excitation (via Z-LTD) would counteract noise-induced reductions in auditory nerve input. Therefore, Z-LTD may contribute to noise-induced adaptation and homeostatic regulation of DCN output.

4.5 Conclusions and future directions

The work in this dissertation has revealed a novel Group 1 mGluR-dependent mechanism of synaptic plasticity in zinc-containing glutamatergic synapses, via the dynamic modulation of synaptic zinc levels and signaling. Given the role of zinc in shaping glutamatergic neurotransmission, sensory processing, and behavior, this mechanism has profound implications for neurotransmission and experience-dependent plasticity in central synapses. The Group 1 mGluR-dependent mechanism shown here may be a general mechanism underlying plasticity in zinc-containing synapses throughout the brain. Future studies will be needed to determine whether this mechanism applies to all zinc-containing brain areas. Moreover, the role of Group 1 mGluR and postsynaptic calcium signaling suggest a working model of zinc plasticity (Figure 13). However, the detailed mechanisms linking calcium release from postsynaptic ER stores to changes in presynaptic zinc levels, likely via retrograde signaling, must be dissected in future studies.

The novel findings presented here highlight the DCN as a model for studying synaptic zinc plasticity, as well as the innovative use of ZX1 and DA-ZP1 to probe this system. Furthermore, in addition to the results presented in Chapters 1 & 2, we characterized a novel photoactivatable fluorescent zinc sensor (Appendix A). This new zinc sensor will be valuable for studying zinc dynamics in live cells and tissues with high spatiotemporal resolution.

In conclusion, this work has elucidated previously unknown mechanisms of plasticity in the brain, and has laid a foundation for future research into the functional roles and clinical implications of synaptic zinc plasticity.

Appendix A Photoactivatable Sensors for Detecting Mobile Zinc

Note: this section is adapted and reprinted with permission from:

Goldberg, J. M., Wang, F., Sessler, C. D., **Vogler, N. W.**, Zhang, D. Y., Loucks, W. H., . . . Lippard, S. J. (2018). Photoactivatable Sensors for Detecting Mobile Zinc. *J Am Chem Soc, 140*(6), 2020-2023. doi:10.1021/jacs.7b12766 (Goldberg et al., 2018)

A.1 Overview

Fluorescent sensors for mobile zinc are valuable for studying complex biological systems. Because these sensors typically bind zinc rapidly and tightly, there has been little temporal control over the activity of the probe after its application to a sample. The ability to control the activity of a zinc sensor in vivo during imaging experiments would greatly improve the time resolution of the measurement. Here, we describe photoactivatable zinc sensors that can be triggered with short pulses of UV light. These probes are prepared by functionalizing a zinc sensor with protecting groups that render the probe insensitive to metal ions. Photoinduced removal of the protecting groups restores the binding site, allowing for zinc-responsive changes in fluorescence that can be observed in live cells and tissues.

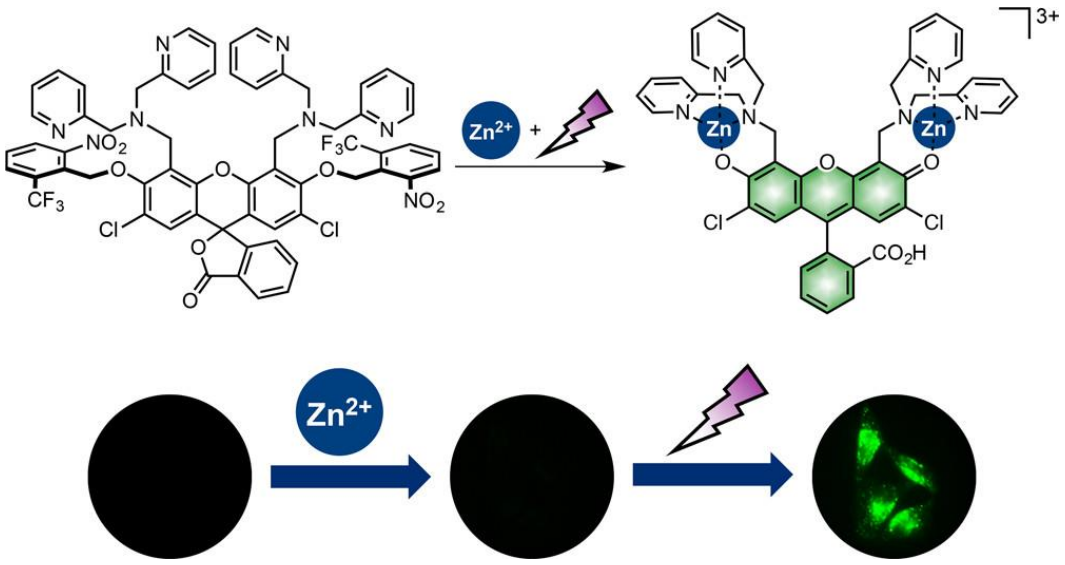

Figure 14: Photoactivatable sensors for detecting mobile zinc

Published in: Jacob M. Goldberg; Fang Wang; Chanan D. Sessler; Nathan W. Vogler; Daniel Y. Zhang; William H. Loucks; Thanos Tzounopoulos; Stephen J. Lippard; *J. Am. Chem. Soc*. 2018, 140, 2020-2023. DOI: 10.1021/jacs.7b12766

A.2 Results

Zinc is an essential element for human health. Throughout the body, zinc is tightly bound to proteins either as a catalytic cofactor or structural element (Maret, 2013). In some tissues, particularly those of the brain, pancreas, prostate, and mammary gland, zinc exists in ion pools that participate in signaling cascades and regulatory networks (Hennigar & Kelleher, 2012). This so-called mobile zinc acts as a brake to attenuate glutamatergic neurotransmission in certain areas of the brain engaged in sensory perception, especially in auditory processing (Anderson et al., 2017; Anderson et al., 2015; Kalappa et al., 2015), and also as a signaling agent in fertilization

(Que et al., 2015). Despite much research, the exact functional role of mobile zinc in these pathways is not completely understood. A critical barrier to understanding the role of mobile zinc is a lack of suitable probes for studying these systems with high spatiotemporal resolution (Barr & Burdette, 2017).

To evaluate our ability to control the activation of [our new photoactivatable] sensor with high spatiotemporal resolution, we tested [the sensor] in live brain slices. For this work, we examined the mouse dorsal cochlear nucleus (DCN), a region of the brain that integrates signals from auditory nerve inputs in the vesicular (synaptic) zinc-lacking deep layer with information arriving from other areas of the brain in the synaptic zinc-rich molecular layer [Figure 15] (Anderson et al., 2015; Frederickson et al., 1988; Kalappa et al., 2015; Oertel & Young, 2004; Rubio & Juiz, 1998). Because the zinc-lacking and zinc-rich layers are anatomically well-separated, the DCN is ideal for testing photoactivation of the sensor. Acute DCN slices incubated with [the photosensor] were irradiated with 355 nm laser light in a square grid pattern spanning both the zinc-rich molecular layer and the zinc-lacking deep layer. As shown in [Figure 15], after 5 ms of irradiation, only sites in the molecular layer exhibited significant increases in fluorescence intensity after photostimulation, while sites in the deep layer did not. Importantly, the fluorescence response was restricted to loci of direct excitation; fluorescence signals from tissue between or outside those regions were not affected. In contrast, the diacetylated derivative of ZP1 fluoresces brightly in the entire molecular layer (Kalappa et al., 2015). This proof-of-principle experiment shows that [the photosensor] can be selectively activated in live tissue slices with at least micrometer spatial resolution and millisecond temporal resolution.

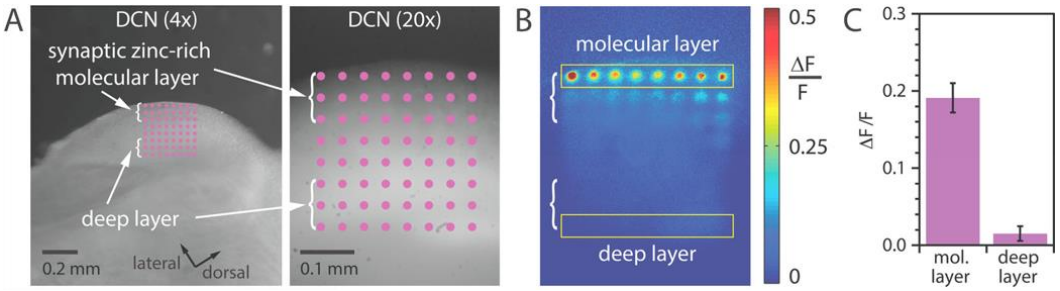

Figure 15: Photoactivatable zinc fluorescence in DCN slices

Published in: Jacob M. Goldberg; Fang Wang; Chanan D. Sessler; Nathan W. Vogler; Daniel Y. Zhang; William H. Loucks; Thanos Tzounopoulos; Stephen J. Lippard; *J. Am. Chem. Soc*. 2018, 140, 2020-2023. DOI: 10.1021/jacs.7b12766

Legend for Figure 15:

Fluorescence of [the photosensor] in brain slices containing the dorsal cochlear nucleus (DCN) after photoactivation. **(A)** 4× image of the DCN slice (left), with overlaid 8 × 8 photostimulation grid (40 μm spacing). 20× image of the DCN (right) with the overlaid grid. The grid was photostimulated 5 times with 1 ms pulses (355 nm, ~5.5 mW). **(B)** Heat map of normalized fluorescent signals. ΔF/F is the fluorescence change after photostimulation divided by the initial fluorescence. **(C)** Comparison of the average photoactivated fluorescence of [the photosensor] in the molecular layer versus the deep layer (regions outlined by yellow boxes in B, $n = 6$, $p < 0.0001$, unpaired *t* test).

A.3 Materials and Methods: Experiments in DCN brain slices

A.3.1 Animals

All procedures were approved by the Institutional Animal Care and Use Committee at the University of Pittsburgh, Pittsburgh, PA.

A.3.2 Preparation of DCN brain slices

Male or female ICR mice (Harlan) aged between postnatal day 20 (P20) and P22 were used. Mice were anesthetized with isoflurane then immediately decapitated and brains were rapidly removed. Brain slices were prepared in warm (34 °C) artificial cerebrospinal fluid (ACSF) containing the following (in mM): 130 NaCl, 3 KCl, 1.2 $CaCl_2 \cdot 2H_2O$, 1.3 $MgCl_2 \cdot 6H_2O$, 20 $NaHCO_3$, 3 HEPES, and 10 D-glucose, saturated with 95% O_2/5% CO_2 (v/v), pH = 7.25-7.35, ~300 mOsm. Coronal slices (210 μm thickness) containing cross sections including the molecular and deep layers of the dorsal cochlear nucleus (DCN) were cut using a Vibratome (VT1200S; Leica), then transferred to a holding chamber containing warm ACSF and incubated for ~60 min at 34 °C before initiating imaging experiments. ACSF used for incubating and imaging had the same composition as cutting ACSF, except contaminating zinc was removed by stirring the ACSF with Chelex 100 resin (Bio-Rad) for 1 hour. Chelex resin was filtered using Nalgene rapid flow filters lined with polyethersulfone (0.2 μm pore size), then high purity $CaCl_2 \cdot 2H_2O$ and $MgCl_2 \cdot 6H_2O$ (99.995%; Sigma-Aldrich) were added to the ACSF. All plastic- and glassware were washed with 5% nitric acid.

A.3.3 Fluorescence imaging and laser photoactivation

Slices were transferred to the imaging chamber and perfused with room temperature recirculating ACSF (1-2 mL/min). Prior to fluorescence imaging, 1 μL [of the sensor] (1 mM) was mixed with 1 μL 20% Pluronic F-127 (Invitrogen), then added to the ACSF for a final concentration of 1 μM [of the sensor]. Slices were allowed to incubate with [the sensor] in the imaging chamber for 20 min before initiating fluorescence imaging. Images were acquired using an upright microscope (Olympus BX5) with a 20× water immersion objective and epifluorescence optics. The excitation source was a blue LED (470 nm wavelength, M470L3, Thorlabs), and green fluorescent signals were isolated using a GFP filter (U-N41017, Olympus) and acquired using a CCD camera (Retiga 2000R, QImaging). Images of fluorescent signals were captured before and after UV laser photostimulation. Photostimulation with UV laser light (355 nm, ~5.5 mW; DPSS Lasers) was performed under the 20× objective, and the photostimulation grid consisted of 8 × 8 sites (40 μm spacing) positioned to encompass the molecular layer and deep layer of the DCN. Each site was photostimulated with a 1 ms pulse of UV laser light (0.4 s between sites), and photostimulation of the entire grid was repeated 5 times.

A.3.4 Data analysis

All analysis was performed with custom routines in MATLAB (Mathworks) or with Prism 6 (GraphPad). For fluorescent images captured before and after photostimulation, a region of interest was selected containing the top row (molecular layer) or bottom row (deep layer) of the photostimulation grid. Fluorescence intensity was averaged within each region, and the change in intensity (ΔF) was calculated by subtracting the intensity before photostimulation from the

intensity after photostimulation. $\Delta F/F$ was calculated by dividing ΔF by the intensity before photostimulation. Statistical comparison of $\Delta F/F$ in the molecular layer versus the deep layer was performed using an unpaired *t* test with Welch's correction.

Bibliography

Abdul-Ghani, M. A., Valiante, T. A., Carlen, P. L., & Pennefather, P. S. (1996). Metabotropic glutamate receptors coupled to IP3 production mediate inhibition of IAHP in rat dentate granule neurons. *J Neurophysiol, 76*(4), 2691-2700. doi:10.1152/jn.1996.76.4.2691

Abraham, W. C., & Tate, W. P. (1997). Metaplasticity: a new vista across the field of synaptic plasticity. *Prog Neurobiol, 52*(4), 303-323.

Adlard, P. A., Parncutt, J., Lal, V., James, S., Hare, D., Doble, P., . . . Bush, A. I. (2015). Metal chaperones prevent zinc-mediated cognitive decline. *Neurobiol Dis, 81*, 196-202. doi:10.1016/j.nbd.2014.12.012

Adlard, P. A., Parncutt, J. M., Finkelstein, D. I., & Bush, A. I. (2010). Cognitive loss in zinc transporter-3 knock-out mice: a phenocopy for the synaptic and memory deficits of Alzheimer's disease? *J Neurosci, 30*(5), 1631-1636. doi:10.1523/JNEUROSCI.5255-09.2010

Aguilar-Alonso, P., Martinez-Fong, D., Pazos-Salazar, N. G., Brambila, E., Gonzalez-Barrios, J. A., Mejorada, A., . . . Leon-Chavez, B. A. (2008). The increase in zinc levels and upregulation of zinc transporters are mediated by nitric oxide in the cerebral cortex after transient ischemia in the rat. *Brain Res, 1200*, 89-98. doi:10.1016/j.brainres.2007.11.077

Aizenman, E., Stout, A. K., Hartnett, K. A., Dineley, K. E., McLaughlin, B., & Reynolds, I. J. (2000). Induction of neuronal apoptosis by thiol oxidation: putative role of intracellular zinc release. *J Neurochem, 75*(5), 1878-1888. doi:10.1046/j.1471-4159.2000.0751878.x

Anderson, C. T., Kumar, M., Xiong, S., & Tzounopoulos, T. (2017). Cell-specific gain modulation by synaptically released zinc in cortical circuits of audition. *Elife, 6*. doi:10.7554/eLife.29893

Anderson, C. T., Radford, R. J., Zastrow, M. L., Zhang, D. Y., Apfel, U. P., Lippard, S. J., & Tzounopoulos, T. (2015). Modulation of extrasynaptic NMDA receptors by synaptic and tonic zinc. *Proc Natl Acad Sci U S A, 112*(20), E2705-2714. doi:10.1073/pnas.1503348112

Andreini, C., Banci, L., Bertini, I., & Rosato, A. (2006). Counting the zinc-proteins encoded in the human genome. *J Proteome Res, 5*(1), 196-201. doi:10.1021/pr050361j

Andrews, G. K. (2000). Regulation of metallothionein gene expression by oxidative stress and metal ions. *Biochem Pharmacol, 59*(1), 95-104. doi:10.1016/s0006-2952(99)00301-9

Anwyl, R. (2009). Metabotropic glutamate receptor-dependent long-term potentiation. *Neuropharmacology, 56*(4), 735-740.

Apostolides, P. F., & Trussell, L. O. (2013). Regulation of interneuron excitability by gap junction coupling with principal cells. *Nat Neurosci, 16*(12), 1764-1772. doi:10.1038/nn.3569

Apostolides, P. F., & Trussell, L. O. (2014). Superficial stellate cells of the dorsal cochlear nucleus. *Front Neural Circuits, 8*, 63. doi:10.3389/fncir.2014.00063

Araque, A., Castillo, P. E., Manzoni, O. J., & Tonini, R. (2017). Synaptic functions of endocannabinoid signaling in health and disease. *Neuropharmacology, 124*, 13-24. doi:10.1016/j.neuropharm.2017.06.017

Armstrong, N., & Gouaux, E. (2000). Mechanisms for activation and antagonism of an AMPA-sensitive glutamate receptor: crystal structures of the GluR2 ligand binding core. *Neuron, 28*(1), 165-181. doi:10.1016/s0896-6273(00)00094-5

Assaf, S. Y., & Chung, S. H. (1984). Release of endogenous Zn2+ from brain tissue during activity. *Nature, 308*(5961), 734-736. doi:10.1038/308734a0

Auerbach, B. D., Rodrigues, P. V., & Salvi, R. J. (2014). Central gain control in tinnitus and hyperacusis. *Front Neurol, 5*, 206. doi:10.3389/fneur.2014.00206

Baizer, J. S., Wong, K. M., Paolone, N. A., Weinstock, N., Salvi, R. J., Manohar, S., . . . Hof, P. R. (2014). Laminar and neurochemical organization of the dorsal cochlear nucleus of the human, monkey, cat, and rodents. *Anat Rec (Hoboken), 297*(10), 1865-1884. doi:10.1002/ar.23000

Barr, C. A., & Burdette, S. C. (2017). The zinc paradigm for metalloneurochemistry. *Essays Biochem, 61*(2), 225-235. doi:10.1042/EBC20160073

Batista, C. M., de Paula, K. C., Cavalcante, L. A., & Mendez-Otero, R. (2001). Subcellular localization of neuronal nitric oxide synthase in the superficial gray layer of the rat superior colliculus. *Neurosci Res, 41*(1), 67-70. doi:10.1016/s0168-0102(01)00268-1

Beaulieu, C., Dyck, R., & Cynader, M. (1992). Enrichment of glutamate in zinc-containing terminals of the cat visual cortex. *Neuroreport, 3*(10), 861-864. doi:10.1097/00001756-199210000-00010

Bender, V. A., Bender, K. J., Brasier, D. J., & Feldman, D. E. (2006). Two coincidence detectors for spike timing-dependent plasticity in somatosensory cortex. *J Neurosci, 26*(16), 4166-4177. doi:10.1523/JNEUROSCI.0176-06.2006

Besser, L., Chorin, E., Sekler, I., Silverman, W. F., Atkin, S., Russell, J. T., & Hershfinkel, M. (2009). Synaptically released zinc triggers metabotropic signaling via a zinc-sensing receptor in the hippocampus. *J Neurosci, 29*(9), 2890-2901. doi:10.1523/JNEUROSCI.5093-08.2009

Bilak, S. R., & Morest, D. K. (1998). Differential expression of the metabotropic glutamate receptor mGluR1alpha by neurons and axons in the cochlear nucleus: in situ hybridization and immunohistochemistry. *Synapse, 28*(4), 251-270. doi:10.1002/(SICI)1098-2396(199804)28:4<251::AID-SYN1>3.0.CO;2-8

Blakemore, L. J., & Trombley, P. Q. (2004). Diverse modulation of olfactory bulb AMPA receptors by zinc. *Neuroreport, 15*(5), 919-923. doi:10.1097/00001756-200404090-00037

Blakemore, L. J., & Trombley, P. Q. (2019). Mechanisms of zinc modulation of olfactory bulb AMPA receptors. *Neuroscience, 410*, 160-175. doi:10.1016/j.neuroscience.2019.05.001

Blasie, C. A., & Berg, J. M. (2002). Structure-based thermodynamic analysis of a coupled metal binding-protein folding reaction involving a zinc finger peptide. *Biochemistry, 41*(50), 15068-15073. doi:10.1021/bi026621h

Brenman, J. E., Chao, D. S., Gee, S. H., McGee, A. W., Craven, S. E., Santillano, D. R., . . . Bredt, D. S. (1996). Interaction of nitric oxide synthase with the postsynaptic density protein PSD-95 and alpha1-syntrophin mediated by PDZ domains. *Cell, 84*(5), 757-767. doi:10.1016/s0092-8674(00)81053-3

Bresink, I., Ebert, B., Parsons, C. G., & Mutschler, E. (1996). Zinc changes AMPA receptor properties: results of binding studies and patch clamp recordings. *Neuropharmacology, 35*(4), 503-509. doi:10.1016/0028-3908(95)00192-1

Brown, C. E., & Dyck, R. H. (2002). Rapid, experience-dependent changes in levels of synaptic zinc in primary somatosensory cortex of the adult mouse. *J Neurosci, 22*(7), 2617-2625. doi:20026255

Brown, C. E., & Dyck, R. H. (2004). Distribution of zincergic neurons in the mouse forebrain. *J Comp Neurol, 479*(2), 156-167. doi:10.1002/cne.20308

Brown, C. E., & Dyck, R. H. (2005). Modulation of synaptic zinc in barrel cortex by whisker stimulation. *Neuroscience, 134*(2), 355-359. doi:10.1016/j.neuroscience.2005.05.011

Bush, A. I., Pettingell, W. H., Multhaup, G., d Paradis, M., Vonsattel, J. P., Gusella, J. F., . . . Tanzi, R. E. (1994). Rapid induction of Alzheimer A beta amyloid formation by zinc. *Science, 265*(5177), 1464-1467. doi:10.1126/science.8073293

Chen, A., Hu, W. W., Jiang, X. L., Potegal, M., & Li, H. (2017). Molecular mechanisms of group I metabotropic glutamate receptor mediated LTP and LTD in basolateral amygdala in vitro. *Psychopharmacology (Berl), 234*(4), 681-694. doi:10.1007/s00213-016-4503-7

Choi, D. W., Yokoyama, M., & Koh, J. (1988). Zinc neurotoxicity in cortical cell culture. *Neuroscience, 24*(1), 67-79. doi:10.1016/0306-4522(88)90312-0

Chorin, E., Vinograd, O., Fleidervish, I., Gilad, D., Herrmann, S., Sekler, I., . . . Hershfinkel, M. (2011). Upregulation of KCC2 activity by zinc-mediated neurotransmission via the mZnR/GPR39 receptor. *J Neurosci, 31*(36), 12916-12926. doi:10.1523/JNEUROSCI.2205-11.2011

Citri, A., & Malenka, R. C. (2008). Synaptic plasticity: multiple forms, functions, and mechanisms. *Neuropsychopharmacology, 33*(1), 18-41. doi:10.1038/sj.npp.1301559

Cole, T. B., Martyanova, A., & Palmiter, R. D. (2001). Removing zinc from synaptic vesicles does not impair spatial learning, memory, or sensorimotor functions in the mouse. *Brain Res, 891*(1-2), 253-265. doi:10.1016/s0006-8993(00)03220-0

Cole, T. B., Robbins, C. A., Wenzel, H. J., Schwartzkroin, P. A., & Palmiter, R. D. (2000). Seizures and neuronal damage in mice lacking vesicular zinc. *Epilepsy Res, 39*(2), 153-169. doi:10.1016/s0920-1211(99)00121-7

Cole, T. B., Wenzel, H. J., Kafer, K. E., Schwartzkroin, P. A., & Palmiter, R. D. (1999). Elimination of zinc from synaptic vesicles in the intact mouse brain by disruption of the ZnT3 gene. *Proc Natl Acad Sci U S A, 96*(4), 1716-1721.

Colvin, R. A., Holmes, W. R., Fontaine, C. P., & Maret, W. (2010). Cytosolic zinc buffering and muffling: their role in intracellular zinc homeostasis. *Metallomics, 2*(5), 306-317. doi:10.1039/b926662c

Conn, P. J., & Pin, J. P. (1997). Pharmacology and functions of metabotropic glutamate receptors. *Annu Rev Pharmacol Toxicol, 37*, 205-237. doi:10.1146/annurev.pharmtox.37.1.205

Cousins, R. J., Liuzzi, J. P., & Lichten, L. A. (2006). Mammalian zinc transport, trafficking, and signals. *J Biol Chem, 281*(34), 24085-24089. doi:10.1074/jbc.R600011200

Cuajungco, M. P., & Lees, G. J. (1998). Nitric oxide generators produce accumulation of chelatable zinc in hippocampal neuronal perikarya. *Brain Res, 799*(1), 118-129. doi:10.1016/s0006-8993(98)00463-6

Czupryn, A., & Skangiel-Kramska, J. (1997). Distribution of synaptic zinc in the developing mouse somatosensory barrel cortex. *J Comp Neurol, 386*(4), 652-660. doi:10.1002/(sici)1096-9861(19971006)386:4<652::aid-cne10>3.0.co;2-m

Danscher, G. (1981). Histochemical demonstration of heavy metals. A revised version of the sulphide silver method suitable for both light and electronmicroscopy. *Histochemistry, 71*(1), 1-16. doi:10.1007/bf00592566

Danscher, G. (1982). Exogenous selenium in the brain. A histochemical technique for light and electron microscopical localization of catalytic selenium bonds. *Histochemistry, 76*(3), 281-293. doi:10.1007/bf00543951

Danscher, G., & Stoltenberg, M. (2005). Zinc-specific autometallographic in vivo selenium methods: tracing of zinc-enriched (ZEN) terminals, ZEN pathways, and pools of zinc ions in a multitude of other ZEN cells. *J Histochem Cytochem, 53*(2), 141-153. doi:10.1369/jhc.4R6460.2005

Davis, K. A., & Young, E. D. (1997). Granule cell activation of complex-spiking neurons in dorsal cochlear nucleus. *J Neurosci, 17*(17), 6798-6806.

Dehmel, S., Pradhan, S., Koehler, S., Bledsoe, S., & Shore, S. (2012). Noise overexposure alters long-term somatosensory-auditory processing in the dorsal cochlear nucleus--possible basis for tinnitus-related hyperactivity? *J Neurosci, 32*(5), 1660-1671. doi:10.1523/JNEUROSCI.4608-11.2012

Demaurex, N., Lew, D. P., & Krause, K. H. (1992). Cyclopiazonic acid depletes intracellular Ca2+ stores and activates an influx pathway for divalent cations in HL-60 cells. *J Biol Chem, 267*(4), 2318-2324.

Deshpande, A., Kawai, H., Metherate, R., Glabe, C. G., & Busciglio, J. (2009). A role for synaptic zinc in activity-dependent Abeta oligomer formation and accumulation at excitatory synapses. *J Neurosci, 29*(13), 4004-4015. doi:10.1523/JNEUROSCI.5980-08.2009

Dreixler, J. C., & Leonard, J. P. (1994). Subunit-specific enhancement of glutamate receptor responses by zinc. *Brain Res Mol Brain Res, 22*(1-4), 144-150. doi:10.1016/0169-328x(94)90042-6

Dyck, R., Beaulieu, C., & Cynader, M. (1993). Histochemical localization of synaptic zinc in the developing cat visual cortex. *J Comp Neurol, 329*(1), 53-67. doi:10.1002/cne.903290105

Dyck, R. H., Chaudhuri, A., & Cynader, M. S. (2003). Experience-dependent regulation of the zincergic innervation of visual cortex in adult monkeys. *Cereb Cortex, 13*(10), 1094-1109.

Frederickson, C. J. (1989). Neurobiology of zinc and zinc-containing neurons. *Int Rev Neurobiol, 31*, 145-238. doi:10.1016/s0074-7742(08)60279-2

Frederickson, C. J., Cuajungco, M. P., LaBuda, C. J., & Suh, S. W. (2002). Nitric oxide causes apparent release of zinc from presynaptic boutons. *Neuroscience, 115*(2), 471-474. doi:10.1016/s0306-4522(02)00399-8

Frederickson, C. J., Howell, G. A., Haigh, M. D., & Danscher, G. (1988). Zinc-containing fiber systems in the cochlear nuclei of the rat and mouse. *Hear Res, 36*(2-3), 203-211.

Frederickson, C. J., Koh, J. Y., & Bush, A. I. (2005). The neurobiology of zinc in health and disease. *Nat Rev Neurosci, 6*(6), 449-462. doi:10.1038/nrn1671

Frederickson, C. J., Suh, S. W., Silva, D., Frederickson, C. J., & Thompson, R. B. (2000). Importance of zinc in the central nervous system: the zinc-containing neuron. *J Nutr, 130*(5S Suppl), 1471S-1483S. doi:10.1093/jn/130.5.1471S

Fujino, K., & Oertel, D. (2003). Bidirectional synaptic plasticity in the cerebellum-like mammalian dorsal cochlear nucleus. *Proc Natl Acad Sci U S A, 100*(1), 265-270. doi:10.1073/pnas.0135345100

Gaither, L. A., & Eide, D. J. (2001). Eukaryotic zinc transporters and their regulation. *Biometals, 14*(3-4), 251-270. doi:10.1023/a:1012988914300

Garthwaite, J. (2008). Concepts of neural nitric oxide-mediated transmission. *Eur J Neurosci, 27*(11), 2783-2802. doi:10.1111/j.1460-9568.2008.06285.x

Garthwaite, J. (2019). NO as a multimodal transmitter in the brain: discovery and current status. *Br J Pharmacol, 176*(2), 197-211. doi:10.1111/bph.14532

Goldberg, J. M., Wang, F., Sessler, C. D., Vogler, N. W., Zhang, D. Y., Loucks, W. H., . . . Lippard, S. J. (2018). Photoactivatable Sensors for Detecting Mobile Zinc. *J Am Chem Soc, 140*(6), 2020-2023. doi:10.1021/jacs.7b12766

Grabrucker, A. M. (2014). A role for synaptic zinc in ProSAP/Shank PSD scaffold malformation in autism spectrum disorders. *Dev Neurobiol, 74*(2), 136-146. doi:10.1002/dneu.22089

Grabrucker, S., Jannetti, L., Eckert, M., Gaub, S., Chhabra, R., Pfaender, S., . . . Grabrucker, A. M. (2014). Zinc deficiency dysregulates the synaptic ProSAP/Shank scaffold and might contribute to autism spectrum disorders. *Brain, 137*(Pt 1), 137-152. doi:10.1093/brain/awt303

Gubellini, P., Saulle, E., Centonze, D., Costa, C., Tropepi, D., Bernardi, G., . . . Calabresi, P. (2003). Corticostriatal LTP requires combined mGluR1 and mGluR5 activation. *Neuropharmacology, 44*(1), 8-16.

Hagmeyer, S., Sauer, A. K., & Grabrucker, A. M. (2018). Prospects of Zinc Supplementation in Autism Spectrum Disorders and Shankopathies Such as Phelan McDermid Syndrome. *Front Synaptic Neurosci, 10*, 11. doi:10.3389/fnsyn.2018.00011

Hansen, K. B., Ogden, K. K., Yuan, H., & Traynelis, S. F. (2014). Distinct functional and pharmacological properties of Triheteromeric GluN1/GluN2A/GluN2B NMDA receptors. *Neuron, 81*(5), 1084-1096. doi:10.1016/j.neuron.2014.01.035

Hardingham, N., Dachtler, J., & Fox, K. (2013). The role of nitric oxide in pre-synaptic plasticity and homeostasis. *Front Cell Neurosci, 7*, 190. doi:10.3389/fncel.2013.00190

Hecker, M., Mulsch, A., & Busse, R. (1994). Subcellular localization and characterization of neuronal nitric oxide synthase. *J Neurochem, 62*(4), 1524-1529. doi:10.1046/j.1471-4159.1994.62041524.x

Hennigar, S. R., & Kelleher, S. L. (2012). Zinc networks: the cell-specific compartmentalization of zinc for specialized functions. *Biol Chem, 393*(7), 565-578. doi:10.1515/hsz-2012-0128

Herring, B. E., & Nicoll, R. A. (2016). Long-Term Potentiation: From CaMKII to AMPA Receptor Trafficking. *Annu Rev Physiol, 78*, 351-365. doi:10.1146/annurev-physiol-021014-071753

Hildebrand, M. S., Phillips, A. M., Mullen, S. A., Adlard, P. A., Hardies, K., Damiano, J. A., . . . Reid, C. A. (2015). Loss of synaptic Zn2+ transporter function increases risk of febrile seizures. *Sci Rep, 5*, 17816. doi:10.1038/srep17816

Holbro, N., Grunditz, A., & Oertner, T. G. (2009). Differential distribution of endoplasmic reticulum controls metabotropic signaling and plasticity at hippocampal synapses. *Proc Natl Acad Sci U S A, 106*(35), 15055-15060. doi:10.1073/pnas.0905110106

Howell, G. A., Welch, M. G., & Frederickson, C. J. (1984). Stimulation-induced uptake and release of zinc in hippocampal slices. *Nature, 308*(5961), 736-738. doi:10.1038/308736a0

Huang, Y. Z., Pan, E., Xiong, Z. Q., & McNamara, J. O. (2008). Zinc-mediated transactivation of TrkB potentiates the hippocampal mossy fiber-CA3 pyramid synapse. *Neuron, 57*(4), 546-558. doi:10.1016/j.neuron.2007.11.026

Huber, K. M., Kayser, M. S., & Bear, M. F. (2000). Role for rapid dendritic protein synthesis in hippocampal mGluR-dependent long-term depression. *Science, 288*(5469), 1254-1257.

Huber, K. M., Roder, J. C., & Bear, M. F. (2001). Chemical induction of mGluR5- and protein synthesis--dependent long-term depression in hippocampal area CA1. *J Neurophysiol, 86*(1), 321-325. doi:10.1152/jn.2001.86.1.321

Ichinohe, N., & Rockland, K. S. (2005). Zinc-enriched amygdalo- and hippocampo-cortical connections to the inferotemporal cortices in macaque monkey. *Neurosci Res, 53*(1), 57-68. doi:10.1016/j.neures.2005.06.002

Izumi, Y., Auberson, Y. P., & Zorumski, C. F. (2006). Zinc modulates bidirectional hippocampal plasticity by effects on NMDA receptors. *J Neurosci, 26*(27), 7181-7188. doi:10.1523/JNEUROSCI.1258-06.2006

Kalappa, B. I., Anderson, C. T., Goldberg, J. M., Lippard, S. J., & Tzounopoulos, T. (2015). AMPA receptor inhibition by synaptically released zinc. *Proc Natl Acad Sci U S A, 112*(51), 15749-15754. doi:10.1073/pnas.1512296112

Kalappa, B. I., & Tzounopoulos, T. (2017). Context-Dependent Modulation of Excitatory Synaptic Strength by Synaptically Released Zinc. *eNeuro, 4*(1). doi:10.1523/ENEURO.0011-17.2017

Kambe, T., Tsuji, T., Hashimoto, A., & Itsumura, N. (2015). The Physiological, Biochemical, and Molecular Roles of Zinc Transporters in Zinc Homeostasis and Metabolism. *Physiol Rev, 95*(3), 749-784. doi:10.1152/physrev.00035.2014

Kantheti, P., Qiao, X., Diaz, M. E., Peden, A. A., Meyer, G. E., Carskadon, S. L., . . . Burmeister, M. (1998). Mutation in AP-3 delta in the mocha mouse links endosomal transport to storage deficiency in platelets, melanosomes, and synaptic vesicles. *Neuron, 21*(1), 111-122. doi:10.1016/s0896-6273(00)80519-x

Kim, C. H., Lee, J., Lee, J. Y., & Roche, K. W. (2008). Metabotropic glutamate receptors: phosphorylation and receptor signaling. *J Neurosci Res, 86*(1), 1-10. doi:10.1002/jnr.21437

Knipp, M., Meloni, G., Roschitzki, B., & Vasak, M. (2005). Zn7metallothionein-3 and the synaptic vesicle cycle: interaction of metallothionein-3 with the small GTPase Rab3A. *Biochemistry, 44*(9), 3159-3165. doi:10.1021/bi047636d

Krezel, A., & Maret, W. (2008). Thionein/metallothionein control Zn(II) availability and the activity of enzymes. *J Biol Inorg Chem, 13*(3), 401-409. doi:10.1007/s00775-007-0330-y

Kujawa, S. G., & Liberman, M. C. (2009). Adding insult to injury: cochlear nerve degeneration after "temporary" noise-induced hearing loss. *J Neurosci, 29*(45), 14077-14085. doi:10.1523/JNEUROSCI.2845-09.2009

Kumar, M., Xiong, S., Tzounopoulos, T., & Anderson, C. T. (2019). Fine Control of Sound Frequency Tuning and Frequency Discrimination Acuity by Synaptic Zinc Signaling in Mouse Auditory Cortex. *J Neurosci, 39*(5), 854-865. doi:10.1523/JNEUROSCI.1339-18.2018

Lavoie, N., Jeyaraju, D. V., Peralta, M. R., 3rd, Seress, L., Pellegrini, L., & Toth, K. (2011). Vesicular zinc regulates the Ca2+ sensitivity of a subpopulation of presynaptic vesicles at hippocampal mossy fiber terminals. *J Neurosci, 31*(50), 18251-18265. doi:10.1523/JNEUROSCI.4164-11.2011

Lee, E. J., Lee, H., Huang, T. N., Chung, C., Shin, W., Kim, K., . . . Kim, E. (2015). Trans-synaptic zinc mobilization improves social interaction in two mouse models of autism through NMDAR activation. *Nat Commun, 6*, 7168. doi:10.1038/ncomms8168

Li, Y., Andereggen, L., Yuki, K., Omura, K., Yin, Y., Gilbert, H. Y., . . . Benowitz, L. (2017). Mobile zinc increases rapidly in the retina after optic nerve injury and regulates ganglion cell survival and optic nerve regeneration. *Proc Natl Acad Sci U S A, 114*(2), E209-E218. doi:10.1073/pnas.1616811114

Li, Y., Hough, C. J., Frederickson, C. J., & Sarvey, J. M. (2001). Induction of mossy fiber --> Ca3 long-term potentiation requires translocation of synaptically released Zn2+. *J Neurosci, 21*(20), 8015-8025.

Liguz-Lecznar, M., Nowicka, D., Czupryn, A., & Skangiel-Kramska, J. (2005). Dissociation of synaptic zinc level and zinc transporter 3 expression during postnatal development and after sensory deprivation in the barrel cortex of mice. *Brain Res Bull, 66*(2), 106-113. doi:10.1016/j.brainresbull.2005.03.019

Lin, W., Mohandas, B., Fontaine, C. P., & Colvin, R. A. (2007). Release of intracellular Zn(2+) in cultured neurons after brief exposure to low concentrations of exogenous nitric oxide. *Biometals, 20*(6), 891-901. doi:10.1007/s10534-007-9082-y

Luscher, C., & Huber, K. M. (2010). Group 1 mGluR-dependent synaptic long-term depression: mechanisms and implications for circuitry and disease. *Neuron, 65*(4), 445-459. doi:10.1016/j.neuron.2010.01.016

MacDonald, R. S. (2000). The role of zinc in growth and cell proliferation. *J Nutr, 130*(5S Suppl), 1500S-1508S. doi:10.1093/jn/130.5.1500S

Malenka, R. C., & Bear, M. F. (2004). LTP and LTD: an embarrassment of riches. *Neuron, 44*(1), 5-21. doi:10.1016/j.neuron.2004.09.012

Malenka, R. C., & Nicoll, R. A. (1993). NMDA-receptor-dependent synaptic plasticity: multiple forms and mechanisms. *Trends Neurosci, 16*(12), 521-527.

Manis, P. B., Spirou, G. A., Wright, D. D., Paydar, S., & Ryugo, D. K. (1994). Physiology and morphology of complex spiking neurons in the guinea pig dorsal cochlear nucleus. *J Comp Neurol, 348*(2), 261-276. doi:10.1002/cne.903480208

Maret, W. (2013). Zinc biochemistry: from a single zinc enzyme to a key element of life. *Adv Nutr, 4*(1), 82-91. doi:10.3945/an.112.003038

Maret, W. (2014). Zinc in the biosciences. *Metallomics, 6*(7), 1174. doi:10.1039/c4mt90021a

Marks, K. L., Martel, D. T., Wu, C., Basura, G. J., Roberts, L. E., Schvartz-Leyzac, K. C., & Shore, S. E. (2018). Auditory-somatosensory bimodal stimulation desynchronizes brain circuitry to reduce tinnitus in guinea pigs and humans. *Sci Transl Med, 10*(422). doi:10.1126/scitranslmed.aal3175

Martel, G., Hevi, C., Friebely, O., Baybutt, T., & Shumyatsky, G. P. (2010). Zinc transporter 3 is involved in learned fear and extinction, but not in innate fear. *Learn Mem, 17*(11), 582-590. doi:10.1101/lm.1962010

Martel, G., Hevi, C., Kane-Goldsmith, N., & Shumyatsky, G. P. (2011). Zinc transporter ZnT3 is involved in memory dependent on the hippocampus and perirhinal cortex. *Behav Brain Res, 223*(1), 233-238. doi:10.1016/j.bbr.2011.04.020

Masters, B. A., Quaife, C. J., Erickson, J. C., Kelly, E. J., Froelick, G. J., Zambrowicz, B. P., . . . Palmiter, R. D. (1994). Metallothionein III is expressed in neurons that sequester zinc in synaptic vesicles. *J Neurosci, 14*(10), 5844-5857.

May, B. J. (2000). Role of the dorsal cochlear nucleus in the sound localization behavior of cats. *Hear Res, 148*(1-2), 74-87. doi:10.1016/s0378-5955(00)00142-8

McAllister, B. B., & Dyck, R. H. (2017). Zinc transporter 3 (ZnT3) and vesicular zinc in central nervous system function. *Neurosci Biobehav Rev, 80*, 329-350. doi:10.1016/j.neubiorev.2017.06.006

McCord, M. C., & Aizenman, E. (2014). The role of intracellular zinc release in aging, oxidative stress, and Alzheimer's disease. *Front Aging Neurosci, 6*, 77. doi:10.3389/fnagi.2014.00077

Molnar, P., & Nadler, J. V. (2001). Synaptically-released zinc inhibits N-methyl-D-aspartate receptor activation at recurrent mossy fiber synapses. *Brain Res, 910*(1-2), 205-207. doi:10.1016/s0006-8993(01)02720-2

Mulkey, R. M., & Malenka, R. C. (1992). Mechanisms underlying induction of homosynaptic long-term depression in area CA1 of the hippocampus. *Neuron, 9*(5), 967-975.

Nakashima, A. S., Butt, R. H., & Dyck, R. H. (2011). Alterations in protein and gene expression within the barrel cortices of ZnT3 knockout mice: experience-independent and dependent changes. *Neurochem Int, 59*(6), 860-870. doi:10.1016/j.neuint.2011.08.007

Nakashima, A. S., & Dyck, R. H. (2009). Zinc and cortical plasticity. *Brain Res Rev, 59*(2), 347-373. doi:10.1016/j.brainresrev.2008.10.003

Nakashima, A. S., & Dyck, R. H. (2010). Dynamic, experience-dependent modulation of synaptic zinc within the excitatory synapses of the mouse barrel cortex. *Neuroscience, 170*(4), 1015-1019. doi:10.1016/j.neuroscience.2010.08.020

O'Connor, D. H., Wittenberg, G. M., & Wang, S. S. (2005). Dissection of bidirectional synaptic plasticity into saturable unidirectional processes. *J Neurophysiol, 94*(2), 1565-1573. doi:10.1152/jn.00047.2005

Oertel, D., & Wu, S. H. (1989). Morphology and physiology of cells in slice preparations of the dorsal cochlear nucleus of mice. *J Comp Neurol, 283*(2), 228-247. doi:10.1002/cne.902830206

Oertel, D., & Young, E. D. (2004). What's a cerebellar circuit doing in the auditory system? *Trends Neurosci, 27*(2), 104-110. doi:10.1016/j.tins.2003.12.001

Ohana, E., Hoch, E., Keasar, C., Kambe, T., Yifrach, O., Hershfinkel, M., & Sekler, I. (2009). Identification of the Zn2+ binding site and mode of operation of a mammalian Zn2+ transporter. *J Biol Chem, 284*(26), 17677-17686. doi:10.1074/jbc.M109.007203

Olesen, R. H., Hyde, T. M., Kleinman, J. E., Smidt, K., Rungby, J., & Larsen, A. (2016). Obesity and age-related alterations in the gene expression of zinc-transporter proteins in the human brain. *Transl Psychiatry, 6*(6), e838. doi:10.1038/tp.2016.83

Oliet, S. H., Malenka, R. C., & Nicoll, R. A. (1997). Two distinct forms of long-term depression coexist in CA1 hippocampal pyramidal cells. *Neuron, 18*(6), 969-982.

Osen, K. K. (1970). Course and termination of the primary afferents in the cochlear nuclei of the cat. An experimental anatomical study. *Arch Ital Biol, 108*(1), 21-51.

Palmiter, R. D., Cole, T. B., Quaife, C. J., & Findley, S. D. (1996). ZnT-3, a putative transporter of zinc into synaptic vesicles. *Proc Natl Acad Sci U S A, 93*(25), 14934-14939.

Pan, E., Zhang, X. A., Huang, Z., Krezel, A., Zhao, M., Tinberg, C. E., . . . McNamara, J. O. (2011). Vesicular zinc promotes presynaptic and inhibits postsynaptic long-term potentiation of mossy fiber-CA3 synapse. *Neuron, 71*(6), 1116-1126. doi:10.1016/j.neuron.2011.07.019

Paoletti, P., Ascher, P., & Neyton, J. (1997). High-affinity zinc inhibition of NMDA NR1-NR2A receptors. *J Neurosci, 17*(15), 5711-5725.

Paoletti, P., Vergnano, A. M., Barbour, B., & Casado, M. (2009). Zinc at glutamatergic synapses. *Neuroscience, 158*(1), 126-136. doi:10.1016/j.neuroscience.2008.01.061

Patrick Wu, H. P., & Dyck, R. H. (2018). Signaling by Synaptic Zinc is Required for Whisker-Mediated, Fine Texture Discrimination. *Neuroscience, 369*, 242-247. doi:10.1016/j.neuroscience.2017.11.020

Pearce, L. L., Wasserloos, K., St Croix, C. M., Gandley, R., Levitan, E. S., & Pitt, B. R. (2000). Metallothionein, nitric oxide and zinc homeostasis in vascular endothelial cells. *J Nutr, 130*(5S Suppl), 1467S-1470S. doi:10.1093/jn/130.5.1467S

Perez-Becerril, C., Morris, A. G., Mortimer, A., McKenna, P. J., & de Belleroche, J. (2016). Common variants in the chromosome 2p23 region containing the SLC30A3 (ZnT3) gene are associated with schizophrenia in female but not male individuals in a large collection of European samples. *Psychiatry Res, 246*, 335-340. doi:10.1016/j.psychres.2016.09.052

Perez-Rosello, T., Anderson, C. T., Schopfer, F. J., Zhao, Y., Gilad, D., Salvatore, S. R., . . . Tzounopoulos, T. (2013). Synaptic Zn2+ inhibits neurotransmitter release by promoting endocannabinoid synthesis. *J Neurosci, 33*(22), 9259-9272. doi:10.1523/JNEUROSCI.0237-13.2013

Peters, S., Koh, J., & Choi, D. W. (1987). Zinc selectively blocks the action of N-methyl-D-aspartate on cortical neurons. *Science, 236*(4801), 589-593. doi:10.1126/science.2883728

Pick, J. E., & Ziff, E. B. (2018). Regulation of AMPA receptor trafficking and exit from the endoplasmic reticulum. *Mol Cell Neurosci*. doi:10.1016/j.mcn.2018.03.004

Pilati, N., Ison, M. J., Barker, M., Mulheran, M., Large, C. H., Forsythe, I. D., . . . Hamann, M. (2012). Mechanisms contributing to central excitability changes during hearing loss. *Proc Natl Acad Sci U S A, 109*(21), 8292-8297. doi:10.1073/pnas.1116981109

Plenge-Tellechea, F., Soler, F., & Fernandez-Belda, F. (1997). On the inhibition mechanism of sarcoplasmic or endoplasmic reticulum Ca2+-ATPases by cyclopiazonic acid. *J Biol Chem, 272*(5), 2794-2800. doi:10.1074/jbc.272.5.2794

Qian, J., & Noebels, J. L. (2005). Visualization of transmitter release with zinc fluorescence detection at the mouse hippocampal mossy fibre synapse. *J Physiol, 566*(Pt 3), 747-758. doi:10.1113/jphysiol.2005.089276

Qian, J., & Noebels, J. L. (2006). Exocytosis of vesicular zinc reveals persistent depression of neurotransmitter release during metabotropic glutamate receptor long-term depression at the hippocampal CA3-CA1 synapse. *J Neurosci, 26*(22), 6089-6095. doi:10.1523/JNEUROSCI.0475-06.2006

Que, E. L., Bleher, R., Duncan, F. E., Kong, B. Y., Gleber, S. C., Vogt, S., . . . O'Halloran, T. V. (2015). Quantitative mapping of zinc fluxes in the mammalian egg reveals the origin of fertilization-induced zinc sparks. *Nat Chem, 7*(2), 130-139. doi:10.1038/nchem.2133

Rachline, J., Perin-Dureau, F., Le Goff, A., Neyton, J., & Paoletti, P. (2005). The micromolar zinc-binding domain on the NMDA receptor subunit NR2B. *J Neurosci, 25*(2), 308-317. doi:10.1523/JNEUROSCI.3967-04.2005

Radford, R. J., & Lippard, S. J. (2013). Chelators for investigating zinc metalloneurochemistry. *Curr Opin Chem Biol, 17*(2), 129-136. doi:10.1016/j.cbpa.2013.01.009

Rassendren, F. A., Lory, P., Pin, J. P., & Nargeot, J. (1990). Zinc has opposite effects on NMDA and non-NMDA receptors expressed in Xenopus oocytes. *Neuron, 4*(5), 733-740. doi:10.1016/0896-6273(90)90199-p

Regehr, W. G., Carey, M. R., & Best, A. R. (2009). Activity-dependent regulation of synapses by retrograde messengers. *Neuron, 63*(2), 154-170. doi:10.1016/j.neuron.2009.06.021

Roberts, M. T., & Trussell, L. O. (2010). Molecular layer inhibitory interneurons provide feedforward and lateral inhibition in the dorsal cochlear nucleus. *J Neurophysiol, 104*(5), 2462-2473. doi:10.1152/jn.00312.2010

Rubio, M. E., & Juiz, J. M. (1998). Chemical anatomy of excitatory endings in the dorsal cochlear nucleus of the rat: differential synaptic distribution of aspartate aminotransferase, glutamate, and vesicular zinc. *J Comp Neurol, 399*(3), 341-358.

Ryugo, D. K., Haenggeli, C. A., & Doucet, J. R. (2003). Multimodal inputs to the granule cell domain of the cochlear nucleus. *Exp Brain Res, 153*(4), 477-485. doi:10.1007/s00221-003-1605-3

Ryugo, D. K., & Willard, F. H. (1985). The dorsal cochlear nucleus of the mouse: a light microscopic analysis of neurons that project to the inferior colliculus. *J Comp Neurol, 242*(3), 381-396. doi:10.1002/cne.902420307

Saadi, R. A., He, K., Hartnett, K. A., Kandler, K., Hershfinkel, M., & Aizenman, E. (2012). SNARE-dependent upregulation of potassium chloride co-transporter 2 activity after metabotropic zinc receptor activation in rat cortical neurons in vitro. *Neuroscience, 210*, 38-46. doi:10.1016/j.neuroscience.2012.03.001

Salazar, G., Craige, B., Love, R., Kalman, D., & Faundez, V. (2005). Vglut1 and ZnT3 co-targeting mechanisms regulate vesicular zinc stores in PC12 cells. *J Cell Sci, 118*(Pt 9), 1911-1921. doi:10.1242/jcs.02319

Salazar, G., Love, R., Styers, M. L., Werner, E., Peden, A., Rodriguez, S., . . . Faundez, V. (2004). AP-3-dependent mechanisms control the targeting of a chloride channel (ClC-3) in neuronal and non-neuronal cells. *J Biol Chem, 279*(24), 25430-25439. doi:10.1074/jbc.M402331200

Salazar, G., Love, R., Werner, E., Doucette, M. M., Cheng, S., Levey, A., & Faundez, V. (2004). The zinc transporter ZnT3 interacts with AP-3 and it is preferentially targeted to a distinct synaptic vesicle subpopulation. *Mol Biol Cell, 15*(2), 575-587. doi:10.1091/mbc.e03-06-0401

Sattler, R., Xiong, Z., Lu, W. Y., Hafner, M., MacDonald, J. F., & Tymianski, M. (1999). Specific coupling of NMDA receptor activation to nitric oxide neurotoxicity by PSD-95 protein. *Science, 284*(5421), 1845-1848. doi:10.1126/science.284.5421.1845

Seidler, N. W., Jona, I., Vegh, M., & Martonosi, A. (1989). Cyclopiazonic acid is a specific inhibitor of the Ca2+-ATPase of sarcoplasmic reticulum. *J Biol Chem, 264*(30), 17816-17823.

Sensi, S. L., Paoletti, P., Koh, J. Y., Aizenman, E., Bush, A. I., & Hershfinkel, M. (2011). The neurophysiology and pathology of brain zinc. *J Neurosci, 31*(45), 16076-16085. doi:10.1523/JNEUROSCI.3454-11.2011

Sensi, S. L., Yin, H. Z., Carriedo, S. G., Rao, S. S., & Weiss, J. H. (1999). Preferential Zn2+ influx through Ca2+-permeable AMPA/kainate channels triggers prolonged mitochondrial superoxide production. *Proc Natl Acad Sci U S A, 96*(5), 2414-2419. doi:10.1073/pnas.96.5.2414

Shen, K. Z., & Johnson, S. W. (2013). Group I mGluRs evoke K-ATP current by intracellular Ca2+ mobilization in rat subthalamus neurons. *J Pharmacol Exp Ther, 345*(1), 139-150. doi:10.1124/jpet.112.201566

Shen, W., Flajolet, M., Greengard, P., & Surmeier, D. J. (2008). Dichotomous dopaminergic control of striatal synaptic plasticity. *Science, 321*(5890), 848-851. doi:10.1126/science.1160575

Shore, S., Zhou, J., & Koehler, S. (2007). Neural mechanisms underlying somatic tinnitus. *Prog Brain Res, 166*, 107-123. doi:10.1016/S0079-6123(07)66010-5

Sindreu, C. B., Varoqui, H., Erickson, J. D., & Perez-Clausell, J. (2003). Boutons containing vesicular zinc define a subpopulation of synapses with low AMPAR content in rat hippocampus. *Cereb Cortex, 13*(8), 823-829. doi:10.1093/cercor/13.8.823

Singla, S., Dempsey, C., Warren, R., Enikolopov, A. G., & Sawtell, N. B. (2017). A cerebellum-like circuit in the auditory system cancels responses to self-generated sounds. *Nat Neurosci, 20*(7), 943-950. doi:10.1038/nn.4567

Slomianka, L. (1992). Neurons of origin of zinc-containing pathways and the distribution of zinc-containing boutons in the hippocampal region of the rat. *Neuroscience, 48*(2), 325-352. doi:10.1016/0306-4522(92)90494-m

Snyder, E. M., Philpot, B. D., Huber, K. M., Dong, X., Fallon, J. R., & Bear, M. F. (2001). Internalization of ionotropic glutamate receptors in response to mGluR activation. *Nat Neurosci, 4*(11), 1079-1085. doi:10.1038/nn746

Steinert, J. R., Chernova, T., & Forsythe, I. D. (2010). Nitric oxide signaling in brain function, dysfunction, and dementia. *Neuroscientist, 16*(4), 435-452. doi:10.1177/1073858410366481

Stoltenberg, M., Bush, A. I., Bach, G., Smidt, K., Larsen, A., Rungby, J., . . . Danscher, G. (2007). Amyloid plaques arise from zinc-enriched cortical layers in APP/PS1 transgenic mice and are paradoxically enlarged with dietary zinc deficiency. *Neuroscience, 150*(2), 357-369. doi:10.1016/j.neuroscience.2007.09.025

Stoltenberg, M., Nejsum, L. N., Larsen, A., & Danscher, G. (2004). Abundance of zinc ions in synaptic terminals of mocha mutant mice: zinc transporter 3 immunohistochemistry and zinc sulphide autometallography. *J Mol Histol, 35*(2), 141-145. doi:10.1023/b:hijo.0000023382.40292.68

Suter, B. A., O'Connor, T., Iyer, V., Petreanu, L. T., Hooks, B. M., Kiritani, T., . . . Shepherd, G. M. (2010). Ephus: multipurpose data acquisition software for neuroscience experiments. *Front Neural Circuits, 4*, 100. doi:10.3389/fncir.2010.00100

Suvarna, Y., Maity, N., & Shivamurthy, M. C. (2016). Emerging Trends in Retrograde Signaling. *Mol Neurobiol, 53*(4), 2572-2578. doi:10.1007/s12035-015-9280-5

Takeda, A., Fuke, S., Ando, M., & Oku, N. (2009). Positive modulation of long-term potentiation at hippocampal CA1 synapses by low micromolar concentrations of zinc. *Neuroscience, 158*(2), 585-591. doi:10.1016/j.neuroscience.2008.10.009

Topolnik, L., Azzi, M., Morin, F., Kougioumoutzakis, A., & Lacaille, J. C. (2006). mGluR1/5 subtype-specific calcium signalling and induction of long-term potentiation in rat hippocampal oriens/alveus interneurones. *J Physiol, 575*(Pt 1), 115-131. doi:10.1113/jphysiol.2006.112896

Tovar, K. R., & Westbrook, G. L. (2012). Amino-terminal ligands prolong NMDA Receptor-mediated EPSCs. *J Neurosci, 32*(23), 8065-8073. doi:10.1523/JNEUROSCI.0538-12.2012

Traynelis, S. F., Wollmuth, L. P., McBain, C. J., Menniti, F. S., Vance, K. M., Ogden, K. K., . . . Dingledine, R. (2010). Glutamate receptor ion channels: structure, regulation, and function. *Pharmacol Rev, 62*(3), 405-496. doi:10.1124/pr.109.002451

Turrigiano, G. (2007). Homeostatic signaling: the positive side of negative feedback. *Curr Opin Neurobiol, 17*(3), 318-324. doi:10.1016/j.conb.2007.04.004

Tzounopoulos, T. (2008). Mechanisms of synaptic plasticity in the dorsal cochlear nucleus: plasticity-induced changes that could underlie tinnitus. *Am J Audiol, 17*(2), S170-175. doi:10.1044/1059-0889(2008/07-0030)

Tzounopoulos, T., Kim, Y., Oertel, D., & Trussell, L. O. (2004). Cell-specific, spike timing-dependent plasticities in the dorsal cochlear nucleus. *Nat Neurosci, 7*(7), 719-725. doi:10.1038/nn1272

Tzounopoulos, T., Rubio, M. E., Keen, J. E., & Trussell, L. O. (2007). Coactivation of pre- and postsynaptic signaling mechanisms determines cell-specific spike-timing-dependent plasticity. *Neuron, 54*(2), 291-301. doi:10.1016/j.neuron.2007.03.026

Vallee, B. L. (1995). The function of metallothionein. *Neurochem Int, 27*(1), 23-33. doi:10.1016/0197-0186(94)00165-q

Vallee, B. L., & Falchuk, K. H. (1993). The biochemical basis of zinc physiology. *Physiol Rev, 73*(1), 79-118. doi:10.1152/physrev.1993.73.1.79

Vergnano, A. M., Rebola, N., Savtchenko, L. P., Pinheiro, P. S., Casado, M., Kieffer, B. L., . . . Paoletti, P. (2014). Zinc dynamics and action at excitatory synapses. *Neuron, 82*(5), 1101-1114. doi:10.1016/j.neuron.2014.04.034

Vogt, K., Mellor, J., Tong, G., & Nicoll, R. (2000). The actions of synaptically released zinc at hippocampal mossy fiber synapses. *Neuron, 26*(1), 187-196.

Waller, H. J., Godfrey, D. A., & Chen, K. (1996). Effects of parallel fiber stimulation on neurons of rat dorsal cochlear nucleus. *Hear Res, 98*(1-2), 169-179. doi:10.1016/0378-5955(96)00090-1

Wenzel, H. J., Cole, T. B., Born, D. E., Schwartzkroin, P. A., & Palmiter, R. D. (1997). Ultrastructural localization of zinc transporter-3 (ZnT-3) to synaptic vesicle membranes within mossy fiber boutons in the hippocampus of mouse and monkey. *Proc Natl Acad Sci U S A, 94*(23), 12676-12681. doi:10.1073/pnas.94.23.12676

Westbrook, G. L., & Mayer, M. L. (1987). Micromolar concentrations of Zn2+ antagonize NMDA and GABA responses of hippocampal neurons. *Nature, 328*(6131), 640-643. doi:10.1038/328640a0

Wisniewski, K., & Car, H. (2002). (S)-3,5-DHPG: a review. *CNS Drug Rev, 8*(1), 101-116.

Wright, D. D., Blackstone, C. D., Huganir, R. L., & Ryugo, D. K. (1996). Immunocytochemical localization of the mGluR1 alpha metabotropic glutamate receptor in the dorsal cochlear nucleus. *J Comp Neurol, 364*(4), 729-745. doi:10.1002/(SICI)1096-9861(19960122)364:4<729::AID-CNE10>3.0.CO;2-K

Wu, J., Harney, S., Rowan, M. J., & Anwyl, R. (2008). Involvement of group I mGluRs in LTP induced by strong high frequency stimulation in the dentate gyrus in vitro. *Neurosci Lett, 436*(2), 235-238. doi:10.1016/j.neulet.2008.03.027

Xie, X., & Smart, T. G. (1994). Modulation of long-term potentiation in rat hippocampal pyramidal neurons by zinc. *Pflugers Arch, 427*(5-6), 481-486. doi:10.1007/bf00374264

Yoo, M. H., Kim, T. Y., Yoon, Y. H., & Koh, J. Y. (2016). Autism phenotypes in ZnT3 null mice: Involvement of zinc dyshomeostasis, MMP-9 activation and BDNF upregulation. *Sci Rep, 6*, 28548. doi:10.1038/srep28548

Zastrow, M. L., Radford, R. J., Chyan, W., Anderson, C. T., Zhang, D. Y., Loas, A., . . . Lippard, S. J. (2016). Reaction-Based Probes for Imaging Mobile Zinc in Live Cells and Tissues. *ACS Sens, 1*(1), 32-39. doi:10.1021/acssensors.5b00022

Zhang, L. H., Wang, X., Stoltenberg, M., Danscher, G., Huang, L., & Wang, Z. Y. (2008). Abundant expression of zinc transporters in the amyloid plaques of Alzheimer's disease brain. *Brain Res Bull, 77*(1), 55-60. doi:10.1016/j.brainresbull.2008.03.014

Zhang, S., & Oertel, D. (1993). Cartwheel and superficial stellate cells of the dorsal cochlear nucleus of mice: intracellular recordings in slices. *J Neurophysiol, 69*(5), 1384-1397. doi:10.1152/jn.1993.69.5.1384

Zhao, Y., & Tzounopoulos, T. (2011). Physiological activation of cholinergic inputs controls associative synaptic plasticity via modulation of endocannabinoid signaling. *J Neurosci, 31*(9), 3158-3168. doi:10.1523/JNEUROSCI.5303-10.2011

Zhou, J., Nannapaneni, N., & Shore, S. (2007). Vessicular glutamate transporters 1 and 2 are differentially associated with auditory nerve and spinal trigeminal inputs to the cochlear nucleus. *J Comp Neurol, 500*(4), 777-787. doi:10.1002/cne.21208